Ann. Henri Poincaré 17 (2016), 1263–1330

1424-0637/16/061263-68
published online December 19, 2015
DOI 10.1007/s00023-015-0452-7

Annales Henri Poincaré

SLE Boundary Visits

Niko Jokela, Matti Järvinen and Kalle Kytölä

Abstract. We study the probabilities with which chordal Schramm–Loewner evolutions (SLE) visit small neighborhoods of boundary points. We find formulas for general chordal SLE boundary visiting probability amplitudes, also known as SLE boundary zig-zags or order refined SLE multi-point Green's functions on the boundary. Remarkably, an exact answer can be found to this important SLE question for an arbitrarily large number of marked points. The main technique employed is a spin chain–Coulomb gas correspondence between tensor product representations of a quantum group and functions given by Dotsenko–Fateev type integrals. We show how to express these integral formulas in terms of regularized real integrals, and we discuss their numerical evaluation. The results are universal in the sense that apart from an overall multiplicative constant the same formula gives the amplitude for many different formulations of the SLE boundary visit problem. The formula also applies to renormalized boundary visit probabilities for interfaces in critical lattice models of statistical mechanics: we compare the results with numerical simulations of percolation, loop-erased random walk, and Fortuin–Kasteleyn random cluster models at $Q = 2$ and $Q = 3$, and find good agreement.

Contents

1. Introduction

1.1. SLE Curves

Schramm–Loewner evolutions (SLE) are conformally invariant random fractal curves in the plane, whose most important characteristics are determined by one parameter $\kappa > 0$. They were introduced by Schramm [42] as the only plausible candidates for the scaling limits of random interfaces in statistical mechanics models that are expected to display conformal invariance, with different models corresponding to different values of the parameter κ.[1] Proofs that interfaces in various critical lattice models do converge to SLEs in the scaling limit have been obtained for example in [13,14,27,28,38,45–47,49,53].

The fundamental example of SLEs is the chordal SLE_κ [37,41]. For a given simply connected domain $\Lambda \subset \mathbb{C}$ with two marked boundary points $a, b \in \partial\Lambda$, the chordal SLE_κ in Λ from a to b is an oriented but unparametrized random curve γ in the closure of Λ starting from a and ending at b. Its two characterizing properties are conformal invariance and domain Markov property:

- Conformal invariance states that the image of a chordal SLE under a conformal map is a chordal SLE in the image domain.
- Domain Markov property states that given an initial segment of a chordal SLE, the conditional law of the continuation is a chordal SLE in the remaining subdomain.

Some features of SLEs vary continuously in κ, notably the Hausdorff dimension of the fractal curve is given by $d_{\mathrm{H}}(\gamma) = 1 + \frac{\kappa}{8}$ for $0 < \kappa \leq 8$ [10]. On the other hand, some qualitative properties of SLEs show abrupt phase transitions with respect to the parameter κ. For the present purposes, it is important to distinguish the following three phases [41]:

[1] Figure 1 shows two SLE curves. Examples of interfaces in lattice models are shown in Figs. 5, 6, and 7, on pages 1305, 1306, and 1307, respectively.

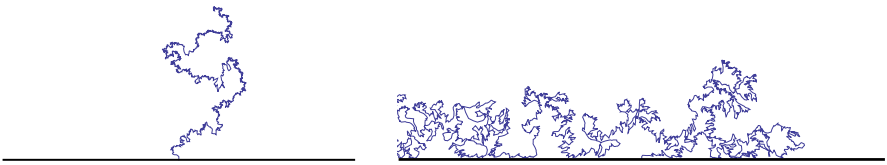

FIGURE 1. Chordal SLE_κ is a random fractal curve. For $\kappa \leq 4$ the curve is simple and does not touch boundary, and for $4 < \kappa < 8$ the curve has double points and touches the boundary on a random Cantor set. The *two pictures* show chordal SLE_κ in the upper half-plane $\mathbb{H}$ from 0 to ∞—in the *left picture* $\kappa = 3$, and the *right picture* $\kappa = 6$

$0 < \kappa \leq 4$ The chordal SLE_κ is a simple curve, i.e., the curve does not have double points, see Fig. 1 (left). The curve does not touch the boundary $\partial\Lambda$ of the domain except at the starting point a and the end point b. The curve avoids any given point $z \in \Lambda$ of the domain with probability one.

$4 < \kappa < 8$ The chordal SLE_κ is a non self-traversing curve with double points, see Fig. 1 (right). The intersection of the curve with the boundary $\partial\Lambda$ of the domain is a random Cantor set. The curve still avoids any given point $z \in \overline{\Lambda} \setminus \{a, b\}$ of the domain or of its boundary with probability one.

$8 \leq \kappa$ The chordal SLE_κ is a space-filling curve; any point $z \in \Lambda$ of the domain is on the curve.

The behavior in the case $\kappa \geq 8$ is somewhat pathological. No interfaces in statistical mechanics models are expected to correspond to $\kappa > 8$.[2] In this article we restrict our attention to the cases $0 < \kappa < 8$.

1.2. Chordal SLE Boundary Visits

The main goal of this article is to find formulas for the probabilities with which the chordal SLE visits small neighborhoods of given boundary points. Partial answers to similar questions have been obtained in [3–5,34,51].

It is easiest to illustrate the question in the upper half-plane

$$\mathbb{H} = \{z \in \mathbb{C} | \Im\mathfrak{m}(z) > 0\},$$

with the chordal SLE_κ curve γ starting from the origin and ending at infinity. We will briefly recall the precise definition of chordal SLE_κ in $\mathbb{H}$ from 0 to ∞ in Sect. 5.1, and we refer the reader to [41] for more thorough background.

[2] In the borderline case $\kappa = 8$, the (space-filling) chordal SLE_8 curve is the scaling limit of the Peano curve of the uniform spanning tree [38].

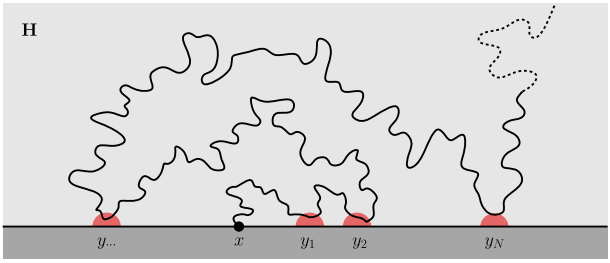

FIGURE 2. A schematic illustration of the boundary zig-zag studied in this article: the chordal SLE_κ curve in the upper half-plane $\mathbb{H}$ starts from x and visits small neighborhoods of boundary points $y_1, y_2, \ldots, y_N$

Denote the half-disk of radius $\varepsilon > 0$ centered at a boundary point $y \in \mathbb{R} \subset \partial\mathbb{H}$ by

$$B_\varepsilon(y) = \{z \in \mathbb{H} | |z - y| < \varepsilon\}.$$

Given points $y_1, y_2, \ldots, y_N \in \mathbb{R}$ and radii $\varepsilon_1, \varepsilon_2, \ldots, \varepsilon_N > 0$, the probability that the curve γ visits all of $B_{\varepsilon_j}(y_j)$, $j = 1, 2, \ldots, N$, tends to zero as a power law as the radius ε_j is taken small. More precisely, the scaling exponent of the power law is

$$h = \frac{8 - \kappa}{\kappa} \tag{1.1}$$

(see Appendix A), and we are interested in the limit[3]

$$C^{(N)}_{(\mathbb{H};0,\infty)}(y_1, y_2, \ldots, y_N) = \lim_{\varepsilon_1,\ldots,\varepsilon_N \searrow 0} \frac{1}{\varepsilon_1^h \ldots \varepsilon_N^h} \mathsf{P}[\gamma \cap B_{\varepsilon_j}(y_j) \neq \emptyset \quad \text{for } j = 1, 2, \ldots, N] \tag{1.2}$$

of probabilities of events illustrated schematically in Fig. 2. In the spirit of [1,33,35,36,39,40], it is appropriate to call the limit (1.2) an SLE boundary Green's function. We emphasize that one could in principle choose to define a boundary visit of SLE differently, for example, for $\kappa > 4$ one could ask the curve γ to touch a boundary segment of length ε, or one could choose the neighborhood shape to be something other than a half-disk. Yet, independently of the precise formulation, the limit remains universal apart from a multiplicative constant which depends on the details of the chosen formulation.[4] Different formulations and universality will be discussed in Sect. 5.

Recalling that γ is an oriented curve, we may even specify the order of the boundary visits, i.e., require that the curve γ first reaches the chosen small neighborhood of y_1, then the neighborhood of y_2 and so on until reaching

[3] The existence of the limit has been proved in [34].

[4] Compare also with the proof [35] that the SLE Green's function defined using conformal radius differs by a multiplicative constant (whose explicit value is not known) from the SLE Green's function defined using Euclidean distance.

the neighborhood of y_N. The order refinement of the SLE boundary Green's function is the limit

$$P^{(N)}_{(\mathbb{H};0,\infty)}(y_1, y_2, \ldots, y_N) = \lim_{\varepsilon_1,\ldots,\varepsilon_N \searrow 0} \frac{1}{\varepsilon_1^h \ldots \varepsilon_N^h} \mathsf{P}[\tau_{y_1;\varepsilon_1} < \tau_{y_2;\varepsilon_2} < \cdots < \tau_{y_N;\varepsilon_N} < \infty], \quad (1.3)$$

where any increasing parametrization $t \mapsto \gamma_t$ of the curve γ is chosen, and we denote by

$$\tau_{y_j;\varepsilon_j} = \inf\{t \geq 0 | \gamma_t \in B_{\varepsilon_j}(y_j)\} \quad (1.4)$$

the stopping time at which the curve γ first reaches the ε_j-neighborhood of y_j. Obviously one can recover the complete correlation function $C^{(N)}_{(\mathbb{H};0,\infty)}$ from the ordered ones $P^{(N)}_{(\mathbb{H};0,\infty)}$ by summing over all possible orders of visits[5]

$$C^{(N)}_{(\mathbb{H};0,\infty)}(y_1, y_2, \ldots, y_N) = \sum_{\sigma \in \mathfrak{S}_N} P^{(N)}_{(\mathbb{H};0,\infty)}(y_{\sigma(1)}, y_{\sigma(2)}, \ldots, y_{\sigma(N)}).$$

In the general form with the order of visits specified, the question of finding the asymptotic amplitudes of the visiting probabilities of chordal SLE_κ was posed in [5], where these quantities were called "(boundary) zig-zag probabilities".

Depending on the details of the precise formulation of the boundary visit question, one would obtain a different non-universal multiplicative constant in the SLE boundary Green's function (1.2) and its order refinement (1.3). We, therefore, prefer to use a generic notation for a quantity of this type, for which we are free to choose a more convenient multiplicative normalization. We also prefer to make explicit the dependence of the question on the starting point $x \in \mathbb{R}$ of the chordal SLE_κ curve, but the end point of the curve will always be kept at infinity. In the rest of this article,

$$\zeta^{(N)}(x; y_1, y_2, \ldots, y_N)$$

denotes a *(boundary) zig-zag amplitude*, which is proportional to any of the interpretations (see Sects. 5.3, 5.4) of the order refined boundary visit question. In particular, we have

$$P^{(N)}_{(\mathbb{H};0,\infty)}(y_1, y_2, \ldots, y_N) = \text{const.} \times \zeta^{(N)}(0; y_1, y_2, \ldots, y_N).$$

Similarly, we denote by

$$\chi^{(N)}(x; y_1, y_2, \ldots, y_N)$$

a *complete (boundary) correlation function*, so that in particular

$$C^{(N)}_{(\mathbb{H};0,\infty)}(y_1, y_2, \ldots, y_N) = \text{const.} \times \chi^{(N)}(0; y_1, y_2, \ldots, y_N),$$

with the same proportionality constant.

[5] In fact in the sum we only need those permutations which respect the order of positive y_j's and reverse the order of negative y_j's; otherwise, the curve essentially disconnects its future passage to a point that it would need to visit later. This will be discussed in some more detail in Sect. 2.2.

Explicit formulas for the above types of quantities are known in the following two special cases:

- The one-point function ($N = 1$) behaves simply as a power law, as follows immediately from the invariance under dilatations $z \mapsto \lambda z$ ($\lambda > 0$) of the chordal SLE_κ in $(\mathbb{H}; 0, \infty)$

$$\zeta^{(1)}(x; y_1) = \chi^{(1)}(x; y_1) \propto |y_1 - x|^{-h} = |y_1 - x|^{1-\frac{8}{\kappa}}. \tag{1.5}$$

- The two-point function when y_1 and y_2 are on the same side of the starting point (either $x < y_1 < y_2$ or $y_2 < y_1 < x$) is given by a hypergeometric function [51] (see also [5])

$$\begin{aligned}\zeta^{(2)}(x; y_1, y_2) &= \chi^{(2)}(x; y_1, y_2) \\ &\propto |y_1 - x|^{1-\frac{8}{\kappa}} |y_2 - y_1|^{1-\frac{8}{\kappa}} \times {}_2F_1\left(\frac{4}{\kappa}, \frac{\kappa - 8}{\kappa}; \frac{8}{\kappa}; \frac{y_2 - y_1}{y_2 - x}\right).\end{aligned} \tag{1.6}$$

In this article we present a method for finding the solutions in the general case. We write down a system of partial differential equations (PDEs) motivated by conformal field theory (CFT) for the quantities of interest, $\zeta^{(N)}$ and $\chi^{(N)}$. Our solutions for them are written in terms of Coulomb gas integrals (Dotsenko–Fateev integrals [17]) and are found by quantum group calculations. This technique is developed in the present article and in [30]; we call it the spin chain–Coulomb gas correspondence. Our primary goal here is to find the explicit formulas and show their wide applicability: the functions $\zeta^{(N)}$ and $\chi^{(N)}$ answer various formulations of boundary visit questions for SLEs as well as for interfaces in lattice models. We also compare the results to numerical simulations of various lattice models and outline a strategy of proof that our formulas give the (order refined) SLE boundary Green's functions.

We emphasize that it is very rarely possible to find the exact solution for an SLE problem involving a large number of marked points—the few existing solutions to such problems rely on finding tricks that appear particular to each problem [1,11,22,23,25,26,43,44,52].[6] The key technique that enables us to find the exact solution here is the spin chain–Coulomb gas correspondence. It provides a systematic method to solve a quite general class of SLE problems.

[6] In contrast, it is almost routine to answer chordal SLE questions which involve only two boundary points or one bulk point in addition to the starting point and end point of the curve. This is so essentially because the three-dimensional group of conformal automorphisms of the domain allows to reduce the problem with four real variables to just one cross ratio, and a standard application of Itô calculus yields a second-order linear ordinary differential equation for the quantity in question. Boundary conditions then pin down the correct answer in the two-dimensional space of solutions. For example, the known formulas (1.5) and (1.6) were found by such methods. For questions depending on a larger number of points, such as the one studied in this article, instead of ordinary differential equations one would need to solve partial differential equations, and the spaces of solutions become substantially harder to manage.

1.3. Organization of the Article

The rest of the article is organized as follows:

In Sect. 2 we formulate the PDE problem which we solve in the subsequent sections to find the zig-zag amplitudes $\zeta^{(N)}$ and the complete correlation functions $\chi^{(N)}$:

- The functions $\zeta^{(N)}$ and $\chi^{(N)}$ are conformally covariant.
- The functions $\zeta^{(N)}$ and $\chi^{(N)}$ satisfy a second order PDE and N third-order PDEs.
- The boundary conditions depend on the order of visits: they are written in terms of asymptotic behaviors of $\zeta^{(N)}$ and their inhomogeneous terms involve the $\zeta^{(N-1)}$ in a recursive manner.

In Sect. 3 we discuss the spin chain–Coulomb gas correspondence, by which the PDE problem is translated to a linear problem in representations of a quantum group:

- We associate functions defined by Coulomb gas integrals to vectors in a finite-dimensional tensor product representation of the quantum group $\mathcal{U}_q(\mathfrak{sl}_2)$.
- The functions associated with highest weight vectors are solutions to the partial differential equations of Sect. 2, and for particular highest weights they also have the correct conformal covariance.
- Projections to subrepresentations in consecutive tensorands determine the asymptotic behaviors of the functions.
- There are unique highest weight vectors of the correct highest weights whose subrepresentation projections correspond to the boundary conditions imposed on the zig-zag amplitudes $\zeta^{(N)}$.

In Sect. 4 the integrals obtained in the spin chain–Coulomb gas correspondence are rewritten as regularized real integrals. The transformation to real integrals concretely exhibits the needed closed homology properties of our solutions.

In Sect. 5 we discuss basic properties, applications, interpretations, and universality of the SLE boundary visit question and outline a strategy of proof.

In Sect. 6, we compare our formula numerically to simulations of lattice models of statistical mechanics. We study random interfaces in percolation, random cluster model, and loop-erased random walk. We perform computer simulations of them and collect frequencies of multi-point boundary visits of the interfaces, and compare renormalized frequencies to the zig-zag amplitudes $\zeta^{(N)}$.

We conclude the article by discussion and outlook in Sect. 7.

The article is complemented with several appendices. Appendix A provides two derivations of the value of the scaling exponent (1.1), and a derivation of the second-order PDE. Appendix B contains relevant background on conformal field theory. Our normalization conventions for some quantum group representations and some explicit four-point solutions are contained in Appendix C. Numerical evaluation of the integrals of Sects. 3 and 4 is treated in Appendix D.

2. The Problem: Partial Differential Equations and Asymptotics

We find the boundary visit amplitudes $\zeta^{(N)}$ and $\chi^{(N)}$ by solving a PDE problem. The system of partial differential equations is given below in Sect. 2.1. This part is the same for $\chi^{(N)}$ and for $\zeta^{(N)}$, and moreover the system is the same for all boundary zig-zag amplitudes corresponding to different orders of visits to the same set of points. The results will be different, however, as each of the functions satisfies different boundary conditions, detailed in Sect. 2.2.

2.1. Differential Equations for Boundary Visit Amplitudes

The linear homogeneous system of PDEs below contains essentially three different types of partial differential equations—all of them can be argued to hold by conformal field theory (see Appendix B.2), but from the point of view of SLE analysis, the argument leading to each of them is different. For $\zeta^{(N)}$ the system reads

$$\left[\frac{\partial}{\partial x}+\sum_{j=1}^{N}\frac{\partial}{\partial y_j}\right]\zeta^{(N)}(x;y_1,\ldots,y_N)=0 \tag{2.1}$$

$$\left[x\frac{\partial}{\partial x}+\sum_{j=1}^{N}y_j\frac{\partial}{\partial y_j}-Nh\right]\zeta^{(N)}(x;y_1,\ldots,y_N)=0 \tag{2.2}$$

$$\left[\frac{\partial^2}{\partial x^2}-\frac{4}{\kappa}\mathcal{L}_{-2}\right]\zeta^{(N)}(x;y_1,\ldots,y_N)=0 \tag{2.3}$$

$$\left[\frac{\partial^3}{\partial y_j^3}-\frac{16}{\kappa}\mathcal{L}_{-2}^{(j)}\frac{\partial}{\partial y_j}+\frac{8(8-\kappa)}{\kappa^2}\mathcal{L}_{-3}^{(j)}\right]\zeta^{(N)}(x;y_1,\ldots,y_N)=0 \quad (j=1,2,\ldots,N), \tag{2.4}$$

where

$$\mathcal{L}_{-2}=\sum_{k=1}^{N}\left(\frac{-1}{y_k-x}\frac{\partial}{\partial y_k}+\frac{h}{(y_k-y_j)^2}\right)$$

and

$$\mathcal{L}_{-n}^{(j)}=\frac{-1}{(x-y_j)^{n-1}}\frac{\partial}{\partial x}+\frac{(n-1)\delta}{(x-y_j)^n}+\sum_{k\neq j}\left(\frac{-1}{(y_k-y_j)^{n-1}}\frac{\partial}{\partial y_k}+\frac{(n-1)h}{(y_k-y_j)^n}\right),$$

and we have used the parameters $h=\frac{8-\kappa}{\kappa}$ and $\delta=\frac{6-\kappa}{2\kappa}$.

The first-order PDEs (2.1) and (2.2) express the translation invariance and homogeneity of the amplitudes. More general conformal covariance of the answer will be discussed in Sect. 5.2 and again from a conformal field theory point of view in Appendix B.1. The second order PDE (2.3) can be interpreted either in terms of the SLE process as the statement of a local martingale property of the answer, see Appendix A.3, or in terms of conformal field theory as a conformal Ward identity associated with a second-order degeneracy of the

boundary field located at x, as will be discussed in Appendix B.2. The N third-order PDEs (2.4) are similarly the conformal Ward identities associated with third-order degeneracies of the boundary fields located at y_j, $j = 1, 2, \ldots, N$, see Appendix B.2. Unlike for the first- and second-order equations we do not know how to explain the third-order equations by SLE analysis directly. As a partial justification, however, we note that Eq. (2.4) coincide with the third-order partial differential equations [19] derived by Dubédat for limiting cases of multiple SLE partition functions, which morally describe the same configurations of curves as our boundary visiting SLEs. Ultimately, the validity of all of the above equations for the SLE boundary visit amplitudes would need to be established by first finding the explicit answer, which is the main task in the present article, and then proving that it gives the SLE boundary Green's function following the strategy that will be outlined in Sect. 5.4.3.[7]

2.2. Asymptotics for Boundary Visit Amplitudes

The system of differential equations of Sect. 2.1 has a large space of solutions. To pin down the correct solution we need boundary conditions, which will be specified in the form of asymptotic behavior of the boundary zig-zag amplitudes. Considerations of the possible asymptotics allowed by conformal field theory can be found in Appendix B.3. The particular requirements that finally specify the solutions are given below.

Consider the question of visiting the neighborhoods of $y_1, y_2, \ldots, y_N$ in this order. Some notation and terminology is needed to conveniently describe the specific asymptotics of $\zeta^{(N)}$ in this case. We say that points y_j such that $y_j < x$ are *on the left* and points y_j such that $x < y_j$ are *on the right*. We say that the points are in an *outwards increasing order* if for any y_j, y_k on the left we have that $j < k$ implies $y_k < y_j$ and for any y_j, y_k on the right we have that $j < k$ implies $y_j < y_k$: in other words, that among points on the same side, the point further away from starting point is visited later.

The boundary visit amplitude vanishes unless the points are in an outwards increasing order—a visit to a small neighborhood of a point further away on the same side almost disconnects the future passage of the curve to the point that would need to be visited later.[8]

It is convenient to use a separate ordering for the points on the left and right. Denote, therefore, $y_1^-, \ldots, y_L^-$ the points on the left in a decreasing order (in the order of visits) and $y_1^+, \ldots, y_R^+$ the points on the right in an increasing

[7] Given that this proposed route to Eq. (2.4) is somewhat indirect, one may wonder if more direct hints of these third-order differential equations exist. To this end, recall that for $N = 1$ and $N = 2$ the explicit zig-zag amplitudes (1.5) and (1.6) can in any case be found by routine SLE calculations. For these already known functions $\zeta^{(1)}$ and $\zeta^{(2)}$, we have by direct calculation verified the validity of the third-order equations, which conformal field theory predicts.

[8] For positive ε it is in principle possible for visits to occur in an order that is not outwards increasing, but these probabilities are suppressed by a higher power of ε, and as such do not survive the limit (1.3) of $\varepsilon \searrow 0$. Rigorous estimates of the appropriate SLE probabilities are of the type considered, e.g., in [10,39], although the present situation is somewhat easier.

order (in the order of visits). The following notation makes the arguments of the zig-zag amplitude appear in the same order as they are on the real axis:

$$\zeta_\omega(y_L^-,\dots,y_1^-;x;y_1^+,\dots,y_R^+)=\zeta^{(N)}(x;y_1,y_2,\dots,y_N),$$

where $\omega=(\omega_1,\omega_2,\dots,\omega_N)\in\{+,-\}^N$ is a sequence of "±"-symbols specifying the sequence of sides of the visits in the sense that $\omega_j=-$ (resp. $\omega_j=+$) if y_j is on the left (resp. on the right). If we fix the number L of points on the left and the number R of points on the right, $N=L+R$, then the number of different outwards increasing orders is $\binom{N}{L}$, corresponding to the choices of $\omega\in\{+,-\}^N$ with L "−"-symbols and R "+"-symbols. The complete correlation function $\chi^{(N)}$ is the sum of these $\binom{N}{L}$ zig-zag amplitudes. In the particular case when all the points are on the same side, the complete correlation function coincides with the zig-zag amplitude.

The specific asymptotics depend on the order of visits, and to describe them we need a few separate cases. We call the consecutive points $y_m^\pm$ and $y_{m+1}^\pm$ on the same side (±) *successively visited points on the same side* if for some j we have $y_m^\pm=y_j$ and $y_{m+1}^\pm=y_{j+1}$.

We claim that for any outwards increasing order ω the boundary zig-zag amplitude ζ_ω satisfies the asymptotics conditions given below,[9] and that up to a multiplicative constant these asymptotics determine all $\zeta^{(N)}$. The conditions are intuitive in view of the possibilities listed in Appendix B.3: they state that the order of magnitude of the amplitude is larger if successively visited points are close and smaller if non-successively visited points are close, and in the former case the leading asymptotic is proportional to an $(N-1)$-point function, where the two close-by points are replaced by a single point. Moreover, they state that the leading behavior when successively visited points are close-by is given by the $(N-1)$-point function with the two close-by points replaced by just one.

- *Asymptotics for successively visited points* If y_j and y_{j+1} are successively visited points on the same side, then

$$\lim_{y_j,y_{j+1}\to y'}\frac{1}{|y_{j+1}-y_j|^{1-\frac{8}{\kappa}}}\zeta^{(N)}(x;\,y_1,\dots,y_j,y_{j+1},\dots,y_N)$$
$$=\text{const.}\times\zeta^{(N-1)}(x;\,y_1,\dots,y_{j-1},y',y_{j+2},y_{j+3},\dots,y_N). \tag{2.5}$$

- *Asymptotics for non-successively visited points* If y_j and y_k are non-successively visited consecutive points on the same side, then

$$\lim_{y_j,y_k\to y'}\frac{1}{|y_k-y_j|^{1-\frac{8}{\kappa}}}\zeta^{(N)}(x;\,y_1,y_2,\dots,y_N)=0. \tag{2.6}$$

[9] The eventual justification of these requirements would be a proof of the fact that the SLE boundary Green's function agrees with our formula obtained by solving the PDE system with these conditions. A strategy of proof is discussed in Sect. 5.4.3.

- *Asymptotics for the first points on the left and right* For the first point y_1 to be visited we have

$$\lim_{x,y_1\to x'} \frac{1}{|y_1-x|^{1-\frac{8}{\kappa}}}\zeta^{(N)}(x;\, y_1,y_2,\ldots,y_N) = \text{const.}\times\zeta^{(N-1)}(x';\, y_2,y_3,\ldots,y_N). \tag{2.7}$$

For the first point on the opposite side, i.e., for $y_1^{\pm}\neq y_1$, we have

$$\lim_{x,y_1^{\pm}\to x'} \frac{1}{|y_1^{\pm}-x|^{1-\frac{8}{\kappa}}}\zeta^{(N)}(x;\, y_1,y_2,\ldots,y_N) = 0. \tag{2.8}$$

The constants in (2.5) and (2.7) are different, but for different pairs of successively visited consecutive points, the constant in (2.5) should be the same.[10] Moreover, the constants should not depend on N.

We conjecture that the solution space to the partial differential Eqs. (2.1)–(2.4) is finite-dimensional and that its dimension is exactly the multiplicity m_N of a certain irreducible direct summand in a tensor product, see Sect. 3.5.5. Under this assumption, it could be shown with the techniques introduced in Sect. 3, that recursively in N the asymptotics conditions (2.5)–(2.8) specify uniquely, up to a multiplicative constant, solutions for all outwards increasing orders of visits ω.

Our choice of normalization of $\zeta^{(N)}$ and $\chi^{(N)}$ will be determined recursively by fixing the constant appearing in Eq. (2.7), see Sect. 3.4. Once this natural choice is made, the different N-point functions ζ_ω obtain correct relative normalizations, with the universal ratios referred to in Sect. 5.4. In particular, the constant appearing in Eq. (2.5) gets automatically fixed as well.

3. Quantum Group and Integral Formulas

3.1. Coulomb Gas Integrals

The main tool that allows us to solve the PDE problem of Sect. 2 and, therefore, to find the explicit formula for the SLE boundary visit amplitudes is the spin chain–Coulomb gas correspondence. In this article, for the sake of concreteness, we describe only the case relevant to the problem of boundary visit amplitudes—a more general treatment can be found in [30].

3.1.1. Standard Coulomb Gas Integrals and Their Properties. The Coulomb gas formalism of conformal field theory, or Dotsenko–Fateev integrals [17], is a way of producing solutions to systems of differential equations of the type of Sect. 2.1 by integrating an auxiliary function, which in our case takes the following form:

[10] As a remark, we have not found any new solutions by relaxing the requirement that the constants for different pairs are equal—even with unspecified constants treated as additional variables, the system of equations forces the correct universal ratios between the constants, at least for small N.

$$f_\ell^{(N)}(x;\ y_1, y_2, \dots, y_N;\ w_1, w_2, \dots, w_\ell)$$
$$= \prod_{j=1}^{N} (y_j - x)^{\frac{4}{\kappa}} \times \prod_{1\le j<k\le N} (y_k - y_j)^{\frac{8}{\kappa}} \times \prod_{s=1}^{\ell} (w_s - x)^{-\frac{4}{\kappa}}$$
$$\times \prod_{j=1}^{N}\prod_{s=1}^{\ell} (w_s - y_j)^{-\frac{8}{\kappa}} \times \prod_{1\le s<r\le \ell} (w_r - w_s)^{\frac{8}{\kappa}}. \tag{3.1}$$

Consider the function

$$F(x; y_1, \dots, y_N) = \int_\Gamma f_\ell^{(N)}(x;\ y_1, \dots, y_N; w_1, \dots, w_\ell)\, \mathrm{d}w_1 \cdots \mathrm{d}w_\ell, \tag{3.2}$$

where Γ is a closed ℓ-surface avoiding the points $x, y_1, \dots, y_N$. The integral of course only depends on the homotopy type of the surface Γ. The function is defined such that while the contour Γ of the w-variables may depend on the positions of $x, y_1, \dots, y_N$, the choice is locally constant. One then observes the following:

- *Translation invariance* F satisfies Eq. (2.1).
- *Scale covariance* F is homogeneous of degree $\Delta_{N;\ell} = \ell + \frac{4}{\kappa}(N^2 + \ell^2 - 2\ell - 2N\ell)$, and in particular if $\ell = N$ it satisfies Eq. (2.2).
- *Second-order differential equation* F satisfies Eq. (2.3).
- *Third-order differential equations* F satisfies Eq. (2.4).

The translation invariance follows immediately from the translation invariance of the integrand $f_\ell^{(N)}$ by considering a shift of the variables $x, y_1, \dots, y_N$ small enough so that the integration contour Γ can be kept constant, and then the same shift of the integration contour, which now does not change the homotopy type. The scaling covariance is shown similarly, starting with scaling close enough to identity. The relevant scaling covariance of the integrand reads

$$f_\ell^{(N)}(\lambda x; \lambda y_1, \dots; \lambda w_1, \dots) = \lambda^{\frac{4}{\kappa}(N^2+\ell^2-2\ell-2N\ell)}\ f_\ell^{(N)}(x; y_1, \dots; w_1, \dots)$$

and an extra factor λ^ℓ comes from the change of variables in the integration—the formal proofs can be found in [30, Lemma 3.3, Theorem 4.17].

The second- and third-order differential equations rely more crucially on the fact that the integration surface Γ is closed. One again starts from a property satisfied by the integrand alone. Starting from the second-order equation, let

$$\mathcal{D}_{1,2} = \frac{\kappa}{2}\frac{\partial^2}{\partial x^2} + \sum_{j=1}^{N}\left(\frac{2}{y_j - x}\frac{\partial}{\partial y_j} - \frac{2h}{(y_j - x)^2}\right)$$

be the differential operator we want to show annihilates F. It is a matter of straightforward verification to see that the integrand satisfies

$$\left[\mathcal{D}_{1,2} + \sum_{s=1}^{\ell}\left(\frac{2}{w_s - x}\frac{\partial}{\partial w_s} - \frac{2}{(w_s - x)^2}\right)\right] f_\ell^{(N)}(x; y_1, \dots; w_1, \dots) = 0$$

and to notice that this can also be read as

$$\mathcal{D}_{1,2}\, f_\ell^{(N)}(x; y_1, \ldots; w_1, \ldots) = -2 \sum_{s=1}^{\ell} \frac{\partial}{\partial w_s} \left(\frac{1}{w_s - x} \times f_\ell^{(N)}(x; y_1, \ldots; w_1, \ldots) \right).$$

Thus when acting on F by the differential operator $\mathcal{D}_{1,2}$, we may take the operator inside the integral and rewrite the integrand as a sum of total derivatives. The integral of these vanish because the contour was assumed to be closed. Hence one gets the second-order differential equation for F. The third-order differential equations are shown to hold similarly—the formal proof of a more general statement can be found in [30, Proposition 4.12, Theorem 4.17].

3.1.2. Spin Chain–Coulomb Gas Basis Functions. Our solution will eventually be of the form (3.2), with $\ell = N$. As in [30,31], we need to unveil an underlying quantum group structure, which will be useful for calculations, and in particular crucial for dealing with the asymptotics. For this purpose, we introduce the functions

$$\varphi_{t_L^-,\ldots,t_2^-,t_1^-;d;t_1^+,t_2^+,\ldots,t_R^+}(y_L^-, \ldots, y_2^-, y_1^-; x; y_1^+, y_2^+, \ldots, y_R^+)$$

indexed by $t_j^\pm \in \{0,1,2\}$ and $d \in \{0,1\}$, which are defined by the integrals

$$\varphi_{t_L^-,\ldots,t_R^+}(y_L^-, \ldots, y_R^+) = \int_{\Gamma_{t_L^-,\ldots,t_R^+}} f^{\ni}_{t_L^-,\ldots,t_R^+}(y_L^-, \ldots, y_R^+; w_1, \ldots, w_\ell)\, \mathrm{d}w_1 \cdots \mathrm{d}w_\ell, \tag{3.3}$$

where:

- The integration surface $\Gamma_{t_L^-,\ldots,t_2^-,t_1^-;d;t_1^+,t_2^+,\ldots,t_R^+}$ is shown in Fig. 3. The dimension of the integration surface, i.e., the number of integration variables w_s, is $\ell = d + \sum_{j=1}^{L} t_j^- + \sum_{j=1}^{R} t_j^+$. In the functions appearing in our final answer this will always be $\ell = N$. The contour of each integration variable w_s is a loop based at an anchor point z_0 to the left of all of the variables, and the loop encircles one of the points in the positive direction. The loops of the first t_L^- variables encircle the point y_L^-, the next t_{L-1}^- variables encircle the point y_{L-1}^- and so on. The loops encircling the same point are nested. The loops encircling different points avoid each other so that the contours to a point further on the right go below.
- The integrand $f^{\ni}_{t_L^-,\ldots,t_1^-;d;t_1^+,\ldots,t_R^+}$ is a rephased branch of the integrand $f_\ell^{(N)}$ defined in Eq. (3.1): we multiply by a suitable complex number of modulus one to make $f^{\ni}_{t_L^-,\ldots,t_R^+}$ real and positive at the point where each of the integration variables is on the real axis to the right of the point it encircles, see Fig. 3.

We make the following remarks about the role and properties of the above functions:

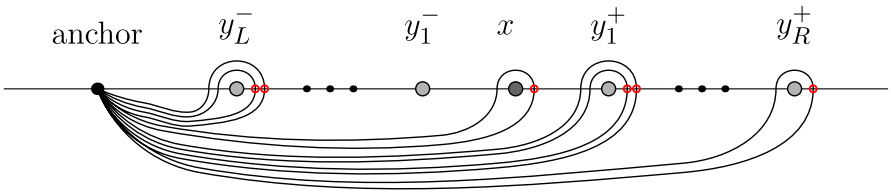

FIGURE 3. The integration contours of the w_j-variables in $\Gamma_{t_L^-,\ldots,t_2^-,t_1^-;d;t_1^+,t_2^+,\ldots,t_R^+}$ and the point (marked by *red circles*) where the integrand $f^{\Subset}$ is rephased to be positive (color figure online)

- Individually the surfaces $\Gamma_{t_L^-,\ldots,t_R^+}$ are not closed, but our solution will be a linear combination which is closed in the appropriate homology [24].
- The individual functions $\varphi_{t_L^-,\ldots,t_R^+}$ depend also on the point z_0 where the loops in $\Gamma_{t_L^-,\ldots,t_R^+}$ are anchored. This dependence will cancel in the final answer—the cancellation will be shown concretely in Sect. 4, and a proof of this property in a general setup is given in [30, Proposition 4.5, Theorem 4.17].

In the spin chain–Coulomb gas correspondence defined in Sect. 3.3.1, we will make basis vectors in a quantum group representation correspond to the functions $\varphi_{t_L^-,\ldots,t_2^-,t_1^-;d;t_1^+,t_2^+,\ldots,t_R^+}$. In Sects. 3.3.2 and 3.3.3 we explain how straightforward quantum group calculations will allow us to decide about the asymptotics of the functions as well as the closedness of the surfaces in an appropriate homology—see also [24,30].

3.2. Quantum Group

We need to recall some facts and fix some notation for the quantum group $\mathcal{U}_q(\mathfrak{sl}_2)$. It should be thought of as a deformation of (the universal enveloping algebra of) the Lie algebra $\mathfrak{sl}_2$, with a deformation parameter q—with a suitable normalization when $q \to 1$ one recovers $\mathfrak{sl}_2$ from the definitions we give below.

We let $q = e^{4\pi \mathrm{i}/\kappa}$, and assume that κ is generic in the sense that $\kappa \notin \mathbb{Q}$.[11] We define the q-integers $[m]$ (for $m \in \mathbb{Z}$)

$$[m] := \frac{q^m - q^{-m}}{q - q^{-1}}.$$

Since we assume $\kappa \notin \mathbb{Q}$, all q-integers $[m]$ with $m \neq 0$ are non-zero.

[11] For irrational κ the parameter q is not a root of unity, and the representation theory of the quantum group is semisimple. To obtain the SLE boundary visit amplitudes in general, we may in the end use continuity in the parameter κ.

3.2.1. Definition of the Quantum Group. The quantum group $\mathcal{U}_q(\mathfrak{sl}_2)$ is the algebra over $\mathbb{C}$ with generators E, F, K, K^{-1} and relations

$$KK^{-1} = 1 = K^{-1}K, \quad KE = q^2 EK, \quad KF = q^{-2} FK,$$
$$EF - FE = \frac{1}{q - q^{-1}} \left(K - K^{-1}\right).$$

Moreover, $\mathcal{U}_q(\mathfrak{sl}_2)$ is equipped with the unique Hopf algebra structure such that the coproducts of the generators are

$$\Delta(K) = K \otimes K, \quad \Delta(E) = E \otimes K + 1 \otimes E, \quad \Delta(F) = F \otimes 1 + K^{-1} \otimes F.$$

The coproduct Δ determines the action of the quantum group in tensor product $M \otimes M'$ of two representations M and M', for example, $E.(v \otimes v') = E.v \otimes K.v' + v \otimes E.v'$. The tensor product of representations is then associative but not commutative: multiple tensor products are well defined, for example $(M \otimes M') \otimes M'' \cong M \otimes (M' \otimes M'')$, but the order of the tensorands is important.

3.2.2. Representations of the Quantum Group. The quantum group $\mathcal{U}_q(\mathfrak{sl}_2)$ is semisimple (for q not a root of unity) in the sense that any finite-dimensional representation is the direct sum of its irreducible subrepresentations. In fact, the representation theory essentially just deforms that of $\mathfrak{sl}_2$. We recall the following standard facts, the proofs of which can be found in, e.g., [30, Lemmas 2.3, 2.4]:

For any $d \in \mathbb{N}$, there exists a d-dimensional irreducible representation M_d with a basis $e_0, e_1, e_2, \ldots, e_{d-1}$ such that the action of the generators on the basis vectors is given by

$$\begin{aligned} K.e_j &= q^{d-1-2j}\, e_j \\ F.e_j &= e_{j+1} \quad \text{(with interpretation } e_d = 0\text{)} \\ E.e_j &= [j]\,[d-j]\, e_{j-1} \quad \text{(with interpretation } e_{-1} = 0\text{)} \end{aligned} \qquad .$$

This representation M_d is the appropriate deformation of the d-dimensional irreducible representation of $\mathfrak{sl}_2$ ("the spin-$\frac{d-1}{2}$ representation"). The tensor products of M_d decompose according to the following formula:

$$M_{d_2} \otimes M_{d_1} \cong M_{d_1+d_2-1} \oplus M_{d_1+d_2-3} \oplus \cdots \oplus M_{|d_1-d_2|+1}.$$

Our calculations will require some specific cases of such (quantum) Clebsch-Gordan decompositions to be made explicit. Formulas for those cases are given in Appendix C.1.

The one-dimensional irreducible $M_1 \cong \mathbb{C}$ is the *trivial representation*; it acts as a neutral element of the tensor products: for any representation M we have the isomorphisms $M_1 \otimes M \cong M \cong M \otimes M_1$. This allows us to omit M_1 in tensor products, when needed.

3.3. Spin Chain–Coulomb Gas Correspondence

3.3.1. Definition of the Correspondence. With the above preparations we can now define the correspondence. The spin chain–Coulomb gas correspondence linearly associates with vectors

$$v \in M_3^{\otimes R} \otimes M_2 \otimes M_3^{\otimes L}$$

in a tensor product of representations of $\mathcal{U}_q(\mathfrak{sl}_2)$ a function so that for the natural tensor product basis vectors the associated functions are those defined in Sect. 3.1.2:

$$e_{t_R^+} \otimes \cdots \otimes e_{t_1^+} \otimes e_d \otimes e_{t_1^-} \otimes \cdots \otimes e_{t_L^-} \;\mapsto\; \varphi_{t_L^-,\ldots,t_1^-;d;t_1^+,\ldots,t_R^+}.$$

Note that in our convention, the order of the variables of the function is the reverse of the order of the corresponding factors in the tensor product.

3.3.2. Asymptotics Via the Correspondence. A key property of the spin chain–Coulomb gas correspondence is that the asymptotics of the functions can be straightforwardly read from the projections to subrepresentations of the corresponding vectors in $M_3^{\otimes R} \otimes M_2 \otimes M_3^{\otimes L}$. For these projections, we use below the notation and normalization conventions of Appendix C.1.

Let $v \in M_3^{\otimes R} \otimes M_2 \otimes M_3^{\otimes L}$ and let φ be the function associated with v by the correspondence of Sect. 3.3.1. The correspondence of asymptotics and subrepresentations is stated precisely in the following:

- Consider two consecutive points $y_m^\pm, y_{m+1}^\pm$ on the right or left (superscript "+" or "−", respectively). For $d \in \{1,3,5\}$, denote accordingly by $\pi_{\pm;m}^{(d)}$ the projection to d-dimensional subrepresentation of $M_3 \otimes M_3$ acting on the m:th and $m+1$:st components on the appropriate side.
  - Suppose that v is in the singlet of the components corresponding to $y_m^\pm, y_{m+1}^\pm$, that is $v = \pi_{\pm;m}^{(1)}(v)$. Then as $y_m^\pm, y_{m+1}^\pm \to y'$, we have

    $$\varphi(x; y_1, \ldots, y_N) \sim B_1 \times |y_{m+1}^\pm - y_m^\pm|^{2-\frac{16}{\kappa}} \times \varphi^{(1)}(x; y_1, \ldots, y_N),$$

    where the variables $y_m^\pm, y_{m+1}^\pm$ have been removed from the right-hand side, the function $\varphi^{(1)}$ is the function of two variables less associated with the vector $\hat{\pi}_{\pm;m}^{(1)}(v)$ interpreted as a vector in either $M_3^{\otimes(R-2)} \otimes M_2 \otimes M_3^{\otimes L}$ or $M_3^{\otimes R} \otimes M_2 \otimes M_3^{\otimes(L-2)}$, and the constant is the generalized beta-function

    $$B_1 = \frac{\Gamma(\frac{\kappa-8}{\kappa})^2\,\Gamma(\frac{\kappa-4}{\kappa})^2\,\Gamma(\frac{\kappa+8}{\kappa})}{2\,\Gamma(2-\frac{8}{\kappa})\,\Gamma(2\frac{\kappa-6}{\kappa})\,\Gamma(\frac{\kappa+4}{\kappa})}.$$

  - Suppose that v is in the triplet of the components corresponding to $y_m^\pm, y_{m+1}^\pm$, that is, $v = \pi_{\pm;m}^{(3)}(v)$. Then as $y_m^\pm, y_{m+1}^\pm \to y'$, we have

    $$\varphi(x; y_1, \ldots, y_N) \sim B_3 \times |y_{m+1}^\pm - y_m^\pm|^{1-\frac{8}{\kappa}} \times \varphi^{(3)}(x; y_1, \ldots, y', \ldots, y_N),$$

    where on the right-hand side the two variables $y_m^\pm, y_{m+1}^\pm$ have been removed and replaced by one y', the function $\varphi^{(3)}$ is the function of one variable less associated with the vector $\hat{\pi}_{\pm;m}^{(3)}(v)$ interpreted as a vector in

either $M_3^{\otimes(R-1)} \otimes M_2 \otimes M_3^{\otimes L}$ or $M_3^{\otimes R} \otimes M_2 \otimes M_3^{\otimes(L-1)}$ and the constant is the beta-function

$$B_3 = \frac{\Gamma(\frac{\kappa-8}{\kappa})^2}{\Gamma(2\frac{\kappa-8}{\kappa})}.$$

– Suppose that v is in the quintuplet of the components corresponding to $y_m^\pm, y_{m+1}^\pm$, that is, $v = \pi^{(5)}_{\pm;m}(v)$. Then as $y_m^\pm, y_{m+1}^\pm \to y'$, we have

$$\varphi(x; y_1, \dots, y_N) \sim |y_{m+1}^\pm - y_m^\pm|^{\frac{8}{\kappa}} \times \varphi^{(5)}(x; y_1, \dots, y', \dots, y_N),$$

where on the right-hand side the two variables $y_m^\pm, y_{m+1}^\pm$ have been removed and replaced by one y'. We will not need any properties of the function $\varphi^{(5)}$, but we nevertheless remark that with a generalization of the present method it becomes in principle explicit (see [30, Proposition 4.4] for details).

- Consider the point x and the first point $y_1^\pm$ on the right or left (superscript "+" or "−", respectively). For $d \in \{2, 4\}$, denote accordingly by $\pi_\pm^{(d)}$ the projection to d-dimensional subrepresentation of $M_3 \otimes M_2$ or $M_2 \otimes M_3$ acting on the middle factor M_2 and the M_3 on the appropriate side of it.
  – Suppose that v is in the doublet of the components corresponding to $x, y_1^\pm$, that is $v = \pi_\pm^{(2)}(v)$. Then as $x, y_1^\pm \to x'$, we have

$$\varphi(x; y_1, \dots, y_N) \sim B_2 \times |y_1^\pm - x|^{1-\frac{8}{\kappa}} \times \varphi^{(2)}(x'; \dots, y_N),$$

where on the right-hand side the two variables $x, y_1^\pm$ have been removed and replaced by one x', the function $\varphi^{(2)}$ is the function of one variable less associated with the vector $\hat{\pi}_\pm^{(2)}(v)$ interpreted as a vector in either $M_3^{\otimes(R-1)} \otimes M_2 \otimes M_3^{\otimes L}$ or $M_3^{\otimes R} \otimes M_2 \otimes M_3^{\otimes(L-1)}$ and the constant is the beta-function

$$B_2 = \frac{\Gamma(\frac{\kappa-4}{\kappa})\Gamma(\frac{\kappa-8}{\kappa})}{\Gamma(2\frac{\kappa-6}{\kappa})}. \tag{3.4}$$

  – Suppose that v is in the quadruplet of the components corresponding to $x, y_1^\pm$, that is $v = \pi_\pm^{(4)}(v)$. Then as $x, y_1^\pm \to x'$, we have

$$\varphi(x; y_1, \dots, y_N) \sim |y_1^\pm - x|^{\frac{4}{\kappa}} \times \varphi^{(4)}(x'; \dots, y_N),$$

where on the right-hand side the two variables $x, y_1^\pm$ have been removed and replaced by one x'. We will not need any properties of the function $\varphi^{(4)}$, although it could also be written explicitly (see [30, Proposition 4.4] for details).

For a general $v \in M_3^{\otimes R} \otimes M_2 \otimes M_3^{\otimes L}$ the asymptotics of φ are obtained by the above formulas and linearity.

The statements are proved by straightforward manipulations of the integrals, which are done in a more general setup in [30, Lemmas 4.2, 4.3, 3.11, Proposition 4.4]. Indeed, when the vector v is of the supposed form, we know from Appendix C.1 explicitly how its two consecutive tensor components must be related. Considering the different possibilities for $y_m^\pm, y_{m+1}^\pm$, namely $v =$

$\pi^{(5)}_{\pm;m}(v)$, $v = \pi^{(3)}_{\pm;m}(v)$, or $v = \pi^{(1)}_{\pm;m}(v)$, one manages to rearrange zero, one, or two integration variables on contours between the points $y^\pm_m$ and $y^\pm_{m+1}$ so that the contours of the rest of the integration variables remain away from these points. Then extracting the asymptotics becomes easy: first of all, there is a factor $|y^\pm_{m+1} - y^\pm_m|^{\frac{8}{\kappa}}$ in the integrand, and second the integral over the contours between the points $y^\pm_m$ and $y^\pm_{m+1}$ can be rescaled to produce (modulo error terms that can be neglected in the limit $y^\pm_m, y^\pm_{m+1} \to y'$) a generalized beta-function

$$B_1 = \int_0^1 \mathrm{d}w_1 \int_{w_1}^1 \mathrm{d}w_2\, w_1^{-\frac{8}{\kappa}} w_2^{-\frac{8}{\kappa}} (w_2 - w_1)^{\frac{8}{\kappa}} (1 - w_1)^{-\frac{8}{\kappa}} (1 - w_2)^{-\frac{8}{\kappa}} \quad \text{or}$$

$$B_3 = \int_0^1 \mathrm{d}w\, w^{-\frac{8}{\kappa}} (1 - w)^{-\frac{8}{\kappa}} \quad \text{or} \quad B_5 = 1,$$

times a power law $|y^\pm_{m+1} - y^\pm_m|^{\Delta_l}$ with $\Delta_l = l + \frac{8}{\kappa}(\frac{(l-1)l}{2} - 2l)$ according to the number $l = 2, 1, 0$ of integration variables on contours between the points $y^\pm_m$ and $y^\pm_{m+1}$. For the rest of the integrations, we may combine the factors in the integrand containing the variables $y^\pm_m, y^\pm_{m+1}$ or any of the integration variables between them, and we get a function of the same type, with fewer variables. The different possibilities for $x, y^\pm_1$ are treated in an entirely parallel fashion.

The multiplicative constants B_1, B_3, and B_2 appear in the derivation as integrals which are a priori convergent only for $\kappa > 8$. The assertions nevertheless remain true by analytic continuation also in the cases of interest $0 < \kappa < 8$, and we have given the constants B_1, B_3, and B_2 explicitly as generalized beta functions which are well defined, non-zero, and analytic in κ apart from certain rational values of κ.

3.3.3. Highest Weight Vectors and Closed Integration Surfaces. For fundamental properties of the Dotsenko–Fateev functions in Sect. 3.1.1, it was important that the integration surface Γ was closed in an appropriate homology related to the multivalued integrand (3.1), see [24]. Our basis functions $\varphi_{t^-_L,\dots,t^-_1,d,t^+_1,\dots,t^+_R}$ for the spin chain–Coulomb gas correspondence, introduced in Sect. 3.1.2, are obtained by integrals along the contours $\Gamma_{t^-_L,\dots,t^-_1,d,t^+_1,\dots,t^+_R}$ of Fig. 3, which do not constitute a closed surface. Remarkably, however, Felder and Wieczerkowski [24] showed that if the vector v is annihilated by the quantum group generator E, i.e., if v is a sum of highest weight vectors of subrepresentations of $M_3^{\otimes R} \otimes M_2 \otimes M_3^{\otimes L}$, then the homology class of the associated linear combination of $\Gamma_{t^-_L,\dots,t^+_R}$ is closed. Less abstractly, as in [30, Proposition 4.5, Corollary 4.8], this can be viewed as a generalization of the manipulations of the integrals we described in the end of Sect. 3.3.2, and we exhibit this property very concretely by transforming the integrals to integrals along the real axis in Sect. 4.1.

Importantly, if $v \in M_3^{\otimes R} \otimes M_2 \otimes M_3^{\otimes L}$ satisfies $E.v = 0$, then the associated function φ has the following properties:

- The function φ does not depend on the choice of the anchor point z_0 of the contours $\Gamma_{t^-_L,\dots,t^+_R}$.

- The function φ satisfies the second-order differential Eq. (2.3).
- The function φ satisfies the third-order differential Eq. (2.4).

Generalizations and formal proofs are given in [30, Propositions 4.5, 4.12].

3.4. Linear Problem in Quantum Group Representations

Recall that we are looking for solutions to the partial differential Eqs. (2.1)–(2.4), with boundary conditions specified in terms of the asymptotics (2.5)–(2.8). We will produce the solution by the spin chain–Coulomb gas correspondence of Sect. 3.3.1: we will find a vector v so that the associated function φ solves the problem.

More precisely, for all order specifications $\omega \in \{+,-\}^N$ with R "+"-symbols and L "−"-symbols, we want vectors

$$v_\omega^{(N)} \in M_3^{\otimes R} \otimes M_2 \otimes M_3^{\otimes L}$$

such that the function associated with v_ω by the spin chain–Coulomb gas correspondence is the boundary zig-zag amplitude $\zeta_\omega(y_L^-, \dots, y_1^-; x; y_1^+, \dots, y_R^+)$. This will be achieved if the vectors v_ω satisfy the following conditions, written in terms of the projections π, $\hat{\pi}$ defined in Appendix C.1:

- *Highest weight vector of a doublet subrepresentation*

$$E.v_\omega^{(N)} = 0 \tag{3.5}$$

$$K.v_\omega^{(N)} = q\, v_\omega^{(N)}. \tag{3.6}$$

- *Projections to singlet and triplet for successively visited points* If $y_m^\pm$ and $y_{m+1}^\pm$ are successively visited points on the same side ($y_m^\pm = y_j$ and $y_{m+1}^\pm = y_{j+1}$), then

$$\begin{aligned} \pi_{\pm;m}^{(1)}(v_\omega^{(N)}) &= 0 \\ \hat{\pi}_{\pm;m}^{(3)}(v_\omega^{(N)}) &= \text{const.} \times v_{\omega'}^{(N-1)}, \end{aligned} \tag{3.7}$$

  where $\omega' = (\omega_1, \omega_2, \dots, \omega_{j-1}, \omega_j, \omega_{j+2}, \omega_{j+3}, \dots, \omega_N)$.
- *Projections to singlet and triplet for non-successively visited points* If $y_m^\pm$ and $y_{m+1}^\pm$ are non-successively visited consecutive points on the same side ($y_m^\pm = y_j$ and $y_{m+1}^\pm = y_k$ with $k - j > 1$), then

$$\begin{aligned} \pi_{\pm;m}^{(1)}(v_\omega^{(N)}) &= 0 \\ \pi_{\pm;m}^{(3)}(v_\omega^{(N)}) &= 0. \end{aligned} \tag{3.8}$$

- *Projections to doublet for the first points on the left and right* Let $\pm$ denote the side of the first visited point, $y_1 = y_1^\pm$, and $\mp$ the opposite side. For the first visited point the condition is

$$\hat{\pi}_{\pm}^{(2)}(v_\omega^{(N)}) = \text{const.} \times v_{\omega'}^{(N-1)}, \tag{3.9}$$

  where $\omega' = (\omega_2, \omega_3, \dots, \omega_N)$. For the first point on the opposite side the condition is

$$\pi_{\mp}^{(2)}(v_\omega^{(N)}) = 0. \tag{3.10}$$

By the closed integration surface considerations of Sect. 3.3.3, Eq. (3.5) guarantees that the function associated with v_ω is independent of the anchor point and satisfies the PDEs (2.3) and (2.4). The translation invariance (2.1) is then obvious. Equation (3.6) guarantees that the associated function is a linear combination of $\varphi_{t_L^-,\ldots,t_1^-,d,t_1^+,\ldots,t_R^+}$ with $d+\sum_j t_j^- + \sum_j t_j^+ = N$, and, therefore, by the results of Sect. 3.1.1, it has the correct scaling covariance (2.2). Finally, by the asymptotics properties of Sect. 3.3.2, we see that Eqs. (3.7)–(3.10), guarantee (2.5)–(2.8), respectively.

As for the choice of multiplicative normalization, we first make an explicit choice for the cases $N = 1$ in Sect. 3.5.1. The rest of the multiplicative factors are fixed recursively in N by requiring that the constant appearing on the right hand side of Eq. (3.9) is equal to one. This corresponds to fixing the multiplicative constant in Eq. (2.7) to the value B_2 given in (3.4).

3.5. Solutions in Terms of Quantum Group Representations

A priori, the system of Eqs. (3.5)–(3.10) given in Sect. 3.4 is a linear algebra problem in the 2×3^N-dimensional tensor product space $M_3^{\otimes R} \otimes M_2 \otimes M_3^{\otimes L}$. The first two Eqs. (3.5) and (3.6) reduce this ambient dimension in a well-understood way: their meaning is that v_ω is a highest weight vector of a sub-representation of dimension two in the tensor product. We have

$$\dim(\mathrm{Ker}(E) \cap \mathrm{Ker}(K - q)) = m_N,$$

where m_N is the multiplicity of M_2 in the semisimple decomposition of the tensor product, determined recursively by the formula of Sect. 3.2.2. Explicitly for small N and asymptotically as $N \to \infty$, the multiplicities m_N are

$$\begin{array}{c|cccccccccc} N & 1 & 2 & 3 & 4 & 5 & 6 & 7 & 8 & 9 & 10 & \ldots \\ \hline m_N & 1 & 2 & 4 & 9 & 21 & 51 & 127 & 323 & 835 & 2188 & \ldots \end{array},$$

$$m_N \sim 3\sqrt{\frac{3}{4\pi}} \times N^{-\frac{3}{2}}\, 3^N.$$

Superficially the system of Sect. 3.4 still seems overdetermined, but we find that in each case the solution space is one-dimensional, so up to multiplicative normalizations the solutions are unique.

Next we give the explicit solutions to the system of equations for a few small values of N.

3.5.1. One-Point Solutions. There are two separate states that we need to solve, $v_-^{(1)} \in M_2 \otimes M_3$ for a visit on the left ($y_1 < x$), and $v_+^{(1)} \in M_3 \otimes M_2$ for a visit on the right ($x < y_1$). The solutions, unique up to normalization, are

$$v_-^{(1)} = \frac{q^4}{1-q^4}\, e_0 \otimes e_1 - \frac{q}{1-q^2}\, e_1 \otimes e_0 \tag{3.11}$$

$$v_+^{(1)} = \frac{q^2}{1-q^2}\, e_0 \otimes e_1 - \frac{q^2}{1-q^4}\, e_1 \otimes e_0. \tag{3.12}$$

The normalization above has been chosen such that the corresponding functions both are equal to

$$\zeta^{(1)}(x;y_1) = B_2\,|y_1 - x|^{1-\frac{8}{\kappa}},$$

where the constant B_2 is given by (3.4) (in particular both functions take positive real values). The calculation of the corresponding integrals is discussed in more detail in Sect. 4.2.1.

3.5.2. Two-Point Solutions. There are four separate states that we need to solve for:

$$\begin{aligned} v^{(2)}_{--} &\in M_2 \otimes M_3 \otimes M_3 \quad (y_2 < y_1 < x)\\ v^{(2)}_{-+} &\in M_3 \otimes M_2 \otimes M_3 \quad (y_1 < x < y_2)\\ v^{(2)}_{+-} &\in M_3 \otimes M_2 \otimes M_3 \quad (y_2 < x < y_1)\\ v^{(2)}_{++} &\in M_3 \otimes M_3 \otimes M_2 \quad (x < y_1 < y_2). \end{aligned}$$

For the normalization of the states, we use the asymptotics as $|y_1 - x| \to 0$, i.e., we fix the constant in either (2.7) or (3.9).

The solutions, unique with the chosen normalization, read

$$\begin{aligned} v^{(2)}_{++} &= \frac{q^4(1+q^2+q^4)}{(1-q^4)^2(1+q^4)}\\ &\quad\times((q^2+q^4)e_{011} - e_{020} - (1+q^2)e_{101} - (1-q^2)e_{110} + e_{200})\\ v^{(2)}_{--} &= \frac{q^3(1+q^2+q^4)}{(1-q^4)^2(1+q^4)}\\ &\quad\times(q^3e_{002} + (q^5-q^3)e_{011} - q^3e_{020} - q^2e_{101} - q^4e_{101} + (1+q^2)e_{110})\\ v^{(2)}_{+-} &= \frac{q^3(1+q^2+q^4)}{(1-q^4)^2(1+q^4)}\\ &\quad\times\left(\frac{q^4}{1+q^2}e_{002} + q^5e_{011} - q^3e_{101} - q^4e_{110} + \frac{1+q^2+q^4}{1+q^2}e_{200}\right)\\ v^{(2)}_{-+} &= \frac{q^3(1+q^2+q^4)}{(1-q^4)^2(1+q^4)}\\ &\quad\times\left(\frac{q^2(1+q^2+q^4)}{1+q^2}e_{002} - qe_{011} - q^3e_{101} + e_{110} + \frac{q^2}{1+q^2}e_{200}\right), \end{aligned}$$

where we use the shorthand notation $e_{t_2t_1d} = e_{t_2} \otimes e_{t_1} \otimes e_d \in M_3 \otimes M_3 \otimes M_2$ in the first case, and similarly for the rest.

3.5.3. Three-Point Solutions. For $N = 3$ there are eight separate states that we need to solve for. For brevity, in the formulas below, we factor out the constant

$$C_3 = \frac{q^5\left(q^4+q^2+1\right)^2}{\left(q^4-1\right)^3\left(q^{12}+q^{10}+2q^8+2q^6+2q^4+q^2+1\right)}.$$

Then, with a shorthand notation similar to above, the unique normalized solutions are

$$\begin{aligned}
v^{(3)}_{+++} &= C_3(-(q^6+2q^4+2q^2+1)\,q^3e_{0021}-(q^2+1)\,(q^6+q^4-1)\,q^3e_{0111}+(q^2+1)^2\,q^3e_{0120}\\
&\quad+(q^2+1)^2\,q^3e_{0201}+(q^6-q^2-1)\,qe_{0210}+(q^3+q)^3\,e_{1011}+(q^6-q^2-1)\,qe_{1020}\\
&\quad+(q^2+1)\,(q^6-q^2-1)\,qe_{1101}+(q^9-q^7-2q^5-q^3+q)\,e_{1110}-(q^6+q^4-1)\,qe_{1200}\\
&\quad-(q^6+2q^4+2q^2+1)\,qe_{2001}-(q^6+q^4-1)\,qe_{2010}+(q^2+1)^2\,qe_{2100})\\
v^{(3)}_{++-} &= C_3\bigg(-(q^4+q^2+1)\,q^4e_{0012}+\Big(-q^8+q^2+\frac{1}{q^2+1}-1\Big)\,e_{0102}-(q^6+q^4-1)\,q^5e_{0111}\\
&\quad+(q^7+q^5)\,e_{0201}+(q^8+q^6)\,e_{0210}+(q^6+q^4)\,e_{1002}+(q^2+1)^2\,q^5e_{1011}\\
&\quad+(q^6-q^2-1)\,q^3e_{1101}+(q^6-q^2-1)\,q^4e_{1110}-(q^4+q^2+1)\,q^4e_{1200}\\
&\quad-(q^4+q^2+1)\,q^3e_{2001}-(q^4+q^2+1)\,q^4e_{2010}+\frac{(q^4+q^2+1)^2\,e_{2100}}{q^2+1}\bigg)\\
v^{(3)}_{+-+} &= C_3\bigg(-(q^4+1)\,(q^4+q^2+1)\,q^2e_{0012}+\Big(q^4+\frac{q^2}{q^2+1}\Big)\,e_{0102}+(q^7+q^5+q^3)\,e_{0111}\\
&\quad-qe_{0201}-q^2e_{0210}+\Big(q^6+q^2+\frac{1}{q^2+1}-1\Big)\,e_{1002}+(q^9+q^7+q^5)\,e_{1011}\\
&\quad-(q^2+1)\,q^3e_{1101}-(q^2+1)\,q^4e_{1110}+\Big(q^2+\frac{1}{q^2+1}\Big)\,e_{1200}-q^5e_{2001}\\
&\quad+q^6\,(-e_{2010})+\Big(q^4+\frac{q^2}{q^2+1}\Big)\,e_{2100}\bigg)\\
v^{(3)}_{+--} &= C_3\bigg(-(q^2+1)\,q^6e_{0012}+\frac{(-q^{10}+q^6+q^4)\,e_{0021}}{q^2+1}-(q^2+1)\,q^7e_{0102}\\
&\quad+(-q^{11}+q^7+q^5)\,e_{0111}+(q^9+q^7+q^5)\,e_{0120}+(q^7+q^5+q^3)\,e_{1002}\\
&\quad+(q^6+q^4-1)\,q^3e_{1011}-(q^2+1)\,q^3e_{1020}+(q^6+q^4-1)\,q^4e_{1101}-(q^2+1)^2\,q^4e_{1110}\\
&\quad-\frac{(q^5+q^3+q)^2\,e_{2001}}{q^2+1}+(q^4+q^2+1)\,e_{2010}+(q^5+q^3+q)\,e_{2100}\bigg)\\
v^{(3)}_{-++} &= C_3\bigg(-(q^4+q^2+1)\,q^4e_{0012}-(q^4+q^2+1)\,q^6e_{0102}+(q^2+1)^2\,q^3e_{0111}\\
&\quad+(q^7+q^5)\,e_{0201}+(-q^4-q^2-1)\,e_{0210}+\frac{(q^5+q^3+q)^2\,e_{1002}}{q^2+1}+(q^6-q^2-1)\,qe_{1011}\\
&\quad+(q^6-q^2-1)\,q^3e_{1101}+(-q^6-q^4+1)\,e_{1110}+\Big(\frac{q^2}{q^2+1}-q^6\Big)\,e_{1200}\\
&\quad-(q^4+q^2+1)\,q^3e_{2001}+(q^2+1)\,e_{2010}+(q^4+q^2)\,e_{2100}\bigg)\\
v^{(3)}_{-+-} &= C_3\bigg(-\frac{(q^{10}+q^8+q^6)\,e_{0012}}{q^2+1}-\frac{(q^4+q^2+1)\,q^8e_{0021}}{q^2+1}+q^3e_{0102}\\
&\quad+(q^7+q^5)\,e_{0111}+q^7e_{0120}+q^5e_{1002}+(q^9+q^7)\,e_{1011}+q^9e_{1020}\\
&\quad-(q^4+q^2+1)\,q^2e_{1101}-(q^4+q^2+1)\,q^4e_{1110}-\frac{(q^8+q^6+q^4)\,e_{2001}}{q^2+1}\\
&\quad-\frac{(q^{10}+q^8+q^6)\,e_{2010}}{q^2+1}+\Big(q^7+q^5+2q^3+q+\frac{1}{q}\Big)\,e_{2100}\bigg)
\end{aligned}$$

$$
\begin{aligned}
v^{(3)}_{--+} = C_3\Bigg(& -\frac{\left(q^4+q^2+1\right)^2 q^4 e_{0012}}{q^2+1} + \left(q^6+q^4+q^2\right) e_{0021} + \left(q^5+q^3+q\right) e_{0102} \\
& + \left(q^6+q^4-1\right) q e_{0111} - \left(q^2+1\right) q e_{0120} + \left(q^7+q^5+q^3\right) e_{1002} + \left(q^6+q^4-1\right) q^3 e_{1011} \\
& - \left(q^2+1\right) q^3 e_{1020} - \left(q^3+q\right)^2 e_{1101} + \left(-q^6+q^2+1\right) e_{1110} - \left(q^2+1\right) q^4 e_{2001} \\
& + \frac{\left(-q^8+q^4+q^2\right) e_{2010}}{q^2+1} + \left(q^5+q^3+q\right) e_{2100} \Bigg) \\
v^{(3)}_{---} = C_3\Bigg(& -\left(q^2+1\right)^2 q^5 e_{0012} + \left(-q^9+q^5+q^3\right) e_{0021} + \left(-q^9+q^5+q^3\right) e_{0102} \\
& + \left(-q^8+q^6+2q^4+q^2-1\right) q^3 e_{0111} + \left(q^6+q^4-1\right) q^3 e_{0120} + \left(q^6+q^4-1\right) q^3 e_{0201} \\
& - \left(q^2+1\right)^2 q^3 e_{0210} + \left(q^2+1\right)\left(q^4+q^2+1\right) q^2 e_{1002} + \left(q^2+1\right)\left(q^6+q^4-1\right) q^2 e_{1011} \\
& - \left(q^3+q\right)^2 e_{1020} - \left(q^2+1\right)^3 q^2 e_{1101} - \left(q^2+1\right)\left(q^6-q^2-1\right) e_{1110} \\
& + \left(q^2+1\right)\left(q^4+q^2+1\right) e_{1200} \Bigg).
\end{aligned}
$$

3.5.4. Four-Point Solutions. For $N = 4$ there are 16 separate states that we need to solve for. The solutions are again unique (with the chosen normalization). In Appendix C.2 we include the results for those vectors that have been used in the plots of Fig. 13.

3.5.5. Well-Posedness of the Problem. The linear problem of Sect. 3.4 is well-posed: one always finds solutions and they are unique (with the chosen normalization). Up to $N = 4$ this was explicitly stated above.

The uniqueness of solutions is checked by considering the homogeneous equations for N-point vectors, where the inhomogeneous terms coming from the $(N-1)$-point vectors on the right-hand sides of Eqs. (3.7) and (3.9) are omitted, that is

$$
\begin{aligned}
& (K-q).v = 0, \quad E.v = 0, \quad \pi^{(1)}_{\pm;m}(v) = 0, \quad \pi^{(3)}_{\pm;m}(v) = 0, \quad \pi^{(2)}_{\pm}(v) = 0 \\
& \quad \text{for } v \in M_3^{\otimes R} \otimes M_2 \otimes M_3^{\otimes L}.
\end{aligned}
$$

The projection conditions here, i.e., the homogeneous versions of Eqs. (3.7)–(3.10), force the vector to lie in the unique subrepresentation of the highest spin $M_{2N+2} \subset M_3^{\otimes R} \otimes M_2 \otimes M_3^{\otimes L}$. On the other hand, the first two equations, i.e., Eqs. (3.5) and (3.6), force the solution to lie in a doublet $M_2 \subset M_3^{\otimes R} \otimes M_2 \otimes M_3^{\otimes L}$. The doublet subrepresentation and the subrepresentation of highest spin intersect only at zero. The homogeneous problem, therefore, has no non-zero solutions, which shows uniqueness.

The easiest way to prove the existence of solutions for all N seems to be by exhibiting an algorithm, which recovers the solutions to our problem from the solutions to a slightly simpler similar problem related to multiple SLEs. This is done in detail in [31, Section 5].

4. Regularized Real Integrals and Evaluation of the Formulas

4.1. Transformation to Real Integration Contours

Let us then analyze further the integrals $\varphi_{t_L^-,\ldots,t_2^-,t_1^-;d;t_1^+,t_2^+,\ldots,t_R^+}$ given by the spin chain–Coulomb gas correspondence. Recall that the integral was defined in Sect. 3.1.2, where the integration surface Γ consists of non-intersecting loop contours for each of the integration variables w_s as depicted in Fig. 3.

First we shall describe a transformation of the contours which makes the integrands explicitly real in general, and examples will follow below. The procedure is, in principle, straightforward. We assume that the anchor point z_0 of the loop integrals lies on the real axis left of the points x and y_L^-. (As stated in Sect. 3.3.3 and as we shall see below, the integrals of interest to us in the end are independent of this anchor point.) We can then deform the loop-shaped contours so that they follow the real line, starting from the innermost loops on the left and proceeding towards right.

There is, however, a complication as the integrals along the real axis may become singular. Notice that as any of the integration variables w_i approaches any of the points y_j, the integrand behaves as $\sim |w_i - y_j|^{1-8/\kappa}$. Thus the resulting integrals will be convergent if $\kappa > 8$. For simplicity, let us, therefore, first assume that $\kappa > 8$, although for the application to SLE boundary visit amplitudes we are ultimately interested in $\kappa < 8$. We will discuss the divergences and the needed regularization for $\kappa < 8$ in Sect. 4.3.

When $\kappa > 8$, a loop contour enclosing, for example, y_k^- can be divided into $2(L-k+1)$ subcontours on the real line. We get two contours (one from both the lower and the upper edges of the loop) between the base point and y_L^- as well as between all consecutive pairs $\{y_j^-, y_{j+1}^-\}$ with $j = k, \ldots, L-1$. The corresponding (one-dimensional) integral thus becomes a sum of integrals over the real line. Extending this procedure to the loops enclosing x and the points y_k^+ right of x, each integral $\varphi_{t_L^-,\ldots,t_2^-,t_1^-;d;t_1^+,t_2^+,\ldots,t_R^+}$ can be written as a linear combination of integrals having all integration contours on the real line.

In order to obtain the explicit linear combination of the integrals, the remaining and most non-trivial task is to calculate the phase factors which arise as the integrand is a multi-valued function. The phase convention for the integrand $f^{\ni}_{t_L^-,\ldots,t_R^+}$ of (3.3) for the loop contours was defined by the red circles in Fig. 3, and this convention leads to rather impractical branch choices for the integrand as the contours are transformed. We shall choose the phases for the contours along the real line as depicted by the red circles in Fig. 4, where the integration contours have been deformed away from the real line to make their multiplicity and the phase convention visible. Let us denote these integrals by $\hat{\rho}_{k_L^-,\ldots,k_2^-,k_1^-;k;k_1^+,k_2^+,\ldots,k_R^+}$, when the number of variables integrated from the anchor to y_L^- is k_L^-, the number of variables integrated from y_L^- to y_{L-1}^- is k_{L-1}^- and so on (we thus choose to index the integrals in terms of the rightmost points of the integration intervals). It is not worthwhile to write down a general formula for the phase factors which appear when expressing each φ as a sum of the integrals $\hat{\rho}$, but it is straightforward to calculate them case by case as

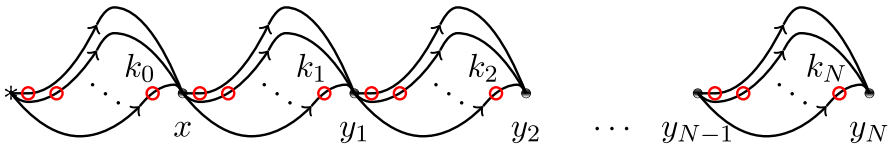

FIGURE 4. The integration contours of the w_j-variables for $\hat{\rho}_{;k;k_1^+,k_2^+,\ldots,k_N^+}$ and the point (marked by *red circles*) where the integrand is rephased to be positive. The *contours* in this figure have been deformed away from the real axis, for the sake of clarity of the phase convention (color figure online)

seen in the examples below. As the phase factors reflect the branch choices of the integrand in (3.2), they will be integer powers of $q = \exp(4\pi \mathrm{i}/\kappa)$, possibly multiplied by -1 if the direction of integration needs to be reversed.

As the final step, we arrange the integration over each interval such that the integration variables have a fixed order. The natural phase convention in this case is that the integrand is real and positive. We denote these integrals by $\rho_{k_L^-,\ldots,k_2^-,k_1^-;k;k_1^+,k_2^+,\ldots,k_R^+}$. The integrals are over products of simplexes of dimensions $k_L^-,\ldots,k_1^-;k;k_1^+,,\ldots,k_R^+$, for example when $L=0$, $R=N$, and $K = k + \sum_{j=1}^N k_j^+$ we have

$$\begin{aligned}
&\rho_{;k;k_1^+,k_2^+,\ldots,k_N^+}(;x;y_1,\ldots,y_N) \\
&\quad = \int\limits_{\substack{x<w_1<w_2<w_3<\cdots<w_k<y_1 \\ y_1<w_{k+1}<\cdots<w_{k+k_1}<y_2 \\ \vdots \qquad\qquad \vdots \\ y_{N-1}<w_{K-k_N+1}<\cdots<w_K<y_N}} \cdots \int \mathrm{d}w_1 \mathrm{d}w_2 \cdots \mathrm{d}w_K \; |f_N^{(N)}(x;y_1,\ldots,y_N;w_1,\ldots,w_N)|.
\end{aligned}$$

The reordering gives a factor of $[k]!\, q^{-k(k-1)/2}$ for each interval with k integrations, where $[k]! = \prod_{m=1}^k [m]$ is a q-factorial (see [30, Lemma 3.2] for details). Thus, we have

$$\begin{aligned}
\hat{\rho}_{k_L^-,\ldots,k_2^-,k_1^-;k;k_1^+,k_2^+,\ldots,k_R^+} &= \prod_{j=1}^L \left[k_j^-\right]! \, q^{-k_j^-\left(k_j^- - 1\right)/2} \times [k]!\, q^{-k(k-1)/2} \\
&\quad \times \prod_{j=1}^R \left[k_j^+\right]! \, q^{-k_j^+\left(k_j^+ - 1\right)/2} \times \rho_{k_L^-,\ldots,k_2^-,k_1^-;k;k_1^+,k_2^+,\ldots,k_R^+}.
\end{aligned}$$

4.2. Solutions in Terms of Real Integrals

Let us then calculate explicitly the solutions obtained in Sect. 3.5 for low numbers of boundary visits N. We shall discuss in detail the case $N=1$, and list the results for the solutions with a higher number of points. Case by case, we will check that the obtained solutions for the boundary zig-zag amplitudes satisfy the following two requirements:

- The integration contour Γ is closed, and, therefore, the solution is independent of the choice of the anchor point of the loop integrals. When the amplitude is expressed in terms of the integrals $\rho_{k_L^-,\dots,k_1^-;k;k_1^+,\dots,k_R^+}$ (or a similar $\hat{\rho}$), this will be clear as the solutions do not depend on the integrals which include integrations starting from the base point—we will only have terms with $k_L^- = 0$ (or if $L = 0$ then $k = 0$).
- The solution is real: when expressed in terms of the integrals ρ, all coefficients will be real.

4.2.1. One-Point Solutions. We start from the $N = 1$ case where the single visit takes place right of the starting point x. In this case we found that the state $v_+^{(1)} \in M_3 \otimes M_2$ in (3.12) which satisfies the constraints is

$$v_+^{(1)} = \frac{q^2}{1-q^2}\, e_0 \otimes e_1 - \frac{q^2}{1-q^4}\, e_1 \otimes e_0.$$

By the spin chain–Coulomb gas correspondence of Sect. 3.3.1, the zig-zag probability amplitude is given by

$$\zeta_+^{(1)}(x; y_1^+) = \frac{q^2}{1-q^2}\, \varphi_{;1;0}(x; y_1^+) - \frac{q^2}{1-q^4}\, \varphi_{;0;1}(x; y_1^+).$$

Let us then do the transformation to the integrals along the real line. The first term $\varphi_{;1;0}$ has the loop integral encircling x, which can only lead to integrals over the real line between the base point and x, i.e., the integral $\hat{\rho}_{;1;0}$. The phase factor from the lower edge of the loop is $q = e^{4\pi \mathrm{i}/\kappa}$ (as the phase conventions of Figs. 3 and 4 differ by a rotation of the integration variable w around x by the angle $-\pi$), whereas the phase factor for the upper edge of the loop is $-q^{-1}$ (where the rotation is in the opposite direction, and the minus sign arises from reversing the direction of integration). Together,

$$\varphi_{;1;0}(x; y_1^+) = \left(q - \frac{1}{q}\right) \hat{\rho}_{;1;0}(x; y_1^+).$$

The other loop integral $\varphi_{;0;1}$ breaks into four integrals along the intervals on the real axis, two integrals between the base point and x, and two integrals between x and y_1^+. The phase factors can be calculated analogously to the case of $\varphi_{;1;0}$, and they are integer powers of q. We find that

$$\varphi_{;0;1}(x; y_1^+) = \left(q^2 - \frac{1}{q^2}\right) \hat{\rho}_{;0;1}(x; y_1^+) + \left(q^3 - \frac{1}{q}\right) \hat{\rho}_{;1;0}(x; y_1^+). \tag{4.1}$$

Substituting in these results, we get

$$\zeta_+^{(1)}(x; y_1^+) = \hat{\rho}_{;0;1}(x; y_1^+) = \rho_{;0;1}(x; y_1^+).$$

In particular, the contributions of the integral $\hat{\rho}_{;1;0}$ cancel. The remaining integral $\hat{\rho}_{;0;1}$ is independent of the anchor point of the loop contours, which shows that the contour Γ was closed. In this case there is only one integration variable, so trivially $\hat{\rho}_{;0;1} = \rho_{;0;1}$. From the final expression we also see that the result is real.

When $N = 1$ the resulting integral can be calculated easily. Using the definitions from (3.2),

$$\begin{aligned}\zeta_+^{(1)}(x;y_1^+) &= (y_1^+ - x)^{4/\kappa} \int_x^{y_1^+} \mathrm{d}w\, (w-x)^{-4/\kappa} (y_1^+ - w)^{-8/\kappa} \\ &= B_2\, (y_1^+ - x)^{1-8/\kappa},\end{aligned}$$

where the constant is given by the same beta function $B_2 = B\left(\frac{\kappa-8}{\kappa}, \frac{\kappa-4}{\kappa}\right) = \Gamma(\frac{\kappa-4}{\kappa})\Gamma(\frac{\kappa-8}{\kappa})/\Gamma(2\frac{\kappa-6}{\kappa})$ as in Eq. (3.4).

For comparison, let us also take a look at the case where the visit takes place left of x. The state $v_-^{(1)} \in W_2 \otimes W_3$ was given in Eq. (3.11), and by the correspondence we get the probability amplitude

$$\zeta_-^{(1)}(y_1^-;x) = \frac{q^4}{1-q^4}\, \varphi_{1;0;}(y_1^-;x) - \frac{q}{1-q^2}\, \varphi_{0;1;}(y_1^-;x).$$

The transformations to real integrals read in this case

$$\begin{aligned}\varphi_{1;0;}(y_1^-;x) &= \left(q^2 - \frac{1}{q^2}\right) \hat{\rho}_{1;0;}(y_1^-;x) \\ \varphi_{0;1;}(y_1^-;x) &= \left(q - \frac{1}{q}\right) \hat{\rho}_{0;1;}(y_1^-;x) + \left(q^3 - q\right) \hat{\rho}_{1;0;}(y_1^-;x).\end{aligned}$$

Inserting these gives again a simple result

$$\zeta_-^{(1)}(y_1^-;x) = \hat{\rho}_{0;1;}(y_1^-;x) = \rho_{0;1;}(y_1^-;x).$$

This evaluates to

$$\zeta_-^{(1)}(y_1^-;x) = (x-y_1^-)^{4/\kappa} \int_{y_1^-}^{x} \mathrm{d}w\, (w-y_1^-)^{-8/\kappa} (x-w)^{-4/\kappa} = B_2\, (x-y_1^-)^{1-8/\kappa}.$$

The results for the left- and right-side visits can be collected in the (well known) $N = 1$ probability amplitude already stated in Eq. (1.5),

$$\zeta^{(1)}(x;y_1) = \chi^{(1)}(x;y_1) = B_2\, |y_1 - x|^{1-\frac{8}{\kappa}},$$

with our multiplicative normalization convention resulting in B_2 given in (3.4).

4.2.2. Two-Point Solutions. Let us start the discussion of the two-point solutions from the case where both visits take place on the right-hand side. The relevant vector $v_{++}^{(2)} \in M_3 \otimes M_3 \otimes M_2$ reads

$$\begin{aligned}v_{++}^{(2)} = &\frac{q^4(1+q^2+q^4)}{(1-q^4)^2(1+q^4)} \\ &\times((q^2+q^4)e_{011} - e_{020} - (1+q^2)e_{101} + (1-q^2)e_{110} + e_{200}),\end{aligned}$$

where $e_{t_2t_1d} \equiv e_{t_2} \otimes e_{t_1} \otimes e_d$. Thus the probability amplitude is

$$\begin{aligned}\zeta^{(2)}_{++}(x;y_1^+,y_2^+) = \frac{q^4(1+q^2+q^4)}{(1-q^4)^2(1+q^4)}((q^2+q^4)\varphi_{;0;1,1}(x;y_1^+,y_2^+)\\ -\varphi_{;0;2,0}(x;y_1^+,y_2^+) - (1+q^2)\varphi_{;1;0,1}(x;y_1^+,y_2^+)\\ +(1-q^2)\varphi_{;1;1,0}(x;y_1^+,y_2^+) + \varphi_{;2;0,0}(x;y_1^+,y_2^+)).\end{aligned}$$

The transformation to real integrals is still straightforward albeit more involved, as one needs to take into account the phases related to the order of the integration variables. The number of terms is also larger, e.g., the integral $\varphi_{;0;2,0}$ breaks into 16 different terms (some of which immediately cancel against each other).

Collecting the results in the expression for the probability amplitude, however, there are again lots of simplifications:

$$\zeta^{(2)}_{++}(x;y_1^+,y_2^+) = \frac{q^{-2}+1+q^2}{q^{-2}+q^2}(\rho_{;0;0,2}(x;y_1^+,y_2^+) + \rho_{;0;1,1}(x;y_1^+,y_2^+)).$$

Again we notice that as the first index of all remaining real integrals is zero, the integration contour is closed. The probability amplitude is also real.

The amplitudes with other orderings of visits can be calculated similarly. The results can be collected as

$$\begin{aligned}\zeta^{(2)}_{--}(y_1^-,y_2^-;x) &= \frac{q^{-2}+1+q^2}{q^{-2}+q^2}(\rho_{0,2;0;}(y_1^-,y_2^-;x) + \rho_{0,1;1;}(y_1^-,y_2^-;x))\\
\zeta^{(2)}_{-+}(y_1^-;x;y_1^+) &= \frac{q^{-2}+1+q^2}{q^{-3}+q^{-1}+q+q^3}\Bigg((q^{-2}+1+q^2)\rho_{0;2;0}(y_1^-;x,y_1^+)\\
&\quad + \frac{q^{-3}+q^{-1}+q+q^3}{q^{-2}+q^2}\rho_{0;1;1}(y_1^-;x;y_1^+) + \rho_{0;0;2}(y_1^-;x;y_1^+)\Bigg)\\
\zeta^{(2)}_{+-}(y_1^-;x;y_1^+) &= \frac{q^{-2}+1+q^2}{q^{-3}+q^{-1}+q+q^3}\Bigg((q^{-2}+1+q^2)\rho_{0;0;2}(y_1^-;x,y_1^+)\\
&\quad + \frac{q^{-3}+q^{-1}+q+q^3}{q^{-2}+q^2}\rho_{0;1;1}(y_1^-;x;y_1^+) + \rho_{0;2;0}(y_1^-;x;y_1^+)\Bigg)\\
\zeta^{(2)}_{++}(x;y_1^+,y_2^+) &= \frac{q^{-2}+1+q^2}{q^{-2}+q^2}(\rho_{;0;0,2}(x;y_1^+,y_2^+) + \rho_{;0;1,1}(x;y_1^+,y_2^+)).\end{aligned}$$

One can check that

$$\begin{aligned}\zeta^{(2)}_{++}(x;y_1^+,y_2^+) = B_2^2\,\frac{\Gamma(\frac{16-\kappa}{\kappa})\,\Gamma(\frac{4}{\kappa})}{\Gamma(\frac{12-\kappa}{\kappa})\,\Gamma(\frac{8}{\kappa})}\,(y_1^+-x)^{1-\frac{8}{\kappa}}(y_2^+-y_1^+)^{1-\frac{8}{\kappa}}\\ \times {}_2F_1\left(\frac{4}{\kappa},\frac{\kappa-8}{\kappa};\frac{8}{\kappa};\frac{y_2^+-y_1^+}{y_2^+-x}\right)\end{aligned}$$

and

$$\zeta^{(2)}_{+-}(y_1^-;x;y_1^+) = B_2^2\,\frac{\Gamma(\frac{16-\kappa}{\kappa})\,\Gamma(\frac{8}{\kappa})}{\Gamma(\frac{12-\kappa}{\kappa})\,\Gamma(\frac{12}{\kappa})}\,(x-y_1^-)^{\frac{4}{\kappa}}(y_1^+-x)^{-\frac{4}{\kappa}}(y_1^+-y_1^-)^{2-\frac{16}{\kappa}} \times {}_2F_1\left(\frac{8}{\kappa},\frac{\kappa-4}{\kappa};\frac{12}{\kappa};-\frac{x-y_1^-}{y_1^+-x}\right),$$

and that $\zeta^{(2)}_{--}(y_2^-,y_1^-;x)$ and $\zeta^{(2)}_{-+}(y_1^-;x;y_1^+)$ are given by the obvious reflection in the above formulas. In particular, our formulas for $\zeta^{(2)}_{++}$ and $\zeta^{(2)}_{--}$ agree up to the choice of normalization with those given in [51].

4.3. Divergences of the Real Integrals

As we mentioned above, the integrals over the real line contain divergences. The integrals converge for $\kappa > 8$, but diverge when $0 < \kappa \leq 8$, which is the range of the most interesting values of κ. There are several strategies to tame the divergences, of which we emphasize two.

First, by construction, the spin chain–Coulomb gas method will result in formulas that are analytic in κ, and the fundamental way of regularizing the divergences of the integrals, therefore, is

- *Analytic Continuation* We can first restrict to $\kappa > 8$, where the integrals converge, and analytically continue the final expressions to smaller values of κ.

As usual, analytic continuation can be done in several ways. The basis functions φ, defined as integrals as in Fig. 3, themselves converge for all values of κ and their suitable linear combinations are thus already the analytic answer that we are looking for. Whenever possible, it is nevertheless desirable to have explicit expressions for the answer in terms of known analytic functions. This is, in fact, essentially what we have been doing so far. Already the multiplicative constants B_1, B_3, B_2 appearing in the asymptotics properties in Sect. 3.3.2 were a priori defined as real integrals convergent only for $\kappa > 8$, but they were expressible in terms of Gamma-functions which readily provide their analytic continuation, e.g., $B_2 = \int_0^1 \mathrm{d}w\ w^{-\frac{4}{\kappa}}(1-w)^{-\frac{8}{\kappa}} = \Gamma(\frac{\kappa-4}{\kappa})\Gamma(\frac{\kappa-8}{\kappa})/\Gamma(2\frac{\kappa-6}{\kappa})$. Furthermore, in Sect. 4.1 we gave formulas for the final answers for the zig-zag amplitudes $\zeta^{(1)}_{\pm}$ and $\zeta^{(2)}_{\omega}$, in terms of, for example, hypergeometric functions which also have known analytic continuations.

Although the real integrals always remain in essence similar to the cases considered above, we cannot in general reduce the answers to such well-known special functions. It is, therefore, useful to have a direct procedure to regularize the divergent real integrals generally, in a way that provides their analytic continuation, has transparent properties, and can be used for their numerical evaluation. We focus on one such procedure:

- *Cutoff Regularization* We can start from the final expressions involving real integrals, and introduce a small cutoff ε to regularize all divergent integrals. More precisely, we require that all integration variables are further away than ε from any of the points x or y_k. With this prescription, the results diverge as $\varepsilon \searrow 0$. All divergent terms are powers of ε, with the exponents

depending on κ. They can be subtracted unambiguously at least for irrational values of κ. The final result is then obtained by taking $\varepsilon \searrow 0$ after subtracting the divergent counterterms. We will discuss the details below.

Let us now sketch how to prove that this regularization leads to the correct final result.

First, the loop integrals φ of Fig. 3 converge for all values of κ and thus can be used to define the analytic continuation of the result from $\kappa > 8$ to $0 < \kappa \leq 8$. We can then do the transformation to real integrals, which was described in Sect. 4.1, in a way that avoids the divergences. We first choose ε which is smaller than half of the separation of any two of the points y_k or x. When deforming the loops into integrals over the real line, we replace the sections of contours on the real line, which are closer than ε to the points y_k or x, by (semi-)circles having radii ε. This approach results in a higher dimensional analogue of the usual Pochhammer contour. In this way a regularization is obtained by modification of the contours, and no terms are dropped. Therefore, it also gives the analytic continuation of the results to small values of κ, independently of the value of ε.

Second, the pieces of the above contour on the real line equal the cutoff regularized integrals. The integrals over the (semi-)circles can be expanded around $\varepsilon = 0$, and the terms which are divergent as $\varepsilon \searrow 0$ provide the counterterms for the cutoff regularization. For generic irrational κ the expansions contain no constant term. Therefore, taking $\varepsilon \searrow 0$, the analytically continued result matches with the cutoff-regularized one for all values of κ for which the cutoff procedure could be defined unambiguously.[12]

Let us then work out the details of the cutoff regularization, i.e., find a method to calculate the counterterms. We already pointed out that this can be done by studying the expansion of the contributions from the (semi-) circles to the integrals above, but tracking the phases of these integrals is quite involved. It turns out to be easier to read off the divergent terms from the real integrals directly. We can first take $\kappa > 8$ and start from the integrals without any cutoff. Then we separate the "divergent" terms by dividing the integrations into several pieces, effectively introducing a "cutoff".

Let us first discuss the generic framework in more detail. We shall also give an example below. We start from the integral ρ where all integrals are along the real line and the integrand is real. We divide the integrals over each of the real intervals into two pieces: the "regular" one where all integration variables are further away than ε from the endpoints, and the "divergent" one where one of the variables (either the first or the last one) is within ε from the endpoints. The basic idea is then to develop the divergent pieces as series at $\varepsilon = 0$.

For an N-point function, the highest possible divergence appears when all integration variables are within ε from different points y_j. Taking into account

[12] For the specific values of κ, where the counterterms of the cutoff procedure involve constants, cutoff regularization can be defined such that it matches with the other schemes. Equivalently we can, e.g., require that the counterterms are analytic in κ.

the behavior of the integrand and the integration measure, such contribution is $\sim \varepsilon^{N(1-8/\kappa)}$. Developing the integrand as series at $\varepsilon = 0$, and taking into account the contributions having divergent terms from $n < N$ integrations, the generic divergent contribution has the power behavior

$$\sim \varepsilon^{n(1-8/\kappa)}\varepsilon^k, \quad \text{where } n = 1, 2, \ldots, N \quad \text{and} \quad k = 0, 1, 2, \ldots \tag{4.2}$$

All such terms can be in principle calculated by analyzing the divergent terms. Analytically continuing to $\kappa < 8$, terms with small k will be divergent as $\varepsilon \searrow 0$. (Alternatively, we could keep $\kappa < 8$ fixed from the start and work with two cutoffs.) Since we started from an integral that was independent of ε, these terms must cancel when all divergent and regular pieces are summed, and they are thus the required counterterms. How all of this works is best illustrated by considering an example.

Let us discuss the $N = 2$ integral

$$\rho_{;0;0,2}(x; y_1, y_2) = \int_{y_1}^{y_2}\int_{w_1}^{y_2} \mathrm{d}w_1\mathrm{d}w_2 \left[\frac{(w_2 - w_1)(y_2 - y_1)}{(y_2 - w_1)(y_2 - w_2)(w_2 - y_1)(w_1 - y_1)}\right]^{\frac{8}{\kappa}} \times F(w_1, w_2; x; y_1, y_2),$$

where $x < y_1 < y_2$ and we denoted by

$$F(w_1, w_2; x; y_1, y_2) = \left[\frac{(y_2 - x)(y_1 - x)}{(w_2 - x)(w_1 - x)}\right]^{\frac{4}{\kappa}}$$

the part which would be replaced by a more complicated function for a higher point integral having a similar structure, i.e., integral of two variables between consecutive points y_j. The regular term is

$$R = \int_{y_1+\varepsilon}^{y_2-\varepsilon}\int_{w_1}^{y_2-\varepsilon} \mathrm{d}w_1\mathrm{d}w_2 \left[\frac{(w_2 - w_1)(y_2 - y_1)}{(y_2 - w_1)(y_2 - w_2)(w_2 - y_1)(w_1 - y_1)}\right]^{\frac{8}{\kappa}} \times F(w_1, w_2; x; y_1, y_2)$$

and the divergent terms can be written as

$$\begin{aligned} &D_1 + D_2 + D_3 + D_4 + D_5 \\ &\quad = \left(\int_{y_1}^{y_1+\varepsilon}\int_{y_1+\varepsilon}^{y_2-\varepsilon} + \int_{y_1+\varepsilon}^{y_2-\varepsilon}\int_{y_2-\varepsilon}^{y_2} + \int_{y_1}^{y_1+\varepsilon}\int_{y_2-\varepsilon}^{y_2} + \int_{y_1}^{y_1+\varepsilon}\int_{w_1}^{y_1+\varepsilon} + \int_{y_2-\varepsilon}^{y_2}\int_{w_1}^{y_2}\right)\mathrm{d}w_1\mathrm{d}w_2 \\ &\qquad \times \left[\frac{(w_2 - w_1)(y_2 - y_1)}{(y_2 - w_1)(y_2 - w_2)(w_2 - y_1)(w_1 - y_1)}\right]^{\frac{8}{\kappa}} F(w_1, w_2; x; y_1, y_2), \end{aligned}$$

where the first two terms include one divergent piece of integration, and the last three include two pieces.

The leading contribution from the divergent pieces is contained in the third term D_3, where $|w_1 - y_1| < \varepsilon$ and $|w_2 - y_2| < \varepsilon$, as the terms D_4 and D_5 are suppressed by the factor $(w_2 - w_1)^{8/\kappa}$. We denote the $\mathcal{O}(\varepsilon)$ integration variables as $\hat{w}_1 = w_1 - y_1$ and $\hat{w}_2 = y_2 - w_2$. Developing at $\varepsilon = 0$ we find

$$\begin{aligned} D_3 = \int_0^\varepsilon\int_0^\varepsilon \mathrm{d}\hat{w}_1\mathrm{d}\hat{w}_2\hat{w}_1^{-8/\kappa}\hat{w}_2^{-8/\kappa}\Bigg[&F(y_1, y_2; x; y_1, y_2) \\ &+ \hat{w}_1\frac{\partial}{\partial w_1}F(w_1, y_2; x; y_1, y_2)\Big|_{w_1=y_1} - \hat{w}_2\frac{\partial}{\partial w_2}F(y_1, w_2; x; y_1, y_2)\Big|_{w_2=y_2} + \mathcal{O}(\varepsilon^2)\Bigg], \end{aligned}$$

where we wrote the terms of the expansions up to next-to-leading order, corresponding to $k = 1$ in (4.2). Doing the integrals gives the counterterms

$$\begin{aligned} D_3 &= \frac{\varepsilon^{2(1-8/\kappa)}}{(1-8/\kappa)^2}\Bigg[F(y_1,y_2;x;y_1,y_2) + \frac{\varepsilon(1-8/\kappa)}{2(1-4/\kappa)} \\ &\quad \times \left(\frac{\partial}{\partial w_1}F(w_1,y_2;x;y_1,y_2)\Big|_{w_1=y_1} - \frac{\partial}{\partial w_2}F(y_1,w_2;x;y_1,y_2)\Big|_{w_2=y_2}\right) + \mathcal{O}(\varepsilon^2)\Bigg] \\ &= \frac{\varepsilon^{2(1-8/\kappa)}}{(1-8/\kappa)^2}\left[1 - \frac{2\varepsilon(1-8/\kappa)(y_2-y_1)}{\kappa(1-4/\kappa)(y_2-x)(y_1-x)} + \mathcal{O}(\varepsilon^2)\right]. \end{aligned}$$

As another example, let us consider the term D_1. Denoting again $\hat{w}_1 = w_1 - y_1$, we find

$$\begin{aligned} D_1 &= \int_0^{\varepsilon}\int_{y_1+\varepsilon}^{y_2-\varepsilon} \mathrm{d}\hat{w}_1\mathrm{d}w_2\hat{w}_1^{-8/\kappa}(y_2-w_2)^{-8/\kappa}\Bigg[F(y_1,w_2;x;y_1,y_2) \\ &\quad + \hat{w}_1\left(\frac{\partial}{\partial w_1}F(w_1,w_2;x;y_1,y_2)\Big|_{w_1=y_1}\right. \\ &\quad \left. - \frac{8(y_2-w_2)}{\kappa(w_2-y_1)(y_2-y_1)}F(y_1,w_2;x;y_1,y_2)\right) + \mathcal{O}(\varepsilon^2)\Bigg] \\ &= \frac{\varepsilon^{1-8/\kappa}}{1-\frac{8}{\kappa}}\int_{y_1+\varepsilon}^{y_2-\varepsilon}\mathrm{d}w_2(y_2-w_2)^{-8/\kappa}\Bigg[F(y_1,w_2;x;y_1,y_2) \\ &\quad + \frac{\varepsilon(1-8/\kappa)}{2(1-4/\kappa)}\left(\frac{\partial}{\partial w_1}F(w_1,w_2;x;y_1,y_2)\Big|_{w_1=y_1}\right. \\ &\quad \left. - \frac{8(y_2-w_2)}{\kappa(w_2-y_1)(y_2-y_1)}F(y_1,w_2;x;y_1,y_2)\right) + \mathcal{O}(\varepsilon^2)\Bigg]. \end{aligned}$$

Thus rather nontrivial integrals remain in these counterterms. Notice that even though the explicit ε-factor which arises from the divergent pieces is of lower order than in D_3, the overall divergence is of the same order as the integral over w_2 also diverges for $\varepsilon \searrow 0$.

The calculation for D_2 is similar as for D_1. The terms D_4 and D_5 only contribute at $\mathcal{O}(\varepsilon^{2-8/\kappa})$, and their calculation is rather involved. Actually we slightly cheated in the calculation of next-to-leading order terms for D_1: we replaced $w_2 - w_1$ by $w_2 - y_1$ even though this approximation fails when w_2 is close to the lower bound of its integration range. Corrections due to this approximation can be combined with the contributions from D_4.

In Appendix D we discuss how the regularized integrals are used to numerically compute the SLE boundary visit amplitudes.

5. Notions of SLE Boundary Visits and Applications

In this section we give the definition of chordal SLE in the upper half-plane $\mathbb{H}$, and give the conformal covariance rule to transport the boundary visit amplitudes from the half-plane to any other domain. We then consider alternative definitions of SLE boundary visits and discuss applications of our main result.

5.1. Definition of Chordal SLE in Half-Plane

By conformal invariance, it is sufficient to define the chordal SLE_κ in one reference domain with marked points. The most common choice is the upper half-plane $\mathbb{H}$, with the curve starting from 0 and ending at ∞. The following definition also gives a convenient time parametrization for the curve. To define the chordal SLE_κ in $(\mathbb{H}; 0, \infty)$, consider the Loewner chain

$$g_0(z) = z, \quad \frac{\mathrm{d}}{\mathrm{d}t} g_t(z) = \frac{2}{g_t(z) - X_t} \quad (\text{for } z \in \mathbb{H}) \tag{5.1}$$

where the driving process $(X_t)_{t \geq 0}$ is taken to be

$$X_t = \sqrt{\kappa}\, B_t$$

a multiple of the standard Brownian motion $(B_t)_{t \geq 0}$ on the real line—the parameter κ gives the variance increment per unit time.

The hull K_t of the chordal SLE_κ at time t is the closure of the set of points $z \in \mathbb{H}$ for which the solution to the Loewner differential equation, Eq. (5.1), has ceased to exist by time t. The hulls are growing compacts, $K_s \subset K_t$ for $s \leq t$. It can be shown [41] that the hulls are generated by a continuous curve $\gamma : [0, \infty) \to \mathbb{H}$ in the sense that the unbounded component of the complement $\mathbb{H} \backslash \gamma[0, t]$ of an initial segment up to time t coincides with the complement $\mathbb{H} \backslash K_t$ of the hull. We think of the chordal SLE_κ simply as this random curve γ.

5.2. Conformal Covariance of Boundary Visit Amplitudes

We content ourselves to writing down the solutions to the boundary visit question in the upper half-plane $\mathbb{H}$ for a chordal SLE_κ from x to ∞. The answer can be transported to other domains by conformal covariance as follows:

Let us denote by $\zeta^{(N)}_{(\Lambda; a, b)}(y_1, \ldots, y_N)$ the boundary zig-zag amplitude for chordal SLE_κ in domain Λ from a to b, defined in a similar manner as in the half-plane, when the points $y_1, \ldots, y_N \in \partial\Lambda$ are on smooth parts of the boundary of the domain. Consider the chordal SLE_κ curve γ in $(\Lambda; a, b)$, and a conformal map $f \colon \Lambda \to f(\Lambda)$. For boundary points $y \in \partial\Lambda$ at which $f'(y)$ exists, a neighborhood of y of radius ε is approximately mapped to a neighborhood of the image $f(y)$ and having radius $\varepsilon \times |f'(y)|$. The SLE curve itself is conformally invariant, that is, $f(\gamma)$ has the law of a chordal SLE_κ in $(f(\Lambda); f(a), f(b))$. Correspondingly, after passing to the limit of small radii in the definition of the amplitude

$$\lim_{\varepsilon \searrow 0} \left(\frac{1}{\prod_j \varepsilon_j^h} \times \mathsf{P}\left[\mathrm{SLE}_\kappa \text{ visits neighborhoods of } y_j \text{ of radii } \varepsilon_j\right] \right),$$

we get that the boundary zig-zag amplitudes satisfy the following conformal covariance rule:

$$\zeta^{(N)}_{(\Lambda;a,b)}(y_1,\dots,y_N) = \left(\prod_{j=1}^{N} |f'(y_j)|^h\right) \times \zeta^{(N)}_{(f(\Lambda);f(a),f(b))}\left(f(y_1),\dots,f(y_N)\right), \tag{5.2}$$

and similarly for the complete correlation functions $\chi^{(N)}_{(\Lambda;a,b)}$.

Appendix B.1 discusses this conformal covariance from the viewpoint of conformal field theory.

5.3. Different Definitions of SLE Boundary Visits

There are several formulations of boundary visits, and one expects many limits of the types of Eq. (1.2) or (1.3) to exist. Consider for example the following alternative formulations:

- *Touching small boundary intervals* (*for* $\kappa > 4$) In the phase $\kappa > 4$, where the curve γ can touch the boundary of the domain, a natural notion of reaching a neighborhood of a point $y_j \in \mathbb{R}\setminus\{x\} \subset \partial\mathbb{H}$ is that the curve γ touches the boundary between the point y_j and a point which is ε_j further away from the starting point x of the curve. If $y_j > x$ set $I_{\varepsilon_j}(y_j) = [y_j, y_j + \varepsilon_j]$ and if $y_j < x$ set $I_{\varepsilon_j}(y_j) = [y_j - \varepsilon_j, y_j]$. The corresponding boundary visit amplitude is given by the limit of

$$\varepsilon_1^{-h}\dots\varepsilon_N^{-h}\,\mathsf{P}[\gamma \cap I_{\varepsilon_j}(y_j) \neq \emptyset \quad \forall j = 1,2,\dots,N] \tag{5.3}$$

  as $\varepsilon_1,\dots,\varepsilon_N \searrow 0$.
- *Reaching small conformal distances from the boundary points* For $\Lambda \subsetneq \mathbb{C}$ a simply connected open domain and $z \in \Lambda$, define the conformal radius $\rho_\Lambda(z)$ such that if $f : \mathbb{D} \to \Lambda$ is a conformal map with $f(0) = z$, then $\rho_\Lambda(z) = |f'(0)|$. By Schwarz lemma and Köbe $\frac{1}{4}$-theorem, $\rho_\Lambda(z)$ is comparable to the distance of z to $\partial\Lambda$:

$$\frac{1}{4}\rho_\Lambda(z) \leq \operatorname{dist}(z, \partial\Lambda) \leq \rho_\Lambda(z).$$

  Now for $y_j \in \mathbb{R}\setminus\{x\} \subset \partial\mathbb{H}$, let U_j be the (unique) connected component of $\mathbb{H}\setminus\gamma$ such that $y_j \in \partial U_j$. Join to U_j its reflection across the real axis, to obtain a larger domain in which y_j is an interior point—more precisely, let V_j be the interior of $U_j \cup \mathbb{R} \cup U_j^*$, where $U_j^* = \{\bar{z} | z \in U_j\}$. The quantity $\rho_{\mathbb{H}\setminus\gamma}(y_j) = \rho_{V_j}(y_j)$ gives a conformally covariant notion of the distance of y_j to γ—recall that $\frac{1}{4}\rho_{\mathbb{H}\setminus\gamma}(y_j) \leq \operatorname{dist}(y_j, \gamma) \leq \rho_{\mathbb{H}\setminus\gamma}(y_j)$. The corresponding boundary visit amplitude is given by the limit of

$$\varepsilon_1^{-h}\dots\varepsilon_N^{-h}\,\mathsf{P}[\rho_{\mathbb{H}\setminus\gamma}(y_j) < \varepsilon_j \quad \forall j = 1,2,\dots,N] \tag{5.4}$$

  as $\varepsilon_1,\dots,\varepsilon_N \searrow 0$.

One could give an endless list of possible formulations: it is essentially possible to define the notion of a boundary visit as the intersection of the curve with a small neighborhood of any imaginable shape. Each of the different formulations admits both a complete correlation function analogous to Eq. (1.2) as exemplified in the two cases above, and an ordered zig-zag amplitude analogous to Eq. (1.3). The formulations (5.3) and (5.4) are convenient for various

reasons. In Appendix A we in particular present a derivation of the correct value of the scaling exponent $h = \frac{8-\kappa}{\kappa}$ given in (1.1) based on each of them.

5.4. Applications of the Results and Universal and Non-Universal Aspects

In Sect. 5.3 we have argued that the SLE boundary visit amplitudes describe the probabilities of events where the SLE trace comes close to marked boundary points, independent of the details of the definition of these events. In this section we mention further applications.

First, however, we emphasize that the details of the formulation or application affect a multiplicative constant in the answer, but not the functional shape of the zig-zag amplitude $\zeta^{(N)}(x; y_1, \ldots, y_N)$ or the correlation function $\chi^{(N)}(x; y_1, \ldots, y_N)$. For example, visiting small neighborhoods of different shapes should happen with comparable but not necessarily equal probabilities. In renormalization group language, the multiplicative constants are non-universal, whereas the functions $\zeta^{(N)}(x; y_1, \ldots, y_N)$ and $\chi^{(N)}(x; y_1, \ldots, y_N)$ are universal as scaling functions (correlation functions). Also some ratios of the multiplicative constants are universal: the most immediate example comes from considering the formula

$$\chi^{(N)}(x; y_1, \ldots, y_N) = \sum_{\sigma \in \mathfrak{S}_N} \zeta^{(N)}(x; y_{\sigma(1)}, \ldots, y_{\sigma(N)})$$

for the complete correlation function as a sum over different orders of visits—for the formula to be meaningful, the ratios of the different multiplicative constants for a given N have to be independent of the formulation.

A slightly trivial but nevertheless illuminating example of the universality of the functional shape and non-universality of the constant factor is to imagine what would have happened in Eq. (1.2) had we chosen to measure the size of the semi-disk neighborhoods with diameter ε instead of radius ε—the limit would obviously have been a factor 2^{Nh} smaller. As a nontrivial example, note that the literature contains two definitions of the SLE Green's function at interior points: one for neighborhoods defined with usual Euclidean distances, and another with conformal radius. It has been shown in [35] that the two Green's functions are the same up to a multiplicative constant (whose value is not explicitly known). In fact, the idea used in [35] is the correct explanation with SLE analysis of the universality of the functional shape of $\zeta_\omega^{(N)}$ and of the non-universality of the multiplicative constant. Roughly, if the SLE curve is conditioned to approach a point y, and one considers the curve locally near y, then in small scale the curve will look like it is drawn from a certain stationary distribution which is independent of what other far away points the curve is conditioned to visit. The curve with stationary law has certain non-zero probabilities of hitting a half-disk, boundary interval, or some other shape, and the ratios of these probabilities give the ratios of the amplitudes in the respective formulations.

In most cases, an exact formula for the non-universal multiplicative constants would be too much to hope for. However, Appendix A.1 contains one

concrete example in which the multiplicative constant is explicit: the $N = 1$ case in the "touching small boundary intervals" formulation is Eq. (A.1).

In Sect. 2 we argued that the amplitudes $\zeta^{(N)}$ and $\chi^{(N)}$ are obtained as solutions to a system of linear partial differential equations and boundary conditions. Solutions to this linear homogeneous problem are at best fixed up to a multiplicative constant, and the above considerations explain that this is only natural.

5.4.1. Boundary Visit Probabilities for Interfaces in Lattice Models. The principal motivation for the introduction and study of SLEs is that these random curves are the scaling limits of interfaces in lattice models of statistical mechanics at criticality. The SLE zig-zag probabilities are closely related to the probabilities for an interface in a lattice model to pass through given boundary points. For some models these probabilities in turn have direct physical interpretations, for example the boundary visit probability of interface in Q-random cluster model (Q-FK model) gives a boundary magnetization in the Q-Potts model via the Edwards–Sokal coupling [20].

For lattice model interfaces, too, the exact meaning of passing through a boundary point involves some choices, and different choices lead to different non-universal constant factors. The idea, however, always is to consider the model on a lattice domain Λ_δ of small lattice mesh size δ so that Λ_δ approximates a given planar domain $\Lambda \subset \mathbb{C}$ as $\delta \searrow 0$. One defines a boundary visit locally by requiring the lattice model interface to use, for example, a given edge or a given vertex near a marked point $y \in \partial\Lambda$ on the boundary. The probabilities of thus visiting N marked points on smooth parts of the boundary $\partial\Lambda$ are of order δ^{Nh}, provided that also the lattice approximations to the boundary have a regular and consistent local structure as $\delta \searrow 0$. Thus the lattice mesh δ serves as a measure of the neighborhood size, and much like in (1.2), the limit of the lattice model interface probability renormalized by δ^{-Nh} should be given by $\zeta^{(N)}$ or $\chi^{(N)}$, correctly conformally transported to the domain Λ by the conformal covariance rule of Sect. 5.2.

In Sect. 6, we discuss in more detail a few well-known lattice models and the details of the question of boundary visits of interfaces for them. We find that our formulas for $\zeta^{(N)}$ and $\chi^{(N)}$ are in very good agreement with the probabilities obtained from numerical simulations of these lattice models.

5.4.2. Covariant Measure of SLE on the Boundary. For lattice models, the most natural way of quantifying boundary proximity of an interface is by counting the number of boundary points visited by it, e.g., within a given boundary segment. In the scaling limit, the count must be renormalized properly by a power of the lattice spacing δ: the probability to visit a given boundary point is of order δ^h and the expected number of boundary points visited in a segment is of order δ^{h-1} (which diverges for $\kappa > 4$ and tends to zero for $\kappa < 4$).

The article [4] presents a construction of a covariant measure of SLEs on the boundary, which is the analogous boundary proximity count in the continuum. Roughly, this SLE boundary measure $\mu_{\Lambda;a,b}$, associated with the chordal SLE_κ in domain Λ from a to b, is a random locally finite measure

$\mu_{\Lambda;a,b}$ on $\partial\Lambda$, supported on the set where the chordal SLE_κ curve $\gamma_{\Lambda;a,b}$ from a to b in Λ touches the boundary $\partial\Lambda$. This measure is conformally covariant with exponent h, i.e., if $f\colon \Lambda \to \Lambda'$ is a conformal map, then $\mu_{\Lambda;a,b}(\mathrm{d}x) = |f'(x)|^h\, \mu_{f(\Lambda);f(a),f(b)}(\mathrm{d}f(x))$ in law. The domain Markov property for the measure states that conditionally on an initial segment of the chordal SLE_κ curve in $(\Lambda; a, b)$, the measure $\mu_{\Lambda;a,b}$ restricted to a set $A \subset \partial\Lambda$ away from the initial segment has the same law as $\mu_{\Lambda\setminus\mathrm{segment};\mathrm{tip},b}$ restricted to the same set. These properties characterize the family of measures $\mu_{\Lambda;a,b}$ up to a multiplicative constant.

The SLE boundary measure is constructed by studying a local martingale associated with the correlation function $\chi^{(1)}$. By construction this function $\chi^{(1)}$ then gives the density of the expectation of $\mu = \mu_{\mathbb{H};0,\infty}$ with respect to the Lebesgue measure on $\mathbb{R}$. The higher complete correlation functions $\chi^{(N)}$ of the present article should be the integral kernels for moments of the SLE boundary measure

$$\varepsilon^{-N}\,\mathsf{E}\left[\prod_{j=1}^{N}\mu([y_j, y_j+\varepsilon])\right] \sim \text{const.} \times \chi^{(N)}(0; y_1, \dots, y_N).$$

In fact the proof [4] of non-triviality of the constructed SLE boundary measure employs the two-point function $\chi^{(2)}$, which had been found in [51].

A convenient way to explicitly characterize a random measure is to give its Laplace transform. Denote briefly $\mu = \mu_{\mathbb{H};0,\infty}$. For a test function $\phi\colon \mathbb{R}\setminus\{0\} \to \mathbb{R}$ let

$$L(\phi) := \mathsf{E}[e^{-\int_{\mathbb{R}}\phi\mathrm{d}\mu}]$$

be the Laplace transform of μ at ϕ. For the sake of concreteness, consider ϕ supported on the positive real axis. Then the expansion of the Laplace transform around the zero function is given by

$$\begin{aligned} L(\varepsilon\phi) &= \mathsf{E}[e^{-\varepsilon\int_{\mathbb{R}}\phi\mathrm{d}\mu}] \\ &= 1 - \varepsilon\mathsf{E}\left[\int_{\mathbb{R}}\phi(y)\mathrm{d}\mu(y)\right] + \frac{\varepsilon^2}{2}\mathsf{E}\left[\iint\phi(y_1)\phi(y_2)\mathrm{d}\mu(y_1)\mathrm{d}\mu(y_2)\right] + \cdots \\ &= 1 + \sum_{N=1}^{\infty}(-\varepsilon)^N c_N \int\cdots\int_{\{y_1<y_2<\cdots<y_N\}}\phi(y_1)\cdots\phi(y_N) \\ &\quad \times \chi^{(N)}(0; y_1, \dots, y_N)\,\mathrm{d}y_1\ldots\mathrm{d}y_N, \end{aligned}$$

where c_N are non-universal multiplicative constants.

The construction of [4] establishes that a unique (up to normalization) random measure satisfying the required abstract properties exists. The results of this article in principle give explicit formulas for the random measure in terms of integral kernels for its moments or the power series expansion of its Laplace transform.

5.4.3. Conditioned SLE and First Visit Point Recursion for the Zig-Zag Amplitudes. Let us discuss one more interpretation of the results, which in

fact also suggests a natural strategy of rigorous proof that our formulas give the order refined SLE Green's functions on the boundary, as defined in Sect. 1 or alternatively in Sect. 5.3.

Consider conditioning the chordal SLE_κ curve γ to visit a boundary point y, for definiteness in $(\mathbb{H}; x, \infty)$ again. As such, this is a zero-probability event (for $\kappa < 8$), and one must perform a limiting procedure to properly define the conditioning: first condition on visiting $B_\varepsilon(y)$ and then let $\varepsilon \searrow 0$. The conditioned curve can be described explicitly: its Radon–Nikodym derivative with respect to the ordinary chordal SLE is proportional to the indicator of the event of the visit, and in the limit $\varepsilon \searrow 0$ we get a Girsanov transform of the ordinary chordal SLE

$$\frac{\mathrm{d}\mathsf{P}^{\mathrm{cond.}}_{(\mathbb{H};x,y,\infty)}}{\mathrm{d}\mathsf{P}_{(\mathbb{H};x,\infty)}}\bigg|_{\mathcal{F}_t} \propto \chi^{(1)}_{\mathbb{H}\setminus K_t}(\gamma(t); y) = |g_t'(y)|^h \, \chi^{(1)}(X_t; g_t(y)).$$

This description of the conditioned curve is equivalent to the more familiar $\mathrm{SLE}_\kappa(\rho)$ with $\rho = \kappa - 8$, i.e., the random Loewner chain (5.1) with driving process given by

$$X_0 = x, \quad \mathrm{d}X_t = \sqrt{\kappa}\,\mathrm{d}B_t + \frac{\rho}{X_t - g_t(y)}\mathrm{d}t, \quad \text{where } \rho = \kappa - 8.$$

After the random time when the conditioned curve reaches y (i.e., when $|X_t - g_t(y)| \to 0$), the curve will continue like an ordinary chordal SLE in the complement of the initial segment of the curve up to that time.

Using the one-point function $\chi^{(1)}$, one may thus describe the SLE conditioned to visit a given boundary point. Conditioning on visiting several points could be similarly done with our functions $\chi^{(N)}$ or $\zeta^{(N)}$. Below we will, however, turn the logic around and see how our formulas could be rigorously proved using this conditioning.

The idea is to use the conditioning to reduce the N-point function question to an $(N-1)$-point question. Namely, for the SLE curve γ to make visits to $B_{\varepsilon_1}(y_1), \dots, B_{\varepsilon_N}(y_N)$ in this order, it needs to make the first visit to y_1 by definition, and we may proceed by conditioning on this. We know, for example by considerations similar to Appendix A.1 or A.2, that the probability of this first visit is of order $\varepsilon_1^h \, \chi^{(1)}(x; y_1)$, and we can describe the conditional law of the curve given this first visit essentially by the $\mathrm{SLE}_\kappa(\rho)$ process above. After the time τ of the first visit, the curve is again a chordal SLE in the random domain $\mathbb{H}\setminus K_\tau$ at that time, and we would like it to visit the neighborhoods of the $N-1$ remaining points $y_2, \dots, y_N$. We may inductively assume that the $(N-1)$-point visit formulas $\zeta^{(N-1)}$ for chordal SLE have been established. Thus we need to be able to average the $(N-1)$-point zig-zag amplitude $\zeta^{(N-1)}_{\mathbb{H}\setminus K_\tau}(\gamma_\tau; y_2, \dots, y_N)$ over the randomness of the domain $(\mathbb{H}\setminus K_\tau; \gamma_\tau, \infty)$ that remains after the first visit. That will be achieved if we can construct a martingale for the conditioned SLE, whose value at the time τ is $\zeta^{(N-1)}_{\mathbb{H}\setminus K_\tau}(\gamma_\tau; y_2, \dots, y_N)$. The key point is that such a martingale is constructed using the formula for $\zeta^{(N)}$ that we

find in the present work—namely we set

$$M_t = \prod_{j=2}^{N} |g_t'(y_j)|^h \times \frac{\zeta^{(N)}(X_t; g_t(y_1), \ldots, g_t(y_N))}{\chi^{(1)}(X_t; g_t(y_1))}.$$

This is a local martingale by the differential Eq. (A.3) that our $\zeta^{(N)}$ satisfies, and its value at time τ is the desired $(N-1)$-point zig-zag amplitude in the random domain $\mathbb{H}\backslash K_\tau$ essentially by the asymptotics conditions (2.7) we impose on $\zeta^{(N)}$. What remains is to show that $(M_t)_{t\in[0,\tau]}$ is a uniformly integrable martingale. This relies partly on a priori estimates of SLE probabilities [10,39] and on careful control of the functions appearing in the spin chain–Coulomb gas correspondence of the present article and in [30]. One also needs to control some approximations made, but roughly speaking at this stage optional stopping for the martingale (M_t) proves that $\zeta^{(N)}$ gives the N-point boundary zig-zag amplitude or N-point order refined SLE Green's function on the boundary.

Carrying out the proof with this strategy is the topic of a subsequent work in collaboration with Konstantin Izyurov.

6. Comparisons with Lattice Model Simulations

It is somewhat intricate and computationally demanding to obtain satisfactory computer simulations of SLE curves [29]. Therefore, comparing our results with direct numerics of SLEs would be difficult. A more practical alternative is to simulate lattice models whose interfaces tend to SLEs in the scaling limit. The boundary visits in such lattice models indeed constitute a natural interpretation and an important physical application of our results, as discussed in Sect. 5.4.1. In the present section we elaborate on the idea in the context of various lattice models. We discuss simulation of these models and their interfaces and boundary visits of the interfaces. Finally, we compare the numerical results obtained from these simulations to our solution presented in Sects. 3 and 4.

On physical grounds it is completely natural to expect that the scaling limit of renormalized lattice interface visit probabilities is proportional to the SLE Green's functions $\chi^{(N)}$ and $\zeta^{(N)}$. We nevertheless remark that even in models whose interface is rigorously known to converge to a chordal SLE in the scaling limit (e.g., Sects. 6.1.2–6.1.4 below), highly nontrivial additional mathematical work would be needed to establish this. Actually, the validity of the physically unsurprising equivalence is highly sensitive to the details of the lattice approximation of the domain boundary, and again even valid approximation schemes lead to different non-universal proportionality constants. Incidentally, the equivalence of the two formulations has been rigorously established for one case: one- and two-point boundary visits of the FK-Ising model interface (Sect. 6.1.4 below) on boundary segments parallel to coordinate axes—the boundary visit probabilities (or equivalent boundary spin correlation functions) were used in [27] as a technique to control the scaling

limit of an interface in a dual model (the Ising model with particular boundary conditions). Our simulation results below of course show a good match to our analytical solution, and thus clearly support the physically expected equivalence of the formulations.

Let us still make general comments about the numerical comparison of simulation data with our main results. Small lattice mesh sizes δ are of course desirable to reduce finite size scaling effects, i.e., to obtain better approximations to the conformally invariant scaling limit situation. As always, however, small mesh size δ or corresponding large size of the simulated system quickly increases needed computational resources, particularly so in critical models that we are interested in. For our question, there is yet another difficulty. With lattice mesh δ, the probability of having N boundary visits by the interface is of order δ^{Nh}, where $h = h_{1,3}(\kappa) = \frac{8-\kappa}{\kappa} > 0$ and κ depends on the model. We are thus interested in rare events, whose probability further decreases with mesh size δ and number of visit points N, so in order to obtain acceptable statistics, we need increasingly large numbers of samples. The trade-off between reducing finite size effects and improving statistics is, therefore, a major issue. High values of the exponent $h_{1,3}(\kappa)$, or correspondingly models with small κ are the most problematic. We have simulated models corresponding to $\kappa = 2$ (LERW, Sect. 6.1.2), $\kappa = \frac{24}{5}$, and $\kappa = \frac{16}{3}$ (different FK-models, Sect. 6.1.4), and $\kappa = 6$ (percolation, Sect. 6.1.3). In the most difficult case $\kappa = 2$ we are essentially limited to $N \leq 2$, and significant finite size effects still remain in the data (see Fig. 10). In the least problematic case $\kappa = 6$, finite size effects can be made reasonably small up to $N = 4$ (see Fig. 13). The issues in numerical evaluation of our analytical results have been separately discussed in Appendix D, and we note that besides large N, difficulties also arise due to small κ.

6.1. Lattice Model Interfaces

6.1.1. Relevant Domains and Conformal Maps. We have simulated different statistical models in lattice approximations of domains of the simplest possible shapes: the square and the equilateral triangle. The frequencies of boundary visits of interfaces have been collected, and for comparison with our formulas they need to be transported to the half-plane $\mathbb{H}$ by conformal maps. The domains, lattice approximations, and the conformal maps are described below.

The unit square

$$S = \{z \in \mathbb{C} | 0 < \Re\mathfrak{e}(z) < 1,\ 0 < \Im\mathfrak{m}(z) < 1\}$$

will be discretized by a square lattice of small mesh size δ: the vertex set is $S_\delta = \delta\mathbb{Z}^2 \cap \overline{S}$ and edges connect vertices at distance δ. A conformal map $f_S \colon S \to \mathbb{H}$ from the square to the half-plane is the Jacobi elliptic sine function sn composed with a Möbius transform, and our choice is

$$f_S(u) = \frac{\mathrm{sn}\left((2u-1)K; m\right) + 1}{\mathrm{sn}\left((2u-1)K; m\right) - 1/\sqrt{m}} \frac{\mathrm{sn}\left(K; m\right) - 1/\sqrt{m}}{\mathrm{sn}\left(K; m\right) + 1},$$

where m is the elliptic modulus of square and $K = K(m)$ is the corresponding complete elliptic integral of the first kind. This choice is such that the lower

left corner is mapped to the origin, the top right corner to infinity, and the bottom right and top left corners to $+1$ and -1, respectively.

The unit equilateral triangle

$$T = \left\{ z \in \mathbb{C} \;\middle|\; -\frac{1}{2} < \Re\mathfrak{e}(z) < \frac{1}{2},\ 0 < \Im\mathfrak{m}(z) < \frac{\sqrt{3}}{2} - \sqrt{3}\,|\Re\mathfrak{e}(z)| \right\}$$

will be discretized by a fine triangular lattice. The small mesh size δ is the distance between its neighboring vertices, and T_δ denotes the set of such triangular lattice vertices in $\overline{T}$. A conformal map $f_T \colon T \to \mathbb{H}$ from the triangle to the half-plane is the inverse of a Schwarz-Christoffel map,

$$f_T^{-1}(z) = \frac{\Gamma(\frac{5}{6})}{\sqrt{\pi}\,\Gamma(\frac{1}{3})} \times \int_0^z (1-w)^{-2/3}(1+w)^{-2/3}\mathrm{d}w.$$

The choice is such that f_T maps the midpoint of the bottom side to the origin, and the left and right bottom corners to -1 and $+1$, respectively.

6.1.2. Loop-Erased Random Walk. The loop-erased random walk (LERW) is a path obtained by performing loop erasure to a finite piece of a simple random walk. The conformal invariance of the scaling limit of interior-to-boundary LERW was shown in [38]. Different LERW variants, including the one we study here, were proven to have conformally invariant scaling limits in [53]. The scaling limit of the path we describe below is chordal SLE_2.

We consider the square lattice domain S_δ, which approximates the unit square, as in Sect. 6.1.1. We send a simple random walk $(W_n)_{n=0}^{\infty}$ at the lower left corner $W_0 = \delta + \mathrm{i}\delta$. We condition on the event that the walk exits the square via the upper right corner, and we denote the time of exit by τ. The loop-erased random walk is the simple path γ_δ which is obtained from $(W_n)_{n=0}^{\tau-1}$ by chronologically erasing all loops (sequences of consecutive steps which start and end at the same vertex). Figure 5 shows a realization of a LERW in S_δ with lattice mesh $\delta = \frac{1}{150}$. The figure also suggests that the loop-erased path is unlikely to come close to the boundary except at the two end points, indicating the difficulties of sampling boundary visits of this model with fine lattice mesh.

We define boundary visit as the event that the path γ_δ passes through a vertex x at distance δ from the boundary ∂S of the square. The behavior of the boundary visit probabilities should be

$$\begin{aligned} &\mathsf{P}[\gamma_\delta \text{ visits } x_1, x_2, \ldots, x_N] \\ &\quad \approx \text{const.} \times \prod_{j=1}^{N} \left(|f'(x_j)|\,\delta\right)^h \times \zeta^{(N)}(0; f(x_1), \ldots, f(x_N)), \end{aligned} \tag{6.1}$$

where $h = h_{1,3}(2) = 3$ and $f = f_S : S \to \mathbb{H}$ is the conformal map from the unit square to the half-plane given in Sect. 6.1.1.

The simulation is done as follows: we sample a conditioned random walk using explicitly calculated transition probabilities, then perform the loop erasure of the random walk, and collect data of visited boundary points of the loop erasure. We correct the boundary visit frequencies obtained from the

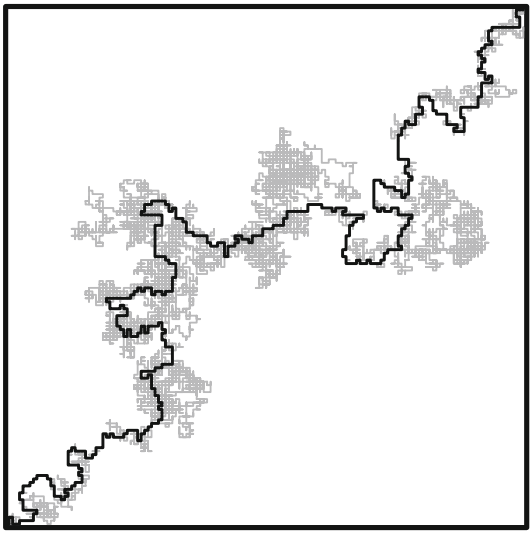

FIGURE 5. A loop-erasure of a random walk in a *box*, from the *bottom-left corner* to the *top-right corner*

simulations by dividing by the factor $\prod_{j=1}^{N} (|f'_S(x_j)|\,\delta)^h$ that appears in (6.1), and then compare with our SLE boundary visit amplitude $\zeta^{(N)}$ at $\kappa = 2$. Note that the probabilities decay as δ^{Nh} and due to the high value of the exponent $h = h_{1,3}(2) = 3$ it is very hard to obtain good statistics with a small mesh size, especially for higher N. Figures 8 and 10 present data from simulations with lattice mesh $\delta = \frac{1}{120}$ and 10^7 realizations and with lattice mesh $\delta = \frac{1}{60}$ and 10^8 realizations, respectively. The agreement with our analytical results is reasonable. The otherwise difficult small κ turns out to have one advantage: the orders of magnitude of the visits in different pieces of the plot are rather different, and one notes in particular that the universal ratio of the boundary visit amplitudes with $y_2 < x = 0$ and $y_2 > y_1 = 1$ obtained by our method is undeniably correct—a single multiplicative constant has been fitted for the two pieces $\zeta^{(2)}_{++}$ and $\zeta^{(2)}_{+-}$ in Fig. 10.

6.1.3. Percolation. Percolation is an easily defined model of statistical physics, showing nevertheless interesting critical behavior. Its conformal invariance had been predicted in [32], and impressive exact results had been predicted using conformal field theory. The proof of conformal invariance of scaling limit of site percolation on triangular lattice was obtained by Smirnov in [45], based on a formula found by Cardy [12]. The interface that we define below converges in the scaling limit to chordal SLE_6, see [14,45].

We take a domain T_δ which is a triangular lattice approximation of an equilateral triangle as in Sect. 6.1.1. Triangular lattice site percolation with parameter $p \in (0,1)$ associates with each vertex of a domain in the triangular lattice (which we portray as a hexagon, a face of the dual lattice) a color:

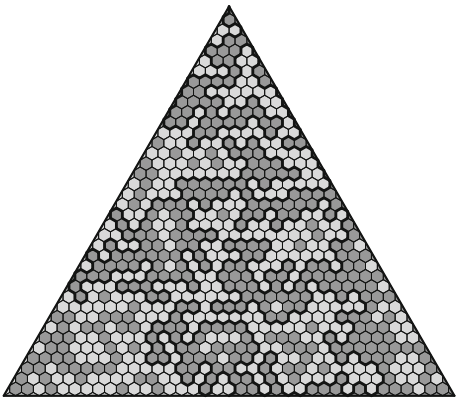

FIGURE 6. Critical percolation in a *triangle*, the exploration path starting from the *middle of the bottom side leaves white hexagons to its left* and *black hexagons to its right*

white with probability p and black with probability $1-p$, independently. One studies questions concerning connected components of sites of one color at the critical parameter value $p = p_c = \frac{1}{2}$. We impose white boundary conditions on the left half of the boundary $\partial T_\delta \cap \{\Re\mathfrak{e}(z) < 0\}$, and black on the right half $\partial T_\delta \cap \{\Re\mathfrak{e}(z) > 0\}$. There is a unique path γ_δ on the dual lattice from the midpoint of the bottom side of the triangle to the top vertex of the triangle, leaving white vertices on the left and black vertices on the right. This path, commonly called the percolation exploration path, is our interface. Figure 6 shows a realization of the exploration path in T_δ with lattice mesh $\delta = \frac{1}{40}$. Quite the contrary to Fig. 5, here there is no shortage of places on the boundary that are visited by the path.

We define boundary visit as the event that the path γ_δ passes through the exteriormost corner x of a hexagon next to the boundary layer. The behavior of the boundary visit probabilities should be given by Eq. (6.1), where now $h = h_{1,3}(6) = \frac{1}{3}$ and $f = f_T \colon T \to \mathbb{H}$ is a conformal map from the triangle to the half-plane given in Sect. 6.1.1.

The simulation of percolation configurations hardly requires any comments. The only computationally intensive step is to extract the interface from the configuration. Another practical issue for high N, small δ, and large number of samples is the storage of the obtained data of boundary visits. Once the data of boundary visit frequencies is collected, we again correct them by dividing by the factor $\prod_{j=1}^{N} (|f_T'(x_j)|\,\delta)^h$ and then compare with our SLE boundary visit amplitude $\zeta^{(N)}$ at $\kappa = 6$. Figures 8, 9, 11, and 13 present data for $N = 1, 2, 3, 4$, respectively, obtained from simulations with lattice mesh $\delta = \frac{1}{500}$ and 10^5 realizations, with lattice mesh $\delta = \frac{1}{300}$ and 2×10^6 realizations, with lattice mesh $\delta = \frac{1}{80}$ and 10^6 realizations, and with lattice mesh $\delta = \frac{1}{160}$ and 2×10^8 realizations, respectively. The agreement with our analytical results is nearly perfect. Note again that for any fixed N, only one

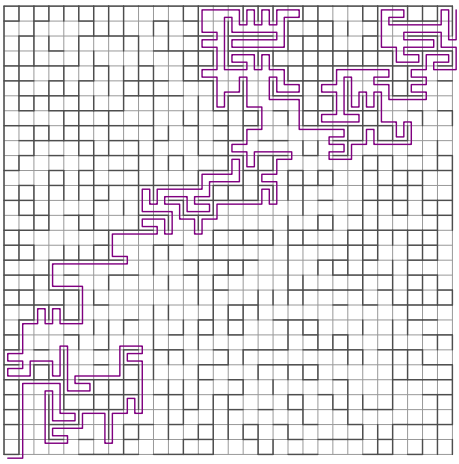

FIGURE 7. FK-model (random cluster model) interface closely follows the outer boundary of the cluster connected to the wired part of the boundary: the *left* and *top sides*

multiplicative constant has been fitted, and the ratios of the magnitudes of boundary visit frequencies in different pieces of the plots are obtained from our results.

6.1.4. FK-Model. The random cluster model (also called FK-model, named after Fortuin and Kasteleyn [21]) with parameters (p, Q) is a generalization of bond percolation, which for integer values of Q is closely related to the Q-Potts model. For $Q \in [0, 4]$ it is expected to undergo a continuous phase transition at the critical value $p = p_c(Q) = \frac{\sqrt{Q}}{1+\sqrt{Q}}$,[13] and behave conformally invariantly at the critical point. With Dobrushin boundary conditions, there is an interface somewhat analogous to the exploration path of percolation, which at the critical point is expected to converge in the scaling limit to (chordal) SLE_κ, where $\kappa = \kappa(Q) = \frac{4\pi}{\arccos(-\sqrt{Q}/2)}$. The SLE scaling limit is rigorously known in two special cases: the case $Q = 2$ is known as the FK-Ising model and the techniques of [46,47] led to a proof [13], and the limiting case $Q = 0$ corresponds to the uniform spanning tree treated in [38]. Figure 7 shows a realization of $Q = 4$ FK-model interface with lattice mesh $\delta = \frac{1}{30}$, together with the interface.

It is worth noticing that the probabilities of boundary visits of the interface can be used to express the boundary magnetization, and more generally boundary spin correlation functions of the Potts model, with one of the boundary arcs having fixed spin. These exemplify some of the physical applications of the boundary visit problem.

For simulations in this article we restrict our attention to the values $Q = 2$ and $Q = 3$. Integer values of Q are convenient because there exists a

[13] That this self-dual value is critical has been established in [9] for $Q \geq 1$.

Monte Carlo Markov chain by Swendsen and Wang, which does not suffer as much of critical slowing down as the more common Markov chains based on local updates [50]. This efficiency of simulation is important, because we need good statistics to get accurate information about the small probability events of multiple boundary visits. Swendsen–Wang algorithm works for all integer Q, but for $Q > 4$ the model has a first-order phase transition and does not exhibit conformal invariance. For $Q = 4$ the finite-size corrections scale too badly for reliable simulations.

We define the model in the lattice approximation S_δ of the unit square S given in Sect. 6.1.1. The random cluster model is a random subset ω of edges of S_δ, with probability proportional to

$$\mathsf{P}_{(p,Q)}[\{\omega\}] \propto \left(\frac{p}{1-p}\right)^{|\omega|} Q^{k(\omega)},$$

where $k(\omega)$ denotes the number of connected components ("clusters") of the subgraph of S_δ defined by all vertices and the edges ω. The appropriate Dobrushin boundary conditions amount to conditioning on the event that all edges of the left and top boundaries of the square are in ω. The interface γ_δ is the path obtained as the boundary of the $\frac{\delta}{4}$-thickening of the component connected to the left and top, i.e., a path closely surrounding the "wired cluster", see Fig. 7.

The interface being defined on a lattice different from the square lattice, it is now natural to define boundary visits to points with half-lattice-unit coordinates. Moreover, the wiring of the boundary introduces some asymmetry in the definition. On the bottom we say that $(x + \frac{1}{2})\delta$ is visited if the path goes outside the domain at $(x + \frac{1}{2})\delta - \frac{\delta}{4}\mathrm{i}$, and on the right a similar definition is used. On the left we say that $\mathrm{i}(y + \frac{1}{2})\delta$ is visited if the path comes to the point $\mathrm{i}(y+\frac{1}{2})+\frac{\delta}{4}$, and on the top a similar definition is used. These definitions are natural, as is illustrated by the figure of the interface. The behavior of the boundary visit probabilities should again be given by Eq. (6.1), where now $h = h_{1,3}(\frac{16}{3}) = \frac{1}{2}$ for $Q = 2$ and $h = h_{1,3}(\frac{24}{5}) = \frac{2}{3}$ for $Q = 3$, and $f = f_S \colon S \to \mathbb{H}$ is the conformal map from the unit square to the half-plane as in Sect. 6.1.1.

Our simulation runs the Swendsen–Wang Monte Carlo Markov chain and collects time averages of the boundary visiting events. Neither the initial transient nor the autocorrelation time at the stationary distribution causes any noticeable statistical errors—the inevitable trade-off between finite size effects and computational time is the main source of numerical error. We correct the boundary visit frequencies obtained from the simulations by dividing by the factor $\prod_{j=1}^{N} (|f_S'(x_j)|\,\delta)^h$ and then compare with our SLE boundary visit amplitude $\zeta^{(N)}$ at $\kappa = \kappa(Q)$. For $N \le 3$ we get good enough statistics and the agreement with our analytical results is very good: Figs. 8 and 9 show $N = 1$ and $N = 2$ data for both $Q = 2$ and $Q = 3$, with $\delta = \frac{1}{100}$ and 10^7 samples in each case. We have included the plot of three-point boundary visit data in Fig. 12 only for $Q = 3$ because the value of κ ($\kappa = \frac{24}{5}$) is sufficiently different

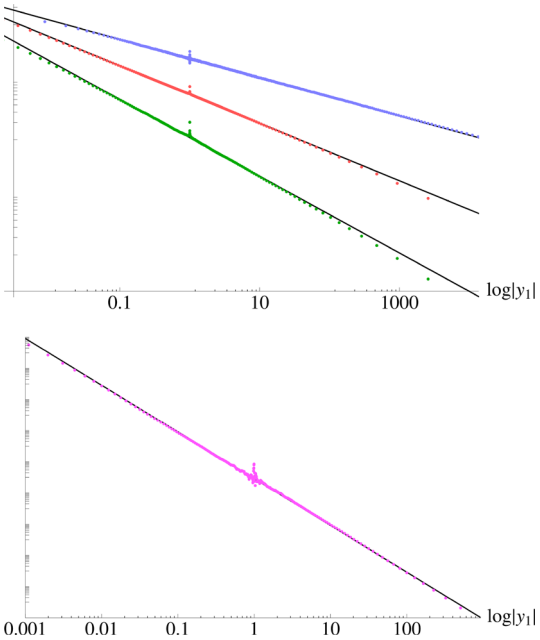

FIGURE 8. Data of one-point boundary visit frequencies collected from simulations of lattice models. We have set $x = 0$ and plotted the conformally corrected frequency of visits as a function of y_1 on log-log scale. The *solid lines* are fitted power laws, in accordance with $\zeta^{(1)}(x, y_1) \propto |y_1 - x|^{-h}$. The simulations are done in polygonal domains (*triangle* for percolation and *square* for the other models), and the bumps in the data in the *middle of the plots* are due to a corner of the polygonal domain. *Upper plot* percolation (*top*, *blue*), FK-Ising model (*middle*, *red*), FK model with $Q = 3$ (*bottom*, *green*). *Lower plot* loop-erased random walk (color figure online)

from the case of percolation ($\kappa = 6$) so that the shapes of the functions are clearly distinct (for this we use $\delta = \frac{1}{100}$ and 5×10^6 samples).

We still point out how remarkably much is known of the FK-Ising case $Q = 2$, largely owing to the techniques of discrete complex analysis [15,16,47,48]. This is the only lattice model for which the scaling limit of renormalized boundary visiting probabilities has in fact been proven to exist, and even the corresponding non-universal constants for $N = 1$ and $N = 2$ have been found explicitly [27]. The exact $N = 1$ formula reads for x away from the corners

$$\frac{1}{\sqrt{\delta}} \frac{1}{\sqrt{|f_S'(x)|}} \mathsf{P}_{\text{FK-Ising}}[\gamma_\delta \text{ visits } x] \underset{\delta \searrow 0}{\longrightarrow} \sqrt{\frac{1+\sqrt{2}}{2\pi}} \times |f_S(x)|^{-1/2}.$$

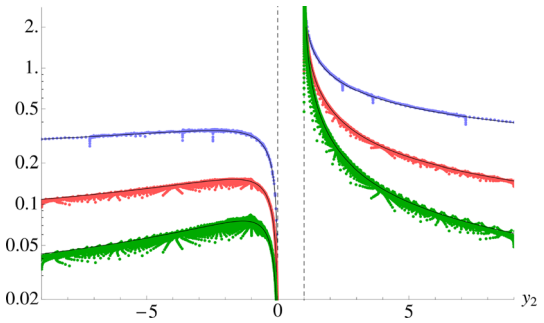

FIGURE 9. Data of two-point boundary visit frequencies collected from simulations of lattice models: percolation (*top*, *blue*), FK-Ising model (*middle*, *red*), FK-model with $Q = 3$ (*bottom*, *green*). We set $x = 0$, $y_1 = 1$ and plot the conformally corrected frequency as a function of y_2 on logarithmic scale. The *solid curves* are multiples of the two-point boundary visit amplitudes $\zeta^{(2)}(x; y_1, y_2)$, with the same multiplicative constant used for the two pieces: $\zeta_{++}(x; y_1, y_2)$ when $y_2 > 1$ and $\zeta_{+-}(y_2; x; y_1)$ when $y_2 < 0$. For FK-Ising we have used the known exact multiplicative constant from [27], for other models this non-universal constant is fitted to data (color figure online)

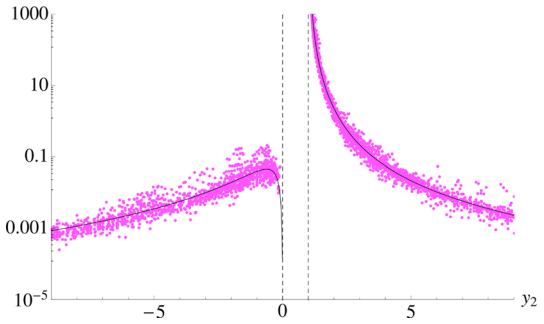

FIGURE 10. Data of two-point boundary visit frequencies collected from simulations of LERW. We set $x = 0$, $y_1 = 1$ and plot the conformally corrected frequency as a function of y_2 on logarithmic scale. The *solid curves* are multiples of the two-point boundary visit amplitudes $\zeta^{(2)}(x; y_1, y_2)$, with again the fitted multiplicative constant being the same for the two pieces

We find excellent numerical agreement of the exponent value (best fit gives 0.499872 instead of $\frac{1}{2}$) and the non-universal multiplicative constant (best fit gives 0.618241 instead of $\sqrt{\frac{1+\sqrt{2}}{2\pi}} \approx 0.619866$). The exact $N = 2$ formula reads

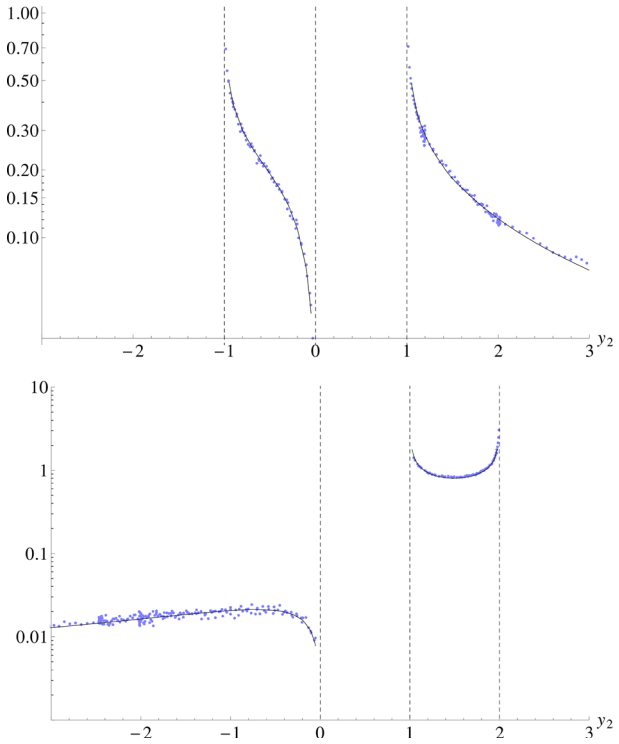

FIGURE 11. Data of three-point boundary visit frequencies collected from simulations of critical percolation. In the *upper plot* we set $x = 0$, $y_1 = 1$, $y_3 = -1$, and in the *lower plot* we set $x = 0$, $y_1 = 1$, $y_3 = 2$. In *both plots* the conformally corrected frequency is shown as a function of y_2 on logarithmic scale. The *solid curves* are multiples of the three-point boundary visit amplitudes $\zeta^{(3)}(x; y_1, y_2, y_3)$ (that is, combinations of ζ_{+--} and ζ_{++-} on the *upper* and of ζ_{+-+} and ζ_{+++} on the *lower plot*). The fitted multiplicative constant is again the same for all the different pieces

for x_1, x_2 away from corners and on the same side

$$\frac{1}{\delta}\,\frac{1}{\sqrt{|f_S'(x_1)|\,|f_S'(x_2)|}}\,\mathsf{P}_{\text{FK-Ising}}\left[\gamma_\delta \text{ visits } x_1 \text{ then } x_2\right]$$
$$\xrightarrow[\delta\searrow 0]{} \frac{(4+2\sqrt{2})\,\Gamma(\frac{3}{4})^2}{\pi^{5/2}} \times \frac{{}_2F_1\left(\frac{-1}{2}, \frac{3}{4}; \frac{3}{2}; 1-\frac{f_Q(x_1)}{f_Q(x_2)}\right)}{\sqrt{f_Q(x_1)}\,\sqrt{f_Q(x_2)-f_Q(x_1)}}.$$

The solid line in the middle plot in Fig. 9 uses this explicit non-universal multiplicative constant. This comparison to an exact scaling limit result gives a fair idea of the finite-size effects present in the simulation data of the FK-Ising model, but one must remember that the finite-size corrections scale differently for other models.

6.2. Simulation Data and Results of the Comparison

Simulation data and corresponding plots of our analytical results are presented in Figs. 8, 9, 10, 11, 12 and 13. The general conclusion is that the boundary visit probabilities of lattice model interfaces are in agreement with the predictions of type (6.1), where the amplitudes $\zeta^{(N)}$ are given by our main results. The main source of numerical error is finite-size effects.

Figure 8 shows one-point visit amplitudes on a log-log scale. The data from all models follow the power law $\zeta^{(1)}(x;y) = |y-x|^{-h}$ over a range of scales. The slope h is so different for $\kappa = 2$ that we have included a separate plot for the LERW case. Particular finite-size effects caused by error near the corners of the polygonal domain (triangle or square) are seen as bumps in the data. This effect diminishes for smaller δ, but it is visibly present in our data for all N. We have centered the $N = 1$ data so that the bump appears in the middle of the plot. For $N \geq 2$ this error affects a part of the data points across the whole range of the plot, resulting in an apparent failure of a perfect data collapse seen as thickness of the data point cloud.

Figures 9 and 10 show two-point boundary visit data on a logarithmic scale both in the case where the points y_1, y_2 to be visited are on the same side and in the case where they are on different sides. We have scaled to the case $y_1 = 1$ and plotted as a function of y_2, so that ideally all data from a given model should collapse on the curve constructed from the two pieces $\zeta^{(2)}_{++}(0;1,y_2)$ (for $y_2 > 1$) and $\zeta^{(2)}_{+-}(0;1,y_2)$ (for $y_2 < 0$). The same fitted multiplicative constant is used on both pieces for each model, and a clear agreement is observed in all cases. For the FK-Ising model case we have even

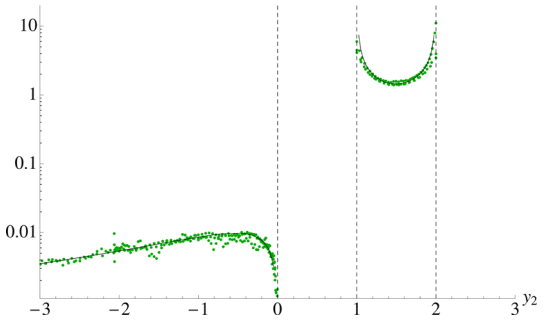

FIGURE 12. Data of three-point boundary visit frequencies collected from simulations of FK random cluster model with $Q = 3$. In this *plot* we set $x = 0$, $y_1 = 1$, $y_3 = 2$. The *plot* shows conformally corrected frequency as a function of y_2 on logarithmic scale. The *solid curves* are multiples of the three-point boundary visit amplitudes $\zeta^{(3)}(x;y_1,y_2,y_3)$ (that is, combinations of ζ_{+-+} and ζ_{+++}). The fitted multiplicative constant is again the same for the different pieces

avoided fitting, as we have been able to use the rare known explicit non-universal constant mentioned in Sect. 6.1.4. Data from all models show some finite-size effects, and roughly these are worse for smaller κ. The functional shape of all plots is nevertheless clearly correct. Again the shape for $\kappa = 2$ is so different from others that we have plotted it separately.

Figures 11 and 12 show three-point boundary visit data on a logarithmic scale for critical percolation and the critical $Q = 3$ FK-model, respectively. Data from percolation are still very well on the curves of our analytical results. In the $Q = 3$ FK-model the finite-size effects are more apparent. Again, a single fitted multiplicative constant has been used for all pieces. In particular the several orders of magnitude difference of the boundary visit frequencies on the two sides of Fig. 12 is in excellent agreement with our analytical results,

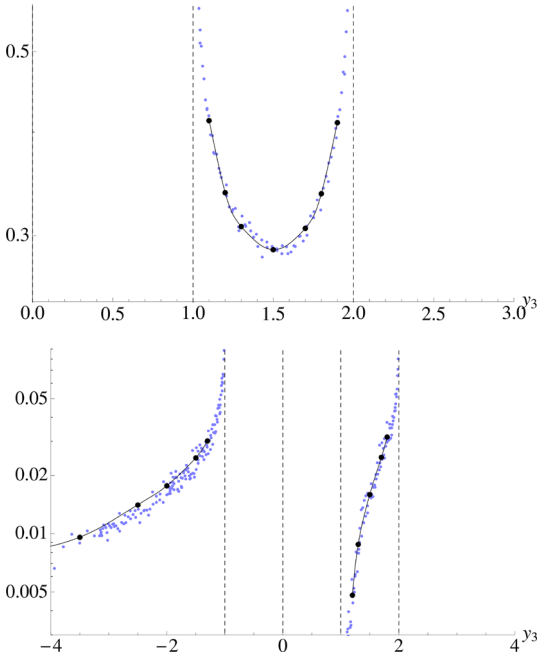

FIGURE 13. Data of four-point boundary visit frequencies collected from simulations of critical percolation. On the *upper plot* we set $x = 0$, $y_1 = -1$, $y_2 = 1$, $y_4 = 2$ and plot as a function of y_3. On the *lower plot* we set $x = 0$, $y_1 = 1$, $y_2 = -1$, $y_4 = 2$ and *plot* as a function of y_3. The conformally corrected frequencies in *both plots* are on a logarithmic scale. The *solid curves* are multiples of the four-point boundary visit amplitudes $\zeta^{(3)}(x; y_1, y_2, y_3, y_4)$ (that is, ζ_{-+++} on the *upper* and combinations of ζ_{+-++} and ζ_{+--+} on the *lower plot*). The fitted multiplicative constant is again the same for all the different pieces

even if, due to finite size effects, the data points otherwise only serve to give a sketchy idea of the shape of the function here.

Figure 13 shows four-point boundary visit data on a logarithmic scale for critical percolation. Both the numerical evaluation of our results $\zeta^{(4)}$ and decent simulation results are starting to be computationally very heavy—we have had to interpolate the analytical result from the calculations at the points shown on the plots. Nevertheless, the plot shows agreement of simulation data with our result.

7. Conclusions and Outlook

We have presented a method based on quantum group calculations, which gives explicit solutions of the chordal SLE_κ boundary visit probability amplitudes $\zeta^{(N)}$ and $\chi^{(N)}$ for arbitrary numbers N of marked boundary points. The answers are expressed in terms of linear combinations of Coulomb gas integrals and can be transformed to regularized real integrals. They give the universal answer to various formulations of the SLE boundary visit question, up to an overall non-universal constant, which depends on the formulation. In particular, they give the renormalized scaling limit boundary visit probabilities for lattice model interfaces.

Our results are obtained by solving a partial differential equation system with boundary conditions given recursively by the solutions with smaller number N of marked points. The system is suggested by plausible considerations of asymptotics, but we have not fully justified the use of this procedure. In an ongoing work with Konstantin Izyurov we plan to implement the strategy outlined in Sect. 5.4.3 to prove rigorously that the formulas obtained in the present article indeed give the SLE multi-point Green's functions on the boundary.

The method we have used is an application of the spin chain–Coulomb gas correspondence presented in a more general setup in [30] and applied to the problem of multiple SLE pure geometries and crossing probabilities in [31]. The method provides a systematic approach to a class of SLE and CFT problems depending on arbitrary numbers of marked points. It works directly only for irrational values of κ, but for questions such as boundary visit amplitudes, one can naturally extend the final results to all κ by requiring continuity. It would be interesting to generalize the spin chain–Coulomb gas correspondence itself to rational values of κ. This would presumably involve non-semisimple representation theory of the corresponding quantum group as well as results that correspond to logarithmic conformal field theory correlation functions.

It would be interesting to find also formulas for boundary visit probabilities for other variants of SLE, such as the radial SLE_κ and dipolar SLE_κ, $\mathrm{SLE}_\kappa(\rho)$, or even more general variants. Finally, one of the most natural remaining open questions about SLE is the bulk analogue of the question answered in the present article: finding a formula for the multi-point Green's function of the chordal SLE (for recent progress on this, see [10,36,39,41]).

Acknowledgements

Konstantin Izyurov and Eveliina Peltola have shared with us many of their insights during related collaborations and discussions. We also thank Dmitry Beliaev, Denis Bernard, Steven Flores, Christian Hagendorf, Clément Hongler, Peter Kleban, Antti Kupiainen, Greg Lawler, Jacob Simmons, and Stanislav Smirnov for interesting discussions and helpful comments. We also thank the anonymous referees for useful comments. This work was initiated in the ISF workshop "Random matrices and integrability: from theory to applications" in Yad Hashmona, and parts of it were carried out at Technion and University of Haifa at Oranim, at the University of Southern Denmark in Odense, and at the University of Geneva—we gratefully acknowledge the hospitality. We also acknowledge the Centro de Supercomputación de Galicia (CESGA) Supercomputing Center for computational time. It would be impossible to list the innumerable breweries which provided constant inspiration during the course of this work. N.J. is funded in part by the Spanish Grant FPA2011-22594, by Xunta de Galicia (Conselleria de Educación, Grants INCITE09-206-121-PR and PGIDIT10PXIB206075PR), by the Consolider-Ingenio 2010 Programme CPAN (CSD2007-00042), and by FEDER. N.J. is also supported by the Juan de la Cierva program. M.J. was supported in part by Grants PERG07-GA-2010-268246, PIF-GA-2011-300984, the EU program "Thales" and "HERAKLEITOS II" ESF/NSRF 2007-2013 and was also co-financed by the European Union (European Social Fund, ESF) and Greek national funds through the Operational Program "Education and Lifelong Learning" of the National Strategic Reference Framework (NSRF) under "Funding of proposals that have received a positive evaluation in the 3rd and 4th Call of ERC Grant Schemes". K.K. is supported by the Academy of Finland grant "Conformally invariant random geometry and representations of infinite dimensional Lie algebras".

Appendix A. SLE Derivations of the Exponent and a PDE

This appendix provides SLE calculations for the $N = 1$ case, to establish the same value of the exponent h with the two alternative notions of boundary visits given in Sect. 5.3. Visits to small boundary intervals are treated in Appendix A.1, and visits to small conformal distance neighborhoods in Appendix A.2. The latter implies up to constant bounds for the probabilities of boundary visits with the notion used in the introduction, since the conformal distance $\rho_{\mathbb{H}\setminus\gamma}(y)$ is proportional to the ordinary distance $d(\gamma, y)$. This up to constants estimate had also been derived differently in [2]. The work [34] establishes the existence of the SLE boundary Green's function in complete generality.

In Appendix A.3 we relate the second-order differential Eq. (2.3) to a martingale for the chordal SLE.

We do not provide a direct justification of the third-order differential Eq. (2.4) for the boundary visit amplitudes with SLE analysis, but instead only discuss them from the point of view of conformal field theory in Appendix B.2.

We nevertheless note that in [18,19,30,31] these equations were shown to hold for limiting cases of multiple SLE partition functions, and it is natural to interpret the boundary visiting SLE as a degeneration of such multiple SLEs.

A.1. Touching a Small Boundary Interval

One can write down the exact solution for the probability of a chordal SLE to hit a boundary interval $[y, y+\varepsilon]$ (for $y > x$) and do the asymptotics as $\varepsilon \searrow 0$, see, e.g., [3,5]. We include the argument briefly here.

Assume that $x < l < r$ and let $P(x,l,r)$ be the probability that a chordal SLE_κ in the half-plane $\mathbb{H}$ from x to ∞ touches the interval $[l,r]$, and note that by translation and scaling invariance it can be reduced to a function of one variable,

$$P(x,l,r) := \mathsf{P}_{(\mathbb{H};x,\infty)}[\gamma \cap [l,r] \neq \emptyset], \quad P(x,l,r) = p\left(\frac{l-x}{r-x}\right).$$

By domain Markov property we create a martingale $(M_t)_{t\geq 0}$: we define M_t as the above probability conditionally on the knowledge of an initial segment $\gamma[0,t]$

$$M_t = \mathsf{P}_{(\mathbb{H};x,\infty)}[\gamma \cap [l,r] \neq \emptyset | \mathcal{F}_t] = \mathsf{P}_{(H_t;\gamma(t),\infty)}[\gamma \cap [l,r] \neq \emptyset].$$

By conformal invariance under the map g_t in (5.1) this can be written as

$$M_t = \mathsf{P}_{(\mathbb{H};X_t,\infty)}\left[\gamma \cap [g_t(l), g_t(r)] \neq \emptyset\right] = P\left(X_t,\, g_t(l),\, g_t(r)\right).$$

Stochastic calculus tells that for this to be a martingale, the drift term

$$\frac{\kappa}{2}\frac{\partial^2}{\partial x^2}P + \frac{2}{l-x}\frac{\partial}{\partial l}P + \frac{2}{r-x}\frac{\partial}{\partial r}P$$

in the Itô derivative must vanish. This is an ordinary differential equation for p,

$$p''(u) + \frac{-4 + (2\kappa - 4)u}{\kappa u(1-u)}\, p'(u) = 0.$$

Integrating with the boundary conditions $p(0) = 1$, $p(1) = 0$ we obtain that (for $4 < \kappa < 8$)

$$\mathsf{P}_{(\mathbb{H};x,\infty)}[\gamma \cap [l,r] \neq \emptyset] = \frac{4\sqrt{\pi}}{2^{8/\kappa}\,\Gamma(\frac{8-\kappa}{2\kappa})\,\Gamma(\frac{\kappa-4}{\kappa})} \int_{\frac{l-x}{r-x}}^1 u^{-\frac{4}{\kappa}}\,(1-u)^{2\frac{4-\kappa}{\kappa}}\,\mathrm{d}u.$$

From this exact answer we find that the probability of hitting a small interval of size ε at y scales as ε^h with amplitude $|y-x|^{-h}$

$$\mathsf{P}_{(\mathbb{H};x,\infty)}[\gamma \cap [y,\, y+\varepsilon] \neq \emptyset] \sim \varepsilon^{\frac{8-\kappa}{\kappa}}\, \frac{4\sqrt{\pi}\,\kappa}{(8-\kappa)\,2^{8/\kappa}\,\Gamma(\frac{8-\kappa}{2\kappa})\,\Gamma(\frac{\kappa-4}{\kappa})}\,(y-x)^{\frac{\kappa-8}{\kappa}}. \tag{A.1}$$

Also the multiplicative constant in

$$\lim_{\varepsilon \searrow 0}\left(\varepsilon^{-h} \times \mathsf{P}[\gamma \cap I_\varepsilon(y) \neq \emptyset]\right) = \text{const.} \times \zeta^{(1)}(x;y)$$

is explicit here, but it is given by a somewhat complicated expression, and such constants are in any case non-universal.

A.2. Reaching a Small Conformal Distance from Boundary Point

Another derivation of the scaling exponent is based on the notion of boundary visit defined in terms of conformal distance. Namely, one can find explicitly the asymptotics of the probability that the chordal SLE reaches a small conformal distance from a marked boundary point. The strategy is similar to the above, but the martingale argument leads to a parabolic partial differential equation, which we do not solve explicitly, but instead we just find the leading eigenvector and eigenvalue of the generator, and hence deduce the small neighborhood size asymptotics of solutions.

For the martingale argument we need to keep track of one more point, the rightmost point r in the image of the SLE hull. Choose, therefore, $x < r < y$ and let $Q(x, r, y, s)$ be the probability that for a chordal SLE_κ γ in the half-plane $\mathbb{H}$ from x to ∞ the conformal radius of y in $\mathbb{H}\backslash(\gamma \cup (-\infty, r])$ (with a Schwarz reflection as before) is at most e^{-s}. In the limit $r \searrow x$ this correctly measures the conformal distance to the curve γ only. By translation and scaling invariance Q can be reduced to a function of two variables,

$$\begin{aligned} Q(x, r, y, s) &:= \mathsf{P}_{(\mathbb{H};x,\infty)}[\rho_{\mathbb{H}\backslash(\gamma\cup(-\infty,r])}(y) \le e^{-s}], \\ Q(x, r, y, s) &= q\left(\frac{r-x}{y-r},\ s + \log(y-r)\right). \end{aligned}$$

By domain Markov property we again create a martingale $(M_t)_{t\ge 0}$

$$M_t = \mathsf{P}_{(\mathbb{H};x,\infty)}[\rho_{\mathbb{H}\backslash(\gamma\cup(-\infty,r])}(y) \le e^{-s} \big| \mathcal{F}_t],$$

and by conformal invariance we write it as

$$\begin{aligned} M_t &= \mathsf{P}_{(\mathbb{H};X_t,\infty)}[\rho_{\mathbb{H}\backslash(\gamma\cup(-\infty,g_t(r)])}(g_t(y)) \le e^{-s+\log|g_t'(y)|}] \\ &= Q\left(X_t,\ g_t(r),\ g_t(y),\ s - \log|g_t'(y)|\right). \end{aligned}$$

For this to be a martingale, the Itô derivative drift term

$$\frac{\kappa}{2}\frac{\partial^2}{\partial x^2}Q + \frac{2}{r-x}\frac{\partial}{\partial r}Q + \frac{2}{y-x}\frac{\partial}{\partial y}Q + \frac{2}{(y-x)^2}\frac{\partial}{\partial s}Q$$

must vanish. This is a parabolic partial differential equation for q,

$$\left[\frac{\partial}{\partial\sigma} - \mathcal{G}\right] q(\theta, \sigma) = 0$$

$$\text{with generator} \quad \mathcal{G} = \frac{\kappa}{4}\theta(1+\theta)^2\frac{\partial^2}{\partial\theta^2} + (1+\theta)(1+2\theta)\frac{\partial}{\partial\theta}.$$

The asymptotics of small neighborhood size $\varepsilon = e^{-s} \to 0$ correspond to $s \to +\infty$ and, therefore, $\sigma \to +\infty$ in the above parabolic equation. In this limit the solution behaves like $q(\theta, \sigma) \sim e^{\lambda_0\sigma} q_0(\theta)$, where q_0 is the positive eigenvector

and λ_0 the corresponding leading eigenvalue of the generator $\mathcal{G}$. One finds explicitly

$$q_0(\theta) = (1+\theta)^{1-\frac{8}{\kappa}}, \quad [\mathcal{G}q_0](\theta) = \left(1 - \frac{8}{\kappa}\right) q_0(\theta), \quad \text{i.e., } \lambda_0 = 1 - \frac{8}{\kappa}.$$

From this asymptotic we find that the probability of reaching a small conformal distance $e^{-s} = \varepsilon$ at y scales as $e^{\lambda_0 s} = \varepsilon^h$ with the correct scaling exponent $h = -\lambda_0 = \frac{8-\kappa}{\kappa}$.

A.3. The Second Order PDE from Stochastic Calculus

Let γ be the chordal SLE_κ curve in $(\mathbb{H}; x, \infty)$ parametrized as in Sect. 5.1. By the domain Markov property, conditionally on an initial segment $\gamma^- = \gamma\big|_{[0,T]}$ of the curve up to a stopping time T, the rest of the curve $\gamma^+ = \gamma\big|_{[T,\infty)}$ is a chordal SLE_κ in the domain $\mathbb{H}\backslash K_T$ from the tip $\gamma(T)$ of the initial segment to ∞. Consider stopping times T smaller than the time at which any boundary visit happens. Then, conditionally on the initial segment γ^-, the contribution to the boundary visit amplitude $\zeta^{(N)}(x; y_1, \ldots, y_N)$ is $\zeta^{(N)}_{(\mathbb{H}\backslash K_T; \gamma(T), \infty)}(y_1, y_2, \ldots, y_N)$. Using the conformal map $g_T \colon \mathbb{H}\backslash K_T \to \mathbb{H}$ and conformal covariance of $\zeta^{(N)}_{(\Lambda; a, b)}$, the conditional contribution equals

$$M_T = \left(\prod_{j=1}^N g_T'(y_j)^h\right) \times \zeta^{(N)}(X_T; g_T(y_1), \ldots, g_T(y_N)). \tag{A.2}$$

By construction, then, $(M_t)_{t\geq 0}$ is a local martingale. We can compute the Itô derivative of M_t and require that the drift term in it vanishes, leading to the second-order partial differential equation

$$\left[\frac{\kappa}{2}\frac{\partial^2}{\partial x^2} + \sum_{j=1}^N \left(\frac{2}{y_j - x}\frac{\partial}{\partial y_j} - \frac{2h}{(y_j - x)^2}\right)\right] \zeta^{(N)}(x; y_1, \ldots, y_N) = 0,$$

which is Eq. (2.3) in the PDE system of Sect. 2.1. The alternative explanation of this equation by conformal field theory is given in Appendix B.2.

Appendix B. Conformal Field Theory Considerations

B.1. Boundary Visit Amplitudes as Conformal Field Theory Correlation Functions

From conformal field theory point of view, the boundary visit amplitudes are essentially correlation functions of boundary primary fields of conformal weights h in a conformal field theory with central charge $c(\kappa) = \frac{(3\kappa-8)(6-\kappa)}{2\kappa}$, see [5]. We remark that the value (1.1) is a conformal weight in the Kac table, $h = h_{1,3}(\kappa) = \frac{8-\kappa}{\kappa}$. This suggests the possibility of a degeneracy at grade three, which we argue to give rise to the third-order PDEs (2.4) below in Appendix B.2.

The covariance rule (5.2) reflects the conformal transformation properties of primary fields. More precisely, the boundary zig-zag amplitude should be thought of as a ratio

$$\zeta^{(N)}(x; y_1, y_2, \dots, y_N) = \frac{\langle \psi_{1,2}(x)\, \psi_{1,3}(y_1) \cdots \psi_{1,3}(y_N)\, \psi_{1,2}(\infty) \rangle}{\langle \psi_{1,2}(x)\, \psi_{1,2}(\infty) \rangle},$$

where

- The numerator $\langle \psi_{1,2}(x)\, \psi_{1,3}(y_1) \dots \psi_{1,3}(y_N)\, \psi_{1,2}(\infty) \rangle$ is a correlation function of N boundary primary fields $\psi_{1,3}$ of conformal weight $h = h_{1,3}(\kappa) = \frac{8-\kappa}{\kappa}$ located at $y_1, y_2, \dots, y_N$, and two boundary primary fields $\psi_{1,2}$ of conformal weight $\delta = h_{1,2}(\kappa) = \frac{6-\kappa}{2\kappa}$ located at x and ∞.
- The denominator $\langle \psi_{1,2}(x)\, \psi_{1,2}(\infty) \rangle$ is the correlation function of two boundary primary fields $\psi_{1,2}$ located at x and ∞. This correlation function is in fact just a constant (independent of x), but the presence of the fields $\psi_{1,2}(x)$ both in the numerator and denominator is the reason why the conformal covariance rule (5.2) does not contain a Jacobian factor $|f'(x)|^{\delta}$.

B.2. Singular Vectors and Differential Equations

From the point of view of conformal field theory, partial differential equations such as (2.3) and (2.4) are consequences of conformal Ward identities if the relevant boundary primary fields have vanishing descendants.

At the tip of the SLE curve, the boundary changing field is a primary field $|\psi_{1,2}\rangle$ of conformal weight $\delta = h_{1,2}(\kappa) = \frac{6-\kappa}{2\kappa}$, which has a vanishing descendant $\left(L_{-1}^2 - \frac{4}{\kappa} L_{-2}\right) |\psi_{1,2}\rangle = 0$ at level 2 [6–8]. The associated conformal Ward identity is the second-order PDE (2.3).

At the points to be visited by the SLE curve, the boundary fields are primaries $|\psi_{1,3}\rangle$ of conformal weights $h = h_{1,3}(\kappa) = \frac{8-\kappa}{\kappa}$, and they have vanishing descendants

$$\left(L_{-1}^3 - \frac{16}{\kappa} L_{-2} L_{-1} + \frac{8(8-\kappa)}{\kappa^2} L_{-3} \right) |\psi_{1,3}\rangle = 0$$

at level 3. The associated conformal Ward identities are the third-order PDEs (2.4).

B.3. Asymptotics from Operator Product Expansions

Conformal field theory allows a finite number of different asymptotics as the distance of any two arguments of $\zeta^{(N)}$ or $\chi^{(N)}$ tends to zero. The reason is that the boundary primary field $\psi_{1,2}(x)$ is degenerate at level two [6–8], and similarly the boundary primary fields $\psi_{1,3}(y_j)$ are degenerate at level three [5] (this level three degeneracy is not a priori granted, but it is suggested by known $N = 1$ and $N = 2$ cases and justified a posteriori by a proof of our formula). The degeneracies imply selection rules for the fusion of the corresponding fields. A fusion of primary fields located at z and w, with respective conformal weights $h^{(z)}$ and $h^{(w)}$, to a field of conformal weight $h^{(\infty)}$ and its descendants, leads to terms of the form

$$(z-w)^{h^{(\infty)} - h^{(z)} - h^{(w)}} \times \text{reg.}$$

in the operator product expansion. Here and below, reg. stands for functions that are holomorphic and non-vanishing on the "diagonal" $z = w$. Taking into account the selection rules, conformal field theory suggests the following:

- *Possible asymptotics as two visit points approach each other* The fusion of the fields at y_j and y_k may contain primary fields of weights $h_{1,1} = 0$, $h_{1,3} = \frac{8-\kappa}{\kappa}$, $h_{1,5} = \frac{2(12-\kappa)}{\kappa}$. Correspondingly the functions $\zeta^{(N)}$ and $\chi^{(N)}$ have the form

$$(y_j - y_k)^{2(1-\frac{8}{\kappa})} \times \text{reg.} + (y_j - y_k)^{1-\frac{8}{\kappa}} \times \text{reg.} + (y_j - y_k)^{\frac{8}{\kappa}} \times \text{reg.} \quad \text{(B.1)}$$

  as $|y_k - y_j| \to 0$.
- *Possible asymptotics as the starting point and a visit point approach each other* The fusion of the fields at x and y_j may contain primary fields of weights $h_{1,2} = \frac{6-\kappa}{2\kappa}$, $h_{1,4} = \frac{3(10-\kappa)}{2\kappa}$. Correspondingly the functions $\zeta^{(N)}$ and $\chi^{(N)}$ have the form

$$(x - y_k)^{1-\frac{8}{\kappa}} \times \text{reg.} + (x - y_k)^{\frac{4}{\kappa}} \times \text{reg.} \quad \text{(B.2)}$$

  as $|y_j - x| \to 0$.

The possible asymptotics above can also be viewed directly as resulting from the indicial equations for the Frobenius series solutions to the system of partial differential equations given in Sect. 2. This point of view to fusion is adopted in the article [19], where also the justification of Frobenius series ansatz and more profound consequences are studied.

Appendix C. Some Explicit Quantum Group Formulas

C.1. Explicit Normalization Conventions for Subrepresentations

In the spin chain–Coulomb gas correspondence, the asymptotics of the functions may be read off from projections to irreducible subrepresentations in consecutive tensorands. We specifically make use of the tensor products

$$M_3 \otimes M_3 \cong M_1 \oplus M_3 \oplus M_5$$

and

$$M_2 \otimes M_3 \cong M_2 \oplus M_4, \qquad M_3 \otimes M_2 \cong M_2 \oplus M_4.$$

We will need projections to the irreducible subrepresentations. Note that if we want to identify the subrepresentations concretely with the irreducibles described in Sect. 3.2.2, we have to fix normalization factors. This corresponds to a choice of embedding of the irreducibles to the tensor products as subrepresentations. Our normalization conventions given below are specializations of [30, Lemma 2.4].

For the former tensor product representation, $M_3 \otimes M_3$, we denote the projections to the three irreducible subrepresentations by $\pi^{(d)} \colon M_3 \otimes M_3 \to M_d \subset M_3 \otimes M_3$, where $d \in \{1, 3, 5\}$. For the latter two, $M_2 \otimes M_3$ and $M_3 \otimes M_2$, we denote the projections to the two irreducible subrepresentations by $\pi^{(d)} \colon M_2 \otimes M_3 \to M_d \subset M_2 \otimes M_3$ and $\pi^{(d)} \colon M_3 \otimes M_2 \to M_d \subset M_3 \otimes M_2$,

where $d \in \{2,4\}$. Although the same notation is used for these latter two different projections, the meaning should always be clear from the context.

Our embeddings of the irreducibles to the tensor products are the following. It is enough to specify the image of the highest weight vector e_0 in the tensor product, and our normalization choices are

$$\begin{aligned} M_1 &\hookrightarrow M_3 \otimes M_3 \colon e_0 \mapsto \frac{1}{(q^2-q^{-2})^2}(e_0 \otimes e_2 - e_1 \otimes e_1 + q^{-2} e_2 \otimes e_0) \\ M_3 &\hookrightarrow M_3 \otimes M_3 \colon e_0 \mapsto \frac{1}{q^2-q^{-2}}(-q^2 e_0 \otimes e_1 + e_1 \otimes e_0) \\ M_5 &\hookrightarrow M_3 \otimes M_3 \colon e_0 \mapsto e_0 \otimes e_0 \end{aligned}$$

and

$$\begin{aligned} M_2 &\hookrightarrow M_2 \otimes M_3 \colon e_0 \mapsto \frac{q^4}{1-q^4} e_0 \otimes e_1 - \frac{q}{1-q^2} e_1 \otimes e_0 \\ M_4 &\hookrightarrow M_2 \otimes M_3 \colon e_0 \mapsto e_0 \otimes e_0 \end{aligned}$$

and

$$\begin{aligned} M_2 &\hookrightarrow M_3 \otimes M_2 \colon e_0 \mapsto \frac{q^2}{1-q^2} e_0 \otimes e_1 - \frac{q^2}{1-q^4} e_1 \otimes e_0 \\ M_4 &\hookrightarrow M_3 \otimes M_2 \colon e_0 \mapsto e_0 \otimes e_0. \end{aligned}$$

These choices of normalizing constants strike a compromise between simplicity of formulas for the quantum group representations and for the asymptotics of the corresponding functions treated in Sect. 3.3.2.

When an identification with a smaller tensor product is implied in a projection to subrepresentation, we indicate this with a hat: we thus define $\hat{\pi}^{(1)} \colon M_3 \otimes M_3 \to \mathbb{C}$, $\hat{\pi}^{(3)} \colon M_3 \otimes M_3 \to M_3$, $\hat{\pi}^{(2)} \colon M_2 \otimes M_3 \to M_2$, and $\hat{\pi}^{(2)} \colon M_3 \otimes M_2 \to M_2$ with the identifications of the subrepresentations given above. We finally need to act on two consecutive components of the following big tensor product:

$$M_3^{\otimes R} \otimes M_2 \otimes M_3^{\otimes L}.$$

We define the following projections to a doublet subrepresentation in the tensor product of the doublet tensorand in the middle and a triplet on either side of it, according to the "±"-symbol:

$$\begin{aligned} \hat{\pi}^{(2)}_+ &\colon M_3^{\otimes R} \otimes M_2 \otimes M_3^{\otimes L} \to M_3^{\otimes (R-1)} \otimes M_2 \otimes M_3^{\otimes L} \\ \hat{\pi}^{(2)}_+ &= (\mathrm{id}_{M_3})^{\otimes (R-1)} \otimes \hat{\pi}^{(d)} \otimes (\mathrm{id}_{M_3})^{\otimes L} \\ \hat{\pi}^{(2)}_- &\colon M_3^{\otimes R} \otimes M_2 \otimes M_3^{\otimes L} \to M_3^{\otimes R} \otimes M_2 \otimes M_3^{\otimes (L-1)} \\ \hat{\pi}^{(2)}_- &= (\mathrm{id}_{M_3})^{\otimes R} \otimes \hat{\pi}^{(2)} \otimes (\mathrm{id}_{M_3})^{\otimes (L-1)}. \end{aligned}$$

Likewise, we define the following projections in two consecutive triplet factors (in the mth and $(m+1)$st factors on the left or on the right)

$$\begin{aligned}
&\hat{\pi}^{(3)}_{+;m}\colon M_3^{\otimes R}\otimes M_2\otimes M_3^{\otimes L}\to M_3^{\otimes(R-1)}\otimes M_2\otimes M_3^{\otimes L}\\
&\hat{\pi}^{(3)}_{+;m}=(\mathrm{id}_{M_3})^{\otimes(R-m-1)}\otimes\hat{\pi}^{(3)}\otimes(\mathrm{id}_{M_3})^{\otimes(m-1)}\otimes\mathrm{id}_{M_2}\otimes(\mathrm{id}_{M_3})^{\otimes L}\\
&\hat{\pi}^{(3)}_{-;m}\colon M_3^{\otimes R}\otimes M_2\otimes M_3^{\otimes L}\to M_3^{\otimes R}\otimes M_2\otimes M_3^{\otimes(L-1)}\\
&\hat{\pi}^{(3)}_{-;m}=(\mathrm{id}_{M_3})^{\otimes R}\otimes\mathrm{id}_{M_2}\otimes(\mathrm{id}_{M_3})^{\otimes(m-1)}\otimes\hat{\pi}^{(3)}\otimes(\mathrm{id}_{M_3})^{\otimes(L-m-1)}.
\end{aligned}$$

Finally, we also define the following projections in two consecutive triplet factors (in the mth and $(m+1)$st factors on the left or on the right)

$$\begin{aligned}
&\hat{\pi}^{(1)}_{+;m}\colon M_3^{\otimes R}\otimes M_2\otimes M_3^{\otimes L}\to M_3^{\otimes(R-2)}\otimes M_2\otimes M_3^{\otimes L}\\
&\hat{\pi}^{(1)}_{+;m}=(\mathrm{id}_{M_3})^{\otimes(R-m-1)}\otimes\hat{\pi}^{(1)}\otimes(\mathrm{id}_{M_3})^{\otimes(m-1)}\otimes\mathrm{id}_{M_2}\otimes(\mathrm{id}_{M_3})^{\otimes L}\\
&\hat{\pi}^{(1)}_{-;m}\colon M_3^{\otimes R}\otimes M_2\otimes M_3^{\otimes L}\to M_3^{\otimes R}\otimes M_2\otimes M_3^{\otimes(L-2)}\\
&\hat{\pi}^{(1)}_{-;m}=(\mathrm{id}_{M_3})^{\otimes R}\otimes\mathrm{id}_{M_2}\otimes(\mathrm{id}_{M_3})^{\otimes(m-1)}\otimes\hat{\pi}^{(1)}\otimes(\mathrm{id}_{M_3})^{\otimes(L-m-1)}.
\end{aligned}$$

Additionally, we denote by $\pi^{(2)}_{\pm},\pi^{(4)}_{\pm},\pi^{(1)}_{\pm;m},\pi^{(3)}_{\pm;m},\pi^{(5)}_{\pm;m}$ the projections

$$M_3^{\otimes R}\otimes M_2\otimes M_3^{\otimes L}\to M_3^{\otimes R}\otimes M_2\otimes M_3^{\otimes L}$$

analogous to the hatted counterparts $\hat{\pi}^{(2)}_{\pm},\hat{\pi}^{(4)}_{\pm},\hat{\pi}^{(1)}_{\pm;m},\hat{\pi}^{(3)}_{\pm;m},\hat{\pi}^{(5)}_{\pm;m}$, respectively, but without the identification of the submodule with a shorter tensor product.

C.2. The Quantum Group Solutions for Some 4-Point Visits

For brevity, we factor out the constant

$$C_4=\frac{q^7\left(q^4+q^2+1\right)^3}{\left(q^2-1\right)^4\left(q^2+1\right)^5\left(\left(q^{12}+2q^8+q^6+2q^4+q^2+2\right)q^4+1\right)}.$$

Then, with a shorthand notation similar to that in Sects. 3.5.2 and 3.5.3, the normalized solutions for the cases needed for Fig. 13 are

$$\begin{aligned}
v^{(4)}_{+-++}=C_4\big(&\left(q^2+1\right)\left(q^4+1\right)q^6e_{00112}-q^4e_{00202}-\left(q^2+1\right)q^5e_{00211}+q^4e_{22000}\\
&+\left(q^2+1\right)\left(q^4+1\right)q^8e_{01012}-\left(q^2+1\right)q^6e_{01102}-\left(q^2+1\right)^2q^7e_{01111}\\
&+\left(q^5+q^3\right)e_{01201}+\left(q^6+q^4\right)e_{01210}-q^8e_{02002}-\left(q^2+1\right)q^9e_{02011}+e_{20200}\\
&+\left(q^7+q^5\right)e_{02101}+\left(q^8+q^6\right)e_{02110}+\left(-q^4-1\right)e_{02200}+\left(q^4-1\right)q^5e_{12001}\\
&-\left(q^2+1\right)\left(q^5+q\right)^2e_{10012}+\left(-q^8+q^6+q^2\right)e_{10102}+\left(q^4-1\right)q^6e_{12010}\\
&+\left(-q^{11}+q^7+q^5+q^3\right)e_{10111}+\left(q^4-1\right)qe_{10201}+\left(q^4-1\right)q^2e_{10210}\\
&+\left(-q^{10}+q^8+q^4\right)e_{11002}+\left(-q^{13}+q^9+q^7+q^5\right)e_{11011}+\left(q^8+q^4\right)e_{20002}\\
&+\left(q^2-1\right)\left(q^2+1\right)^2q^3e_{11101}+\left(q^2-1\right)\left(q^2+1\right)^2q^4e_{11110}+\left(-q^6-q^2+1\right)e_{11200}\\
&-\left(q^6+q^2-1\right)q^2e_{12100}+\left(q^2+1\right)\left(q^4+1\right)q^5e_{20011}-\left(q^2+1\right)q^3e_{20101}\\
&-\left(q^2+1\right)q^4e_{20110}-\left(q^2+1\right)q^5e_{21001}-\left(q^2+1\right)q^6e_{21010}+\left(q^4+q^2\right)e_{21100}\big)
\end{aligned}$$

$$
\begin{aligned}
v^{(4)}_{+--+} = C_4\Bigg(& \frac{\left(q^4+1\right)\left(q^4+q^2+1\right)q^5 e_{00022}}{q^2+1} + \left(q^4+1\right)\left(q^4+q^2+1\right)q^6 e_{00112} + \left(q^3-q^9\right)e_{21100} \\
& - \left(q^4+1\right)\left(q^4+q^2+1\right)q^2 e_{00121} - \left(q^4+q^2+1\right)q^4 e_{01012} + \left(q^2-q^8\right)e_{01021} \\
& - \left(q^4+q^2+1\right)q^5 e_{01102} + \left(-q^{11}-q^9+q^5+q^3\right)e_{01111} + \left(q^7+q^5+q^3\right)e_{01120} \\
& + \left(q^3+\frac{q}{q^2+1}\right)e_{02002} + \left(q^4+q^2-1\right)q e_{02011} + \left(q^2+\frac{1}{q^2+1}-2\right)q e_{02020} \\
& + \left(q^4+q^2-1\right)q^2 e_{02101} + \left(q^4-q^2-1\right)q^2 e_{02110} - \left(q^4+q^2+1\right)q^6 e_{10012} \\
& + \left(q^4-q^{10}\right)e_{10021} - \left(q^4+q^2+1\right)q^7 e_{10102} + \left(q^2-q^8\right)e_{21010} + \left(q^6+2q^4-1\right)q^3 e_{11011} \\
& + \left(q^9+q^7+q^5\right)e_{10120} + \left(q^7+q^5+q^3\right)e_{11002} - \left(q^8+q^6-q^2-1\right)q^5 e_{10111} \\
& + \left(q^4-q^2-1\right)q^3 e_{11020} + \left(q^6+2q^4-1\right)q^4 e_{11101} + \left(q^6-2q^2-1\right)q^4 e_{11110} \\
& - \left(q^4+q^2+1\right)q^2 e_{12001} + \left(1-q^6\right)e_{12010} + \left(q-q^7\right)e_{12100} + \frac{\left(q^9+q^7+q^5\right)e_{20002}}{q^2+1} \\
& - \frac{\left(-q^9+q^7+q^5\right)e_{20020}}{q^2+1} - \left(q^4+q^2+1\right)q^4 e_{21001} + \frac{\left(q^4+1\right)\left(q^4+q^2+1\right)q e_{22000}}{q^2+1} \\
& + \left(q^4+q^2-1\right)q^5 e_{20011} + \left(q^4-q^2-1\right)q^6 e_{20110} + \left(q^4+q^2-1\right)q^6 e_{20101}\Bigg)
\end{aligned}
$$

$$
\begin{aligned}
v^{(4)}_{-+++} = C_4\big(& \left(q^2+1\right)\left(q^4+q^2+1\right)q^6 e_{00112} + \left(q^4+1\right)\left(q^4+q^2+1\right)q^2 e_{20002} \\
& + \left(q^8+q^6-q^2-1\right)q^4 e_{01012} + \left(q^8+q^6-q^2-1\right)q^6 e_{01102} + \left(q^6+q^4+q^2\right)e_{22000} \\
& - \left(q^6+2q^4-1\right)q^5 e_{01201} + \left(q^2+1\right)\left(q^4+q^2+1\right)q^2 e_{01210} - \left(q^4+q^2+1\right)q^6 e_{02002} \\
& + \left(-q^9+2q^5+q^3\right)e_{02011} + \left(-q^{11}+2q^7+q^5\right)e_{02101} + \left(q^8+q^6-q^2-1\right)e_{02110} \\
& + \left(q^6-1\right)q^2 e_{02200} - \left(q^2+1\right)\left(q^4+q^2+1\right)q^4 e_{10012} - \left(q^2+1\right)\left(q^4+q^2+1\right)q^6 e_{10102} \\
& + \left(-q^{12}+2q^6+q^4+q^2\right)e_{11002} + \left(-q^{11}+2q^7+q^5\right)e_{10201} + \left(q^8+q^6-q^2-1\right)e_{10210} \\
& - \left(q^2+1\right)^2\left(q^4-q^2-1\right)q^3 e_{10111} - \left(q^2+1\right)^2\left(q^4+q^2-1\right)q^3 e_{01111} \\
& - \left(q^2+1\right)\left(q^8-2q^6-q^4+1\right)q^3 e_{11101} + \left(q^2+1\right)\left(q^8-q^4-2q^2+1\right)e_{11110} \\
& + \left(q^{10}-q^6-2q^4+q^2\right)e_{11200} + \left(q^8+q^6-q^2-1\right)q^3 e_{12001} + \left(1-q^4\left(q^2+2\right)\right)e_{12010} \\
& + \left(-q^8-2q^6+q^2\right)e_{12100} + \left(q^8+q^6-q^2-1\right)q e_{20011} + \left(q^4+q^2+1\right)q^8 e_{00202} \\
& + \left(q^8+q^6-q^2-1\right)q^3 e_{20101} + \left(1-q^4\left(q^2+2\right)\right)e_{20110} - \left(q^4+q^2-1\right)q^2 e_{20200} \\
& - \left(q^2+1\right)\left(q^4+q^2+1\right)q^3 e_{21001} + \left(-q^6+2q^2+1\right)e_{21010} + \left(-q^8+2q^4+q^2\right)e_{21100} \\
& - \left(q^2+1\right)\left(q^8-2q^6-q^4+1\right)q e_{11011} - \left(q^2+1\right)\left(q^4+q^2+1\right)q^3 e_{00211}\big).
\end{aligned}
$$

Appendix D. Numerical Evaluation of the Integrals

Let us then describe how the integral expressions can be evaluated numerically in practice. We have implemented two methods with symbolic computation software:

1. Direct evaluation of the complex loop integrals $\varphi_{t_L^-,\ldots,t_2^-,t_1^-;d;t_1^+,t_2^+,\ldots,t_R^+}$.
2. Evaluation of the (real) integrals $\rho_{t_L^-,\ldots,t_2^-,t_1^-;d;t_1^+,t_2^+,\ldots,t_R^+}$ by using the ε-regularization scheme described above.

Both of these approaches have advantages and disadvantages. The loop integrals are well defined as such for all values of κ, but involve complex integrands

and complicated numerical contours which slow down the integration. Real ε-regularized integrals are faster to evaluate, but one needs to add counterterms which also involve integrals, thus increasing the total number of integrations. In addition, the remaining ε-dependence of the result needs to be controlled.

In both methods, low values of κ are the most challenging. In the loop integrals, the variations in the absolute value of the integrand increase with decreasing κ, leading to more and more precise cancellations between contributions from different sections of the integrations contours. In order to make the ε-regularization work, a larger number of counterterms is necessary at small κ than at values of κ close to $\kappa = 8$, which practically limits this method to $\kappa \gtrsim 4$. As it turns out, probability amplitudes with $N = 3$ boundary visits are still relatively fast to evaluate, in particular when κ is close to eight, whereas it is already computationally demanding to evaluate the $N = 4$ amplitudes. For $N = 3$ the calculation of the loop integrals is the faster method. We have controlled the numerical errors by comparing the results obtained by the two methods for the final result of the probability amplitude.

D.1. Evaluation of the Loop Integrals

In order to evaluate the loop integrals, we first need to specify the integration contours. We choose the anchor point in the lower half plane. Each contour is chosen to be a combination of two straight lines and an arc of a circle, with the center of the circle located at the encircled charge, and the lines being tangential to the circle (see Fig. 14). The radii of the circles are chosen such that the minimum distance between any pair of charges is (approximately) maximized. The contours $w_k = c_k(s_k)$ are parametrized in terms of the real variables $s_k \in [0, 1]$, such that w_k moves around the charge in the counterclockwise direction with increasing s_k. The parametrization can be chosen such that $c_k'(s_k)$ is continuous at the points where the arc joins with the lines.

The most tricky step is to write the multi-branched integrand in terms of the principal branches of the power functions such that it is an analytic function on the integration contours, and the phase convention of Fig. 3 is

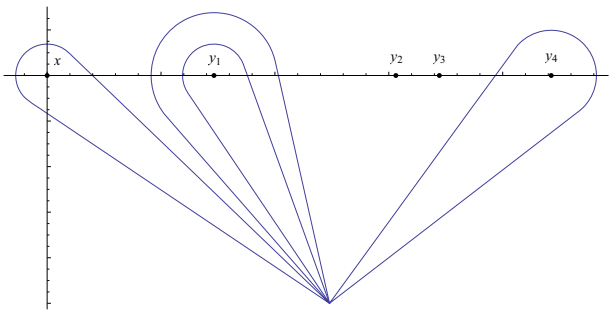

FIGURE 14. An example of the integration contours used for numerical evaluation of our results

realized. By the principal branch we mean that

$$x^y = \exp\left(y\,\log(x)\right),$$

where the principal branch of the logarithm satisfies $-\pi < \Im\mathfrak{m}\left(\log(x)\right) \leq \pi$ for all complex $x \neq 0$. Let us denote by $\hat{s}_k$ the value of s_k where $\Im\mathfrak{m}\, w_k$ takes its largest value. It is then easy to check that the various terms of the integrand can be defined as follows:

- If the contours with indices k_1 and k_2 encircle two different charges y_{j_1} and y_{j_2}, with $y_{j_1} < y_{j_2}$, we take

$$(w_{k_2} - w_{k_1})^{8/\kappa} = \exp\left(\frac{8}{\kappa}\,\log(w_{k_2} - w_{k_1})\right).$$

  Similar definition holds when either of the contours is around x.
- If the contours with indices k_1 and k_2 encircle the same charge, with c_{k_1} being the innermost contour, we take

$$(w_{k_2} - w_{k_1})^{8/\kappa} = \exp\left(\frac{8}{\kappa}\,\log(w_{k_2} - w_{k_1})\right) \quad \text{if } 0 \leq s_{k_2} \leq \hat{s}_{k_2}$$

$$(w_{k_2} - w_{k_1})^{8/\kappa} = \exp\left(\frac{8\pi}{\kappa}\mathfrak{i} + \frac{8}{\kappa}\,\log(w_{k_1} - w_{k_2})\right) \quad \text{if } \hat{s}_{k_2} < s_{k_2} \leq 1.$$

- If the contour c_k encircles y_{j_1} we take for each $y_{j_2} \neq y_{j_1}$

$$(w_k - y_{j_2})^{-8/\kappa} = \exp\left(-\frac{8}{\kappa}\,\log(w_k - y_{j_2})\right) \quad \text{if } y_{j_1} > y_{j_2}$$

$$(y_{j_2} - w_k)^{-8/\kappa} = \exp\left(-\frac{8}{\kappa}\,\log(y_{j_2} - w_k)\right) \quad \text{if } y_{j_1} < y_{j_2},$$

  and for the contribution from the charge y_{j_1} we use

$$(w_k - y_{j_1})^{-8/\kappa} = \exp\left(-\frac{8}{\kappa}\,\log(w_k - y_{j_1})\right) \quad \text{if } 0 \leq s_k \leq \hat{s}_k$$

$$(w_k - y_{j_1})^{-8/\kappa} = \exp\left(-\frac{8\pi}{\kappa}\mathfrak{i} - \frac{8}{\kappa}\,\log(y_{j_1} - w_k)\right) \quad \text{if } \hat{s}_k < s_k \leq 1.$$

  The terms involving w_k and x are treated analogously.

The numerical integration can then be done after changing the integration variables to s_k. It turns out that the integration on our symbolic computation software is often faster, if each of the contours is explicitly divided into the three pieces containing the two lines and the arc, and the contributions are integrated separately.

The probability amplitudes $\zeta^{(N)}$ often have zeroes of poles at the rational values of κ of interest to us, but then one may just straightforwardly modify the normalizing constants. For example, at $\kappa = 6$, $N = 3$ we can add a normalization factor $\propto 1/(\kappa - 6)$ and study $\zeta^{(3)}/(\kappa - 6)$ in the limit $\kappa \to 6$. The numerical integration cannot be done, however, arbitrary close to $\kappa = 6$, because the integrals contributing to $\zeta^{(3)}$ do not vanish term by term, and noise due to the limited numerical precision of such integrals will grow as $1/|\kappa - 6|$ as $\kappa \to 6$. We evaluated the amplitude for values of κ near the critical one,

say, at $\kappa = 6.05$ and $\kappa = 5.95$, and estimated the amplitude at $\kappa = 6$ as the average of the results. More elaborate fitting, as a function of κ, can also be done.

D.2. Evaluation of the ε-Regularized Integrals

The most involved step in the evaluation of the ε-regularized integrals is the identification of the counterterms. In Sect. 4.3 we already discussed how this can be done, and considered explicitly a simple example. Computation of the terms at higher N and to higher order in ε is in principle straightforward, but the complexity of the expressions grows relatively fast. We have written a code on symbolic computation software which automatically finds the counterterms for a given integral. All leading order terms in the expansion of the divergent terms at $\varepsilon = 0$ [i.e., the $k = 0$ terms $\mathcal{O}\left(\varepsilon^{-n(8/\kappa-1)}\right)$ in (4.2), with $n = 1, 2, \ldots, N$] and at least the leading divergence from the next-to-leading order term of the series [i.e., the terms $\mathcal{O}\left(\varepsilon^{-(N-1)(8/\kappa-1)}\varepsilon\right)$] are generated. Including these terms, the method converges for $N = 2$ integrals when $\kappa > 4$, and for $N = 3$ integrals when $\kappa > 16/3$. In practice the limits can be somewhat higher due to limited numerical precision.

After the counterterms have been identified, it is straightforward to evaluate the sum of the regularized integral and all counterterms for any fixed value of the cutoff ε. Notice also that since we are not able to subtract counterterms to all orders, some dependence on ε remains, and we need to extrapolate the result down to $\varepsilon = 0$. It is useful to calculate the amplitude at various values of ε, and fit the remaining ε-dependence by using the highest order term which was not subtracted. Moreover, a similar interpolation as a function of κ, as was described above for the loop integrals, is usually also required.

References

[1] Alberts, T., Kozdron, M.J., Lawler, G.F.: The Green's function for the radial Schramm–Loewner evolution. J. Phys. A Math. Theor. **45**, 494015 (2012)

[2] Alberts, T., Kozdron, M.J.: Intersection probabilities for a chordal SLE path and a semicircle. Electron. Commun. Probab. **13**, 448–460 (2008)

[3] Alberts, T., Sheffield, S.: Hausdorff dimension of the SLE curve intersected with the real line. Electron. J. Probab. **13**(40), 1166–1188 (2008)

[4] Alberts, T., Sheffield, S.: The covariant measure of SLE on the boundary. Probab. Theory Relat. Fields **149**(3), 331–371 (2011)

[5] Bauer, M., Bernard, D.: SLE, CFT and zig-zag probabilities. In: Proceedings of the Conference 'Conformal Invariance and Random Spatial Processes', Edinburgh (2003)

[6] Bauer, M., Bernard, D.: Conformal field theories of stochastic Loewner evolutions. Commun. Math. Phys. **239**(3), 493–521 (2003)

[7] Bauer, M., Bernard, D.: SLE martingales and the Virasoro algebra. Phys. Lett. B **557**(3-4), 309–316 (2003)

[8] Bauer, M., Bernard, D.: Conformal transformations and the SLE partition function martingale. Ann. Henri Poincaré, **5**(2), 289–326 (2004)

[9] Beffara, V., Duminil-Copin, H.: The self-dual point of the two-dimensional random-cluster model is critical for $q \geq 1$. Probab. Theory Relat. Fields **153**(3–4), 511–542 (2012)

[10] Beffara, V.: The dimension of the SLE curves. Ann. Probab. **36**(4), 1421–1452 (2008)

[11] Beliaev, D., Izyurov, K.: Proof of a factorization formula for critical percolation. Commun. Math. Phys. **310**, 611–623 (2012)

[12] Cardy, J.L.: Critical percolation in finite geometries. J. Phys. A **25**, L201–L206 (1992)

[13] Chelkak, D., Duminil-Copin, H., Hongler, C., Kemppainen, A., Smirnov, S.: Convergence of Ising interfaces to Schramm's SLE curves. Comptes Rendus Math. de l'Acad. Des Sci. **352**(2), 157–161 (2014)

[14] Camia, F., Newman, C.M.: Critical percolation exploration path and SLE_6: a proof of convergence. Probab. Theory Relat. Fields **139**(3-4), 473–519 (2007)

[15] Chelkak, D., Smirnov, S.: Discrete complex analysis on isoradial graphs. Adv. Math. **228**, 1590–1630 (2011)

[16] Chelkak, D., Smirnov, S.: Universality in the 2D Ising model and conformal invariance of fermionic observables. Invent. Math. **189**(3), 515–580 (2012). arXiv:0910.2045

[17] Dotsenko, V.S., Fateev, V.A.: Conformal algebra and multipoint correlation functions in 2D statistical models. Nucl. Phys. B **240**, 312 (1984)

[18] Dubédat, J.: SLE and Virasoro representations: localization. Commun. Math. Phys. **336**(2), 695–760 (2015)

[19] Dubédat, J.: SLE and Virasoro representations: fusion. Commun. Math. Phys. **336**(2), 761–809 (2015)

[20] Edwards, R.G., Sokal, A.D.: Generalization of the Fortuin–Kasteleyn–Swendsen–Wang representation and Monte Carlo algorithm. Phys. Rev. D **38**, 2009–2012 (1988)

[21] Fortuin, C.M., Kasteleyn, P.W.: On the random-cluster model. I. Introduction and relation to other models. Physica **57**, 536–564 (1972)

[22] Flores, S.M., Kleban, P.: A solution space for a system of null-state partial differential equations. Part I. Commun. Math. Phys. **333**(1), 389–434 (2015)

[23] Flores, S.M., Kleban, P., Ziff, R.M.: Cluster pinch-point densities in polygons. J. Phys. A Math. Theor. **45**, 505002 (2012)

[24] Felder, G., Wieczerkowski, C.: Topological representation of the quantum group Uq(sl2). Commun. Math. Phys. **138**, 583–605 (1991)

[25] Hagendorf, C.: A generalization of Schramm's formula for SLE2. J. Stat. Mech. Theory Exp. P02033 (2009)

[26] Hagendorf, C., Le Doussal, P.: SLE on doubly-connected domains and the winding of loop-erased random walks. J. Stat. Phys. **133**, 231–254 (2008)

[27] Hongler, C., Kytölä, K.: Ising interfaces and free boundary conditions. J. Am. Math. Soc. **26**, 1107–1189 (2013)

[28] Izyurov, K.: Critical Ising interfaces in multiply-connected domains (2013). arXiv:1309.5302

[29] Kennedy, T.: A fast algorithm for simulating the chordal Schramm–Loewner evolution. J. Stat. Phys. **128**, 1125–1137 (2007)

[30] Kytölä, K., Peltola, E.: Conformally covariant boundary correlation functions with a quantum group (2014). arXiv:1408.1384

[31] Kytölä, K., Peltola, E.: Pure partition functions of multiple SLEs (2015). arXiv:1506.02476

[32] Langlands, R.P., Pichet, C., Pouliot, P., Saint-Aubin, Y.: On the universality of crossing probabilities in two-dimensional percolation. J. Stat. Phys. **67**(3–4), 553–574 (1992)

[33] Lawler, G.: Fractal and Multifractal Properties of SLE. Clay Mathematics Summer School, Buzios (2010)

[34] Lawler, G.F.: Minkowski content of the intersection of a Schramm–Loewner evolution (SLE) curve with the real line. J. Math. Soc. Japan **67**(4), 1631–1669 (2015). http://www.math.uchicago.edu/~lawler/minkreal.pdf

[35] Lawler, G.F., Rezaei, M.A.: Minkowski content and natural parameterization for the Schramm–Loewner evolution. Ann. Probab. **43**(3), 1082–1120 (2015)

[36] Lawler, G.F., Sheffield, S.: A natural parametrization for the Schramm–Loewner evolution. Ann. Probab. **39**(5), 1896–1937 (2011)

[37] Lawler, G.F., Schramm, O., Werner, W.: Values of Brownian intersection exponents. I. Half-plane exponents. Acta Math. **187**(2), 237–273 (2001)

[38] Lawler, G.F., Schramm, O., Werner, W.: Conformal invariance of planar loop-erased random walks and uniform spanning trees. Ann. Probab. **32**(1B), 939–995 (2004)

[39] Lawler, G.F., Werness, B.M.: Multi-point Green's functions for SLE and an estimate of Beffara. Ann. Probab. **41**(3A), 1513–1555 (2013)

[40] Lawler, G.F., Zhou, W.: SLE curves and natural parametrization. Ann. Probab. **41**(3A), 1556–1584 (2013)

[41] Rohde, S., Schramm, O.: Basic properties of SLE. Ann. Math. (2) **161**(2), 883–924 (2005)

[42] Schramm, O.: Scaling limits of loop-erased random walks and uniform spanning trees. Isr. J. Math. **118**, 221–288 (2000)

[43] Simmons, J.J.H., Kleban, P.: Complete conformal field theory solution of a chiral six-point correlation function. J. Phys. A Math. Theor. **44**, 315403 (2011)

[44] Simmons, J.J.H., Kleban, P., Flores, S.M., Ziff, R.M.: Cluster densities at 2-d critical points in rectangular geometries. J. Phys. A Math. Theor. **44**, 385002 (2011)

[45] Smirnov S.: Critical percolation in the plane: conformal invariance, Cardy's formula, scaling limits. C. R. Acad. Sci. Paris **333**, 239–244 (2001). arXiv:0909.4499

[46] Smirnov, S.: Towards conformal invariance of 2d lattice models. In: Proceedings of the International Congress of Mathematicians (2006)

[47] Smirnov, S.: Conformal invariance in random cluster models. I. Holomorphic fermions in the Ising model. Ann. Math. **172**, 1435–1467 (2010). arXiv:0708.0039

[48] Smirnov, S.: Discrete complex analysis and probability. In: Proceedings of the ICM, Hyderabad (2010)

[49] Schramm, O., Sheffield, S.: Harmonic explorer and its convergence to SLE_4. Ann. Probab. **33**(6), 2127–2148 (2005)

[50] Swendsen, R.H., Wang, J.-S.: Nonuniversal critical dynamics in Monte Carlo simulations. Phys. Rev. Lett. **58**, 86–88 (1987)

[51] Schramm, O., Zhou, W.: Boundary proximity of SLE. Probab. Theory Relat. Fields **146**(3-4), 435–450 (2010)

[52] Simmons, J.J.H., Ziff, R.M., Kleban, P.: Factorization of percolation density correlation functions for clusters touching the sides of a rectangle. J. Stat. Mech. Theory Exp. P02067 (2009)

[53] Zhan, D.: The scaling limits of planar LERW in finitely connected domains. Ann. Probab. **36**(2), 467–529 (2008)

Niko Jokela
Departamento de Física de Partículas
Universidade de Santiago de Compostela
Santiago de Compostela
Spain

and

Present Address:
Department of Physics
Helsinki Institute of Physics
University of Helsinki
POB 64
00014 Helsinki
Finland
e-mail: niko.jokela@helsinki.fi

Matti Järvinen
Department of Physics
Crete Center for Theoretical Physics
University of Crete
71003 Heraklion
Greece

and

Present Address:
Laboratoire de Physique Théorique
Ecole Normale Supérieure
Institut de Physique Théorique Philippe Meyer
24, rue Lhomond
75231 Paris
France
e-mail: jarvinen@lpt.ens.fr

Kalle Kytölä
Department of Mathematics and Statistics
University of Helsinki
P.O. Box 68
00014 Helsinki
Finland

and

Present Address:
Department of Mathematics and Systems Analysis
Aalto University
POB 11100
00076 Espoo
Finland
e-mail: kalle.kytola@aalto.fi

Communicated by Denis Bernard.
Received: December 13, 2014.
Accepted: July 6, 2015.